The influence of structure on the fracture of brittle ceramic materials.

Alderson, J. P.

Award date:
1977

Awarding institution:
University of Bath

The Influence of Structure on the Fracture of Brittle Ceramic Materials.

Submitted by J.P.Alderson
for the degree of Ph. D.
of the University of Bath.
1977

Copyright

J.P. Alderson

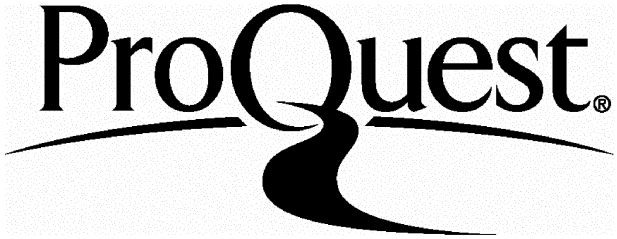

to my wife

Abstract

The thesis reviews the historical development of stress analysis for the solution of stress functions in the neighbourhood of cracks or flaws. The analysis assumes the material is a brittle continuum obeying the laws of linear elasticity. The influence of material structure on such analysis is considered both from the experimental and the theoretical point of view.

For the experimental investigation, clay ceramics based on Kaolinite are used to provide a range of different coarse polyphase structures in the form of test pieces suitable for fracture testing in a three point bend rig. The values of the fracture stress σ_F, the critical stress intensity K_{Ic} and the modulus of elasticity E obtained in this way, are found to follow similar trends and to vary with the clay formulation.

Scanning electron microscopy has been employed to study the intrinsic structure of the material. It is found that the measured values, not only of K_{Ic} and E, but also of σ_F can be related to the structure. Thus in these materials, σ_F is <u>not</u> random flaw controlled and σ_F, K_{Ic} and E are all material influenced parameters.

The validity of applying the stress equations to structured materials is shown to depend on the stress field at the crack tip being of the same form for both σ_F and K_{Ic} determinations. It is argued that in the case of quasi brittle materials, this is ensured by the plastic zone at the crack tip. In the case of the brittle ceramic

materials investigated here, it is shown that similarity of stress at the crack tip is produced by subcritical crack growth.

With subcritical crack growth, a physical significance can be attributed to derived variables such as the equivalent elastic crack, and the material dependence of σ_F can be explained.

Contents

1. Introduction

Brittle fracture is a form of material failure in which no yielding or plastic flow takes place and in which ideally the only energy involved is that required to form the new surfaces. The fracture is generally assumed to originate at some flaw or crack in the material which acts as a stress intensifier and gives rise to catastrophic failures at an applied stress considerably less than the intrinsic strength of the material. In this respect fracture can be considered flaw dependent and extrinsic to the nature of the material. However, this can be only part of the picture as the nature and structure of the material will determine the stress field developed around the flaw and should therefore influence the applied stress at which catastrophic fracture occurs.

The aims of this thesis are

a) to investigate the part played by the structure of a material on the values of the fracture stress σ_F, the critical stress intensity K_{Ic} and the modulus of elasticity E.

b) to examine the validity of applying the various classically derived equations connecting σ_F, K_{Ic} and E which are based on assumptions of continuum mechanics and linear elasticity, to polyphase and complex structural materials.

c) to consider the theoretical significance of the calculated values of the derived variables, such as the energy for the initiation of fracture γ_i, with particular

regard to the difference between the quasi brittle and the fully brittle material.

Clay bodied ceramics provided a convenient source of brittle materials which was the primary reason for their choice. By taking kaolinite as the base material, adding various fillers and firing at different temperatures it was possible to produce a series of materials with different structures in test piece form. Additionally, the test pieces proved to be easily reproducible giving good agreement between batches made on separate occassions.

The structure of the fracture surfaces were examined on a scanning electron microscope (S.E.M.). An etching technique was used to remove the glassy phase and to reveal the underlying structure of the material which was not always readily visible on the fracture surface. Additional confirmation, that the firing reactions were in general agreement with those expected from the chemistry of kaolinite, was obtained by X-ray spectroscopy.

The values of σ_F, K_{Ic} and E were measured on test pieces in a three point bend test rig and relationships were looked for between the fracture surfaces shown by the S.E.M. and the measured fracture values.

The now standard bend test formulae were considered satisfactory for brittle ceramics both from the evidence of other workers and, since for this thesis the test procedures were standardised and the numbers would be comparative.

2. Theoretical Background and Literature Review

The building of any structure or the making of an article requires a knowledge of the way in which it is likely to fail, and the use of the correct design criteria if failure is to be avoided. This applies whether one is constructing a bridge, making a pressure vessel or manufacturing turbine blades. Apart from failure due to environmental causes such as corrosion or temperature, several types of mechanical failure can occur, three of which are usually the most important.

2.1. Modes of Mechanical Failure.

2.1.1. Buckling - this is where, for example, a strut is overloaded and bends elastically until such time as the load is greater than the elastic restoring force and collapse by buckling occurs.

2.1.2. General Yielding - this is where plastic deformation occurs to such an extent that none of the applied load is carried by elastic forces. It can occur in a beam forming part of a larger structure or, its energy absorbing properties can be utilised to advantage in, for example, car seat belts. It is necessary to distinguish between general yield and local yield - often associated with fracture, which can occur in small highly stressed areas whilst the main load is still carried elastically in the main bulk of the material.

2.1.3. Cracking - unlike buckling and yielding where

there is no visible separation of the material, in the case of cracking (or brittle fracture), failure occurs due to cracks travelling through the material dividing it into two or more parts. Cracks normally propagate very rapidly and are completely catastrophic, as for example in the breaking of a ceramic plate. Brittle fracture is the type of material failure with which this thesis is concerned and although a more formal definition is given later,* the following comments are made now.

2.2. Brittle Fracture.

Intuitively one is inclined to say cast iron is brittle and mild steel is not or glass is more brittle when cold than when hot. One is inferring that cast iron or cold glass will shatter or fracture if struck with say a hammer, whereas the mild steel or the hot glass will bend or yield and absorb the energy.

It is also well known that scale effects play an important part in determining whether or not a material breaks in a brittle fashion. Catastrophic fractures have occurred in many large structures such as bridges, ships and aircraft at well below their design loads. The understanding of the reasons for these failures and the precautions necessary to avoid their repetition, lie in the field of fracture mechanics.

It is more relevant to talk of a 'brittle fracture' rather than of a 'brittle material' bearing in mind nevertheless, that materials such as ceramics are more

*p. 23

likely to exhibit brittle fracture than others such as mild steel.

On the basis of what has been said so far, a possible definition of a brittle fracture would be one in which fracture occurs from the elastic state before general yielding; and conversely, a non brittle or ductile failure would be one in which yielding occurred in preference to fracture.

2.3. Stress

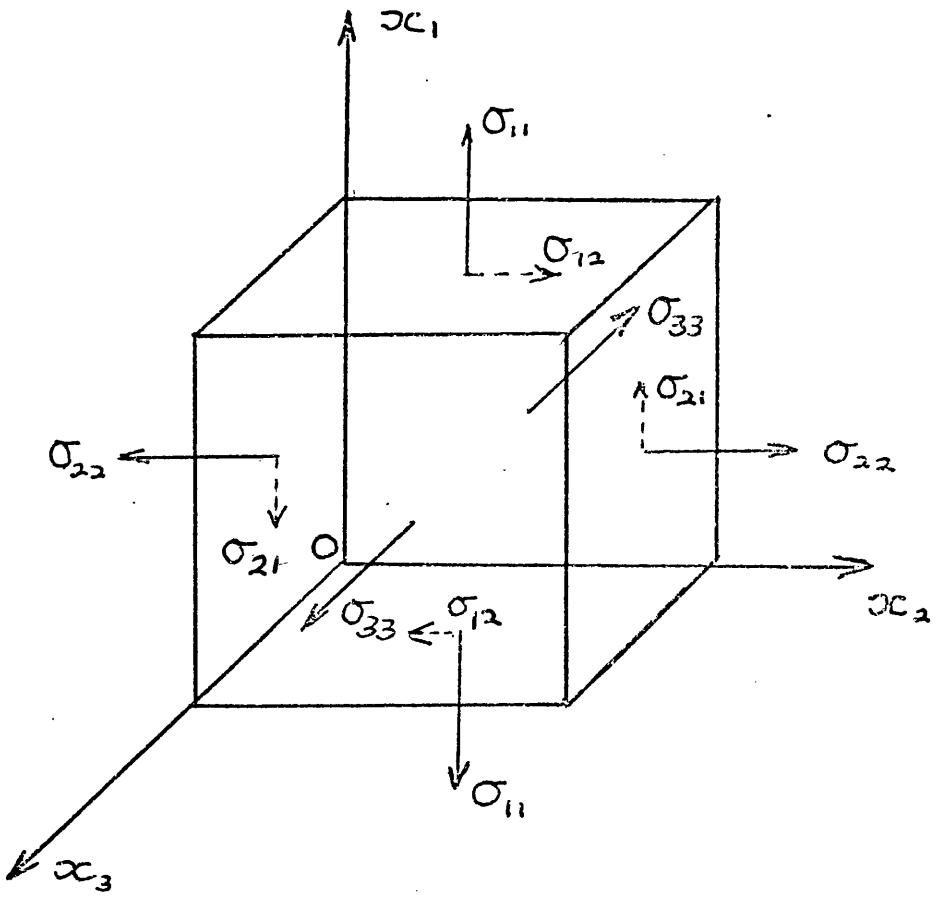

Although many structures such as cranes and bridges are rated to take a load quoted in tons, it is usually more convenient from the point of view of design or experiment to work in terms of the load per unit area

or 'stress'. In the case of failure by fracture, tensile stress is almost always the stress involved and can be defined more exactly by reference to the diagram on the previous page.

A body is shown in relation to the x_1, x_2 and x_3 axes which are drawn with the orientation usual in fracture mechanics. Components of stress are shown and the subscript notation is the accepted one - i.e. the first subscript denotes the direction of the normal from the face concerned and the second subscript denotes the direction of the force. Thus σ_{11} is a tensile stress rigidly defined as,

$$\sigma_{11} = \lim_{A \to 0} \left(\frac{F}{A} \right)$$

where F is the force in the x_1 direction normal to the plane A.

For comparison shown dashed are two shear stresses σ_{21} and σ_{12} which must be equal if the body is not to rotate.

A body with three tensile stresses σ_{11}, σ_{22} and σ_{33} is said to be under 'triaxial stress' and if the stresses are equal under 'hydraulic stress'.

2.3.1. Plane stress - in the case where one of the stresses is equal to zero, the body is in a state of bi-axial or 'plane stress'. Such a condition occurs in a thin sheet where little or no stress is developed through the thickness of the sheet in resistance to an applied stress. It is conventional to choose σ_{11} as the applied stress and σ_{33} equal to zero. Thus in plane stress,

$$\sigma_{11} > \sigma_{22} > \sigma_{33} = 0$$

2.4. Strain

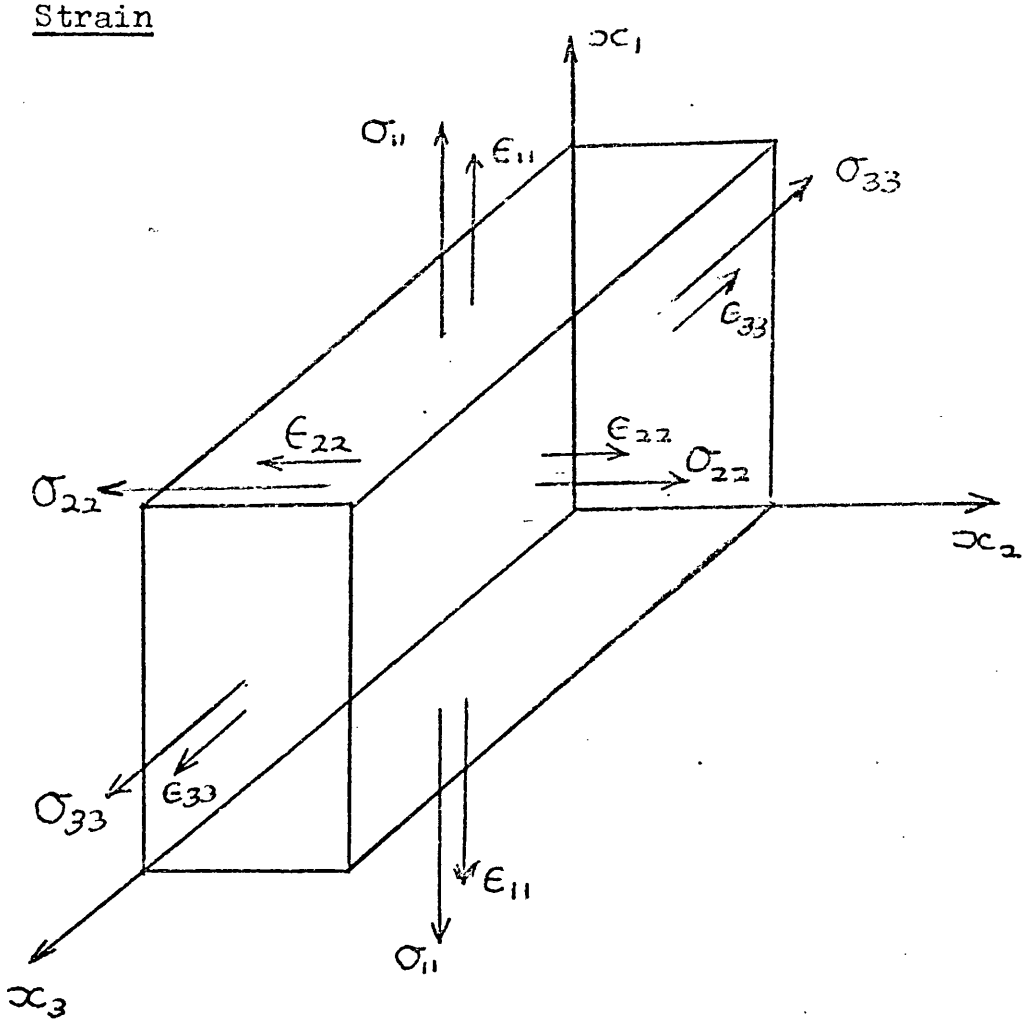

When a stress is applied to a body, deformation of the body occurs and it is said to be strained. If on the removal of the stress, the body returns to its original shape, it is said to be an elastic strain and is the type of strain involved in cases of brittle fracture. When the body does not return to its original shape, yielding or plastic strain has occurred.

The diagram shows a body under tensile stresses σ_{11}, σ_{22} and σ_{33} giving rise to tensile strains ϵ_{11}, ϵ_{22} and ϵ_{33} when, for example, the tensile strain ϵ_{11} is

defined as,

$$\epsilon_{11} = \frac{\text{increase in length in direction } x_1}{\text{original length in direction } x_1} = \frac{\delta l_1}{l_1}$$

it being understood that the change in length is small.

2.4.1. Plane strain - as with stress, various states of strain can be identified; triaxial, uniaxial and in particular bi-axial or 'plane strain'. With a body of the shape indicated in the diagram, the change in length along the x_3 axis will be very much less than along the x_1 and x_2 axes and towards the centre of the body ϵ_{33} will be virtually zero. In this condition of plane strain,

$$\sigma_{11} > \sigma_{33} > \sigma_{22} = 0.$$

Thus the second largest principle stress is σ_{33} in plane strain and σ_{22} in plane stress. It can be shown that this has the effect of reducing the size of any plastic zone at a crack tip by up to three times for the case of plane strain in relation to plane stress. This is one of the factors that feature in the design of experimental test pieces.

2.4.2. Poisson's Ratio ν It will be apparent that, if the body is extended by a stress along the x_1 axis, if $\epsilon_{33} \neq 0$ and the material remains un-cracked or continuous, then the body must contract along the x_2 axis. The ratio of the contraction to the extension is known as Poisson's ratio, and has a value between 0 and 0.5 with a figure of about 0.25 for ceramics.

2.4.2. Modulus of Elasticity E It was found empirically by Hooke experimenting with uniaxial stresses on thin wires, that for small strains, and providing the strain

remained elastic, there was a linear relationship

$\sigma_{11} = E\epsilon_{11}$ or more generally $\sigma = E\epsilon$

where E is the modulus of elasticity or Young's modulus.

2.5. Mechanism of Fracture

It has been suggested that brittle fracture is the cracking of the material from the elastic state in preference to general yielding. When one considers that the force required to fracture interatomic bonds is greater than the force required to cause them to slide or yield across each other, and that fracture commonly occurs at values one thousandth of the theoretical bond strength; it is apparent some additional mechanism is responsible for the fracture. This mechanism is the variation in stress pattern brought about by flaws in the material which may be a change in the crystal alignment, or an existing hole or crack. As early as 1921, Griffith was able to show that microscopic flaws were likely to be present in apparently flaw free material. Such flaws act as stress raisers causing a local increase in stress, which can be many times the overall applied stress and which can account for the low stress values associated with brittle fracture.

An idea of stress intensification which occurs is obtainable from the comparison of values for elastic modulus E and the measured fracture stress σ_F. It can be shown that the theoretical fracture stress is approximately $E/10$. The table overleaf gives typical values of E and σ_F for some common materials.

Material		E in GNm^{-2}	σ_F in MNm^{-2}
Sintered Alumina	1	366	200-350
Sintered Magnesia	1	210	103
Hot pressed Boron nitride	1	83	48
" " " carbide	1	290	345
" " Silicon nitride	2	275	$\sim$1000
" " " carbide	2	414	$\sim$ 800
Zirconia	1	152	83
Silica glass	1	72	107
Mullite porcelain	1	69	69
Fire clay brick	1	96	5

1. Kingery W.D. 1960 Introduction to Ceramics.
2. Godfrey D.J. 1973 Proc. Brit. Cer. Soc. 22.

Table 1.

2.6. Stress Analysis for Crack Geometries.

The problem of calculating theoretically the stress functions associated with different crack geometries - in particular with elliptical forms, has been approached in a number of ways. Three will be discussed briefly here.

2.6.1. Linear Elastic Stress Analysis Approach.

The theory of linear elastic stress analysis rests on two main requirements.

a) that all the stress applied to the body shall be in equilibrium.

b) the strains produced by these stresses must be such that elastic continuity is preserved throughout the body - known as the compatibility condition.

Additional to these two requirements and almost implicit in the second is that the body is a continuum and not made of discreet particles -atoms, molecules, crystals.

Whilst the two requirements are general and apply

in three dimension, the derivation of suitable stress functions and their analytical solutions for the stresses involved in particular cases, is exceedingly complex. It is usually sufficient to consider the more tractable two dimensional case. Airy 1862 was able to show that for two dimensionsa funtion existed for which the stresses to satisfy requirements a) were given by,

$$\sigma_{11} = \frac{\partial^2 \phi}{\partial x_2^2} \qquad \ldots\ldots\ldots(1a)$$

$$\sigma_{22} = \frac{\partial^2 \phi}{\partial x_1^2} \qquad \ldots\ldots\ldots(1b)$$

$$\sigma_{12} = -\frac{\partial^2 \phi}{\partial x_1 \partial x_2} \qquad \ldots\ldots\ldots(1c)$$

and the compatability requirement b) was satisfied by the biharmonic equation,

$$\frac{\partial^4 \phi}{\partial x_1^4} + 2\frac{\partial^4 \phi}{\partial x_1^2 \partial x_2^2} + \frac{\partial^4 \phi}{\partial x_2^4} \equiv \nabla^2(\nabla^2 \phi) = 0 \quad \ldots(2)$$

where ∇^2 is the Laplacian operator

and the diagram indicates the other variables.

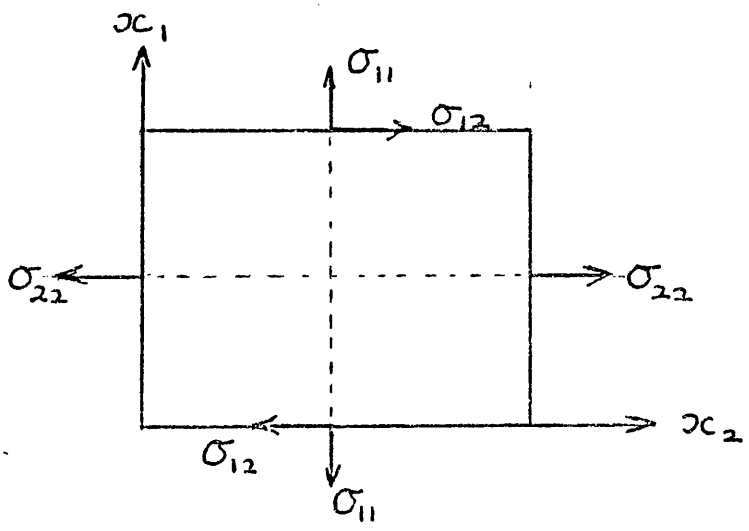

(note - The discussion and functions have been developed in terms of the stresses in the body. It is assumed throughout that the strains involved are small - for ceramics this is always the case at ambient temperatures. With this assumption, Hooke's empirical law

Stress = E x Strain

will hold and a set of strain functions essentially identical to the stress functions will exist.)

If the function satisfies equation (2), then it follows that the stress will be given by equation (1) provided also that the boundary conditions associated with the geometry of the body are met. Apart from a few idealised shapes, even in two dimensions the boundary conditions impose severe difficulties on the analytical solutions for stress values. Nowadays with the advent of computers, numerical methods are being applied to extend the range of shapes for which solutions are available.

2.6.1.1. Stresses at a Crack Tip

In 1939, Westergaard considered the stress near a sharp crack in an infinite plate. His problem was to find a suitable stress function which satisfied equation (2) and which by the application of the boundary conditions associated with the crack would give the stress involved by the solution of equation (1).

The details of his approach given in Knott p 54-56 are edited here.

Consider a harmonic function $\phi(Z) = \phi(x_1 + ix_2)$ and denote the first and second derivatives and the first

and a second integrals of $\phi(Z)$ by,

$\phi'(z)$, $\phi''(z)$, $\bar{\phi}(z)$ and $\bar{\bar{\phi}}(z)$ respectively.

Let a stress function $\bar{\Phi} = \text{Re}\ \bar{\phi}(Z) + x_2\ \text{Im}\ \bar{\phi}(Z)$

where Re stands for Real Part and Im for Imaginary Part.

Then from a knowledge of the properties of complex variables,

$$\sigma_{11} = \frac{\partial^2 \bar{\Phi}}{\partial x_2^2} = \text{Re}\ \phi(z) - x_2\ \text{Im}\ \phi'(z) \quad \ldots(3a)$$

$$\sigma_{22} = \frac{\partial^2 \bar{\Phi}}{\partial x_1^2} = \text{Re}\ \phi(z) + x_2\ \text{Im}\ \phi'(z) \quad \ldots(3b)$$

$$\sigma_{12} = \frac{\partial^2 \bar{\Phi}}{\partial x_1 \partial x_2} = -x_2\ \text{Re}\ \phi'(z) \quad \ldots(3c)$$

It can be shown that these stresses satisfy both the equilibrium requirement (a) and the compatability requirement (b).

Consider now the situation at the crack shown in the diagram below.

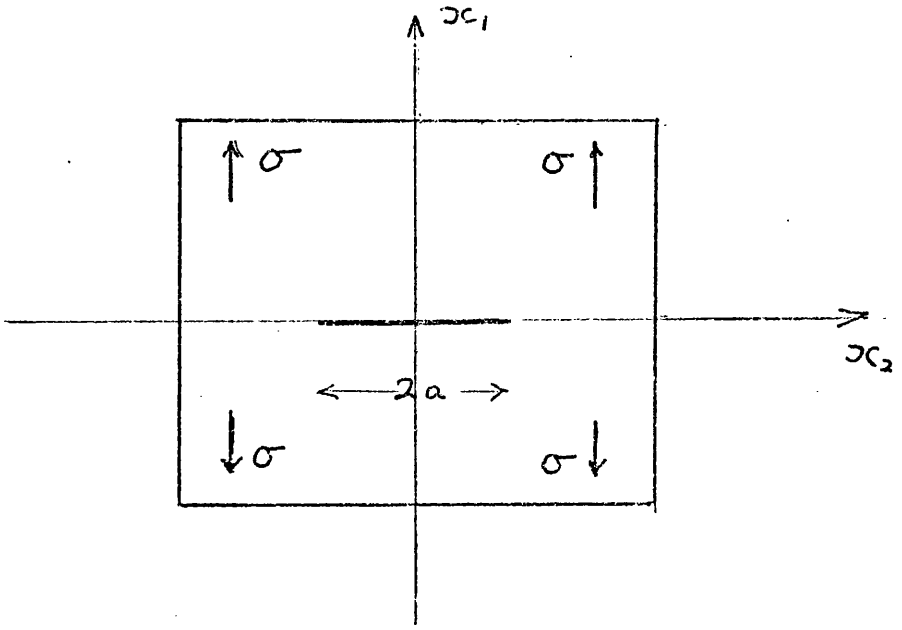

When the crack is under uniaxial tension

$\sigma_{22} = \mathrm{Re}\,\phi(Z) + x_1 \mathrm{Im}\,\phi'(Z)$

$= \mathrm{Re}\,\phi(Z)$ since the crack lies along $x_1 = 0$

To satisfy the boundary conditions that

$\sigma_{11} \to \sigma$ as $x_2 \to \pm\infty$.

and $\sigma_{11} > 0$ when $|x_2|$ is just greater than $|a|$

the simplest form of $\phi(Z)$ is $\dfrac{\sigma}{1 - a^2/x_2^2}$.

To satisfy also the conditon that

$\sigma_{11} = 0$ when $-a < x_2 < a$

the form of $\phi(Z)$ is $\dfrac{\sigma}{\sqrt{1 - a^2/x_2^2}}$.

i.e. $\sigma_{11} = \dfrac{\sigma}{\sqrt{1 - a^2/x_2^2}}$ .....(4)

At a point r just ahead of the crack tip where $r/a \ll 1$ equation (4) becomes to a first approximation,

$$\sigma_r \equiv \sigma_{11} = \sigma\sqrt{a/2r} \qquad \text{.....(5)}$$

It is also possible to shcw that the displacement associated with this stress is given in plane strain by,

$$u_{11} = \frac{2(1-\nu^2)\sigma}{E}\sqrt{a^2 - x_2^2} \qquad \text{.....(6)}$$

Previously Inglis 1913 had, by a mathematically more direct approach, obtained an expression for the stress distribution around an elliptical hole in an infinite plate. In particular, the stress σ_t at the tip of the ellipse drawn overleaf is given by,

$$\sigma_t = \sigma\left(1 + 2\sqrt{a/\rho}\right) \qquad \text{.....(7)}$$

and when $\rho << a$, the equation reduces to,

$$\sigma_t = 2\sigma\sqrt{a/\rho} \qquad \text{.....(8)}$$

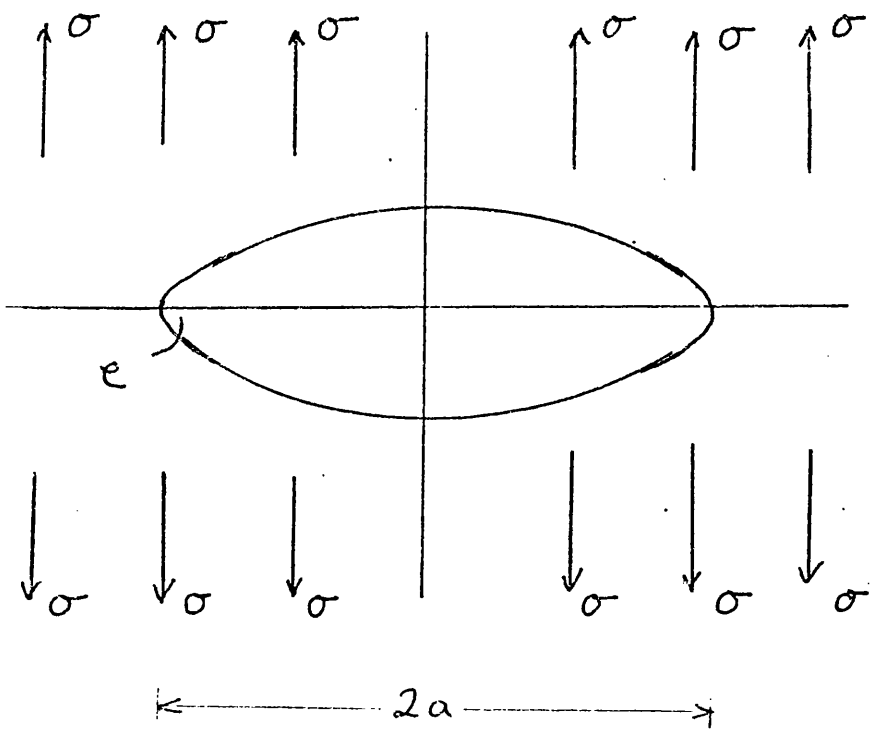

In equations (5) and (8) we have two expressions derived by elastic stress analysis for the stresses close to the tip of a crack. There is no reason from the point of view of the analysis why r and ρ should not be allowed to approach zero, it already having been mentioned that the analysis assumes the body is a continuum. In real materials however it is obviously unreasonable to assume the analysis will hold down to molecular dimensions when any resemblance to a countinuum structure has disappeared. This limitation restricts the increase in localised stress to, at the very most, a figure representative of the interatomic bond strength.

2.6.1.2. Stress Intensity Factor K Before considering an alternative thermodynamic approach by Griffith 1921, it is convenient to introduce the concept of 'stress intensity'.

If a function K_1 is chosen so that $K_1 = \sigma\sqrt{\pi a}$ and substituted in equation(5)

$$\sigma_{11} = \sigma\sqrt{\frac{a}{2r}} = \frac{K_1}{\sqrt{2\pi r}} \qquad \ldots\ldots\ldots(9)$$

K_1 is then known as the 'Stress Intensity Factor' for the opening mode of stress and combines the applied stress and the geometry of the system into a single parameter for points close to the crack tip. (Equation 5 is an approximation dependent on $r \ll a$). Put in another way for emphasis, K is a parameter that characterises the stress at a point just ahead of the crack tip.

K_1 is chosen to be $\sigma\sqrt{\pi a}$ for a crack in an infinite plate, in the case of an edge crack of length 'a' in semi-infinite plate, K_1 is found to be $1.12\sigma\sqrt{\pi a}$ so again $\sigma_{11} = \frac{K_1}{\sqrt{2\pi r}}$

There is sometimes confusion as to whether or not K_1 is always by definition $\sigma\sqrt{\pi a}$ and a separate correction factor (1.12 in the case of an edge crack) should be applied to allow for different geometries. In this thesis, K_1 will be defined to include any correction factor necessary to obtain the $\frac{1}{\sqrt{2\pi r}}$ dependency and thus K_1 is a direct measure of the stress amplification.

Stress analysis functions have now been evaluated by numerical methods on computers to provide K calibrations for a number of configurations suitable for use as

tensile test pieces. These calibrations allow the critical stress intensity factor K_{1c} (or fracture toughness (the K_1 value at fracture) for brittle materials to be measured in terms of the applied stress and the geometry of the system. Providing the boundary conditions are met, the measured value of K_{1c} will not be dependent on the extraneous factors affecting σ_F. In essence, this is possible because the test piece for the K_{1c} measurement contains a deliberate, large and measureable crack which swamps any incipient cracks elsewhere in the material. As defined K is not dimensionless and has the units $MNm^{-3/2}$, occasionally quoted $Pm^{\frac{1}{2}}$.

2.6.2. Energetic or Thermodynamic Approach

For the reasoning behind this approach it is unlikely that Griffith's own words in his 1921 paper can be bettered.

'The fundamental conception of the new theory is this. Just as in a liquid, so in a solid the bounding surfaces possess a surface tension which implies the existence of a corresponding amount of potential energy. If owing to the action of a stress a crack is formed or a pre-existing crack is caused to extend, therefore, a quantity of energy proportional to the area of the new surface must be added, and the condition that this shall be possible is that such addition of energy shall take place without any increase in the total potential energy of the system. This means that the increases of potential energy due to the surface tension of the crack

must be balanced by the decrease in the potential of the strain energy and the applied forces.'

The advantage of the approach is that by considering the energy changes in the body as whole, a useful formula for the fracture stress can be obtained without a detailed understanding of the stresses in the immediate vicinity of the crack tip. However, this advantage is not without its drawbacks which Griffith, if not all his successors, fully appreciated. The requirement that the system as a whole shall contain sufficient energy to provide for the energy intake of the new surfaces formed, is a necessary condition for crack propagation. It is not the only condition. A further condition requires that the stress at the crack tip is sufficiently high to cause rupture of the material, and, by its very concept, the thermodynamic approach does not provide a measure of this stress. It is thus possible to have a situation in which from thermodynamic considerations, there is adequate strain energy in the system for crack propagation, but in which from stress analysis considerations, none of the cracks are sufficiently sharp (ie ρ in equation (8) sufficiently small) to raise the stress high enough for fracture to occur.

Griffith approached the calculation for the fracture stress σ_F by considering the energy requirements to extend an existing crack in an infinite plate by an infinitesimal amount. He argues that for such an extension, the new crack would be essentially similar to the old. The energy change involved would be the conversion of potential or strain energy in the system

into the thermodynamic surface energy associated with the new surfaces. This he obtained by integrating the stress-strain product over the whole plate. He obtained two equations for the fracture stress (Griffith 1924)

$$\sigma_F = \sqrt{\frac{2E\gamma_t}{\pi(1-\nu^2)a}} \qquad \text{in plane strain} \quad \ldots(10)$$

$$\sigma_F = \sqrt{\frac{2E\gamma_t}{\pi a}} \qquad \text{in plane stress} \quad \ldots(11)$$

where E is Young's Modulus

ν is Poisson's Ratio

and γ_t is the thermodynamic surface energy per unit extension.

2.6.2.1. Strain Energy Release Rate G. With the introduction of surface energies, their connection with a function known as the 'strain energy release rate' can be considered.

γ_t, the thermodynamic surface energy used in the Griffith equation (10) and (11) is the energy associated with the formation of unit area of new surface. Thus to extend unit width of crack by a length δa, the work done δU is given by,

$$\delta U = 2\gamma_t \delta a \quad \text{(two surfaces are formed)}$$

The rate at which strain or potential energy is released from the system to extend the crack is given by

$$\frac{\delta U}{\delta a} = 2\gamma_t \equiv G$$

The strain energy release rate defined in this way is strictly G_t and like γ_t is concerned only with fully reversible thermodynamis energy changes. It is however not usual to apply the suffix 't', but the point

will be considered in more detail later* when the significance of G as a material parameter is explored.

2.6.3. Stress Intensity Approach - essentially a combination of the other two. Originally suggested by Irwin 1958, the details of the approach are as follows - Knott p106-109

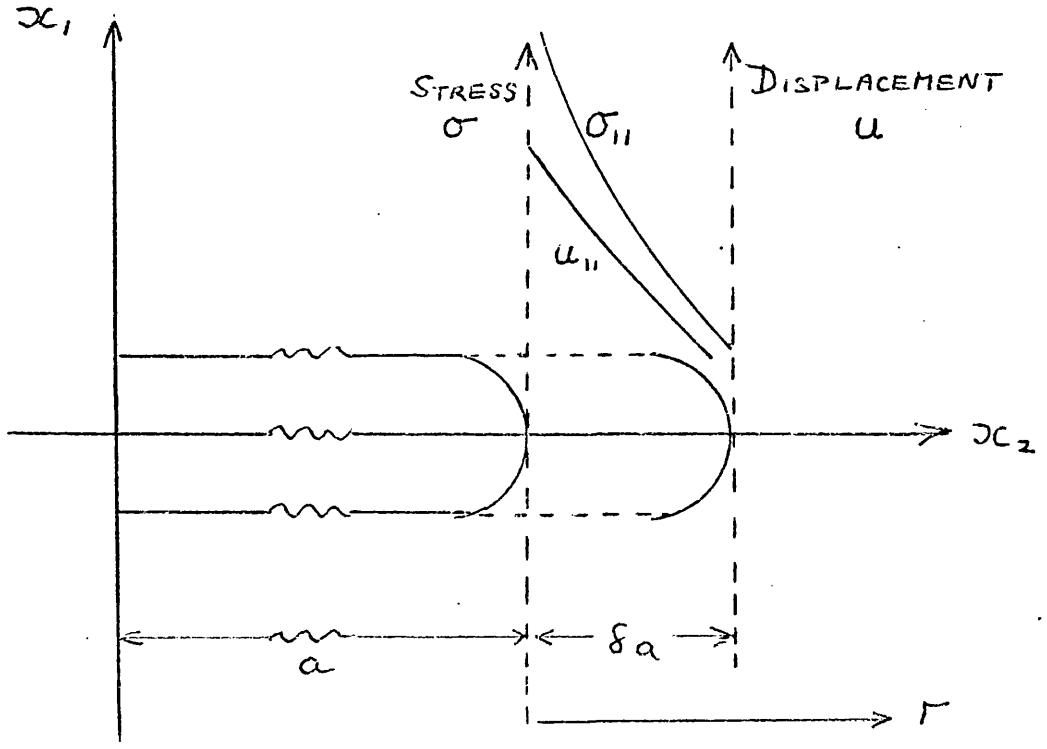

The diagram shows a crack extended by an amount δa which is sufficiently large compared with molecular dimensions to allow the laws of elastic stress analysis to apply. Then from equation (6),

$$u_{11} = \frac{2(1-\nu^2)\sigma}{E} \cdot \sqrt{a^2 - x_2^2}$$

and putting $r = (x_2 - a)$ and neglecting terms in δa^2 and r^2 gives,

*p. 128

$$u_{11} = \frac{2(1-\nu^2)\sigma}{E}\sqrt{2a(\delta a - r)}$$

and from equation (5)

$$\sigma_{11} = \sigma\sqrt{\frac{a}{2r}}$$

The virtual work principle may be applied to determine the work done by the surface forces acting along the length δa if the crack were closed from length $(a+\delta a)$ to length a. The energy change is then expressed as;

$$G\,\delta a = \int_0^{\delta a} \sigma_{11}\, u_{11}\, dr$$

$$= 2(1-\nu^2)\frac{\sigma^2 a}{E}\int_0^{\delta a}\left(\frac{\delta a - r}{r}\right)^{1/2} dr$$

making the substitution $r = \delta a \sin^2\omega$ the integral gives,

$$G\,\delta a = \frac{\sigma^2 \pi a}{E}(1-\nu^2)\,\delta a$$

and substituting $K_1 = \sigma\sqrt{\pi a}$

$$G = \frac{K_1^2}{E}(1-\nu^2) \quad \ldots\ldots \text{ in plane strain} \quad (12)$$

starting with the plane stress equation for U_{11}

$$G = \frac{K_1^2}{E} \quad \ldots\ldots \text{ in plane stress} \quad (13)$$

The expressions for G have been written in terms of K_1, the opening mode of stress which is used in this thesis. The equations are however general and K_1 may be replaced by K which includes components of other modes.

As with the Griffith approach, no suggestion has been made in the derivation of the formula that crack propagation will occur. The value of formula is, that if fracture occurs, they give a measure of the energy absorption in terms of K_1 and E, both of which are measureable quantities.

The formula do, of course, reduce to the Griffith expressions, equations (10) and (11), if $2\gamma_t$ is substituted for G and $\sigma_F\sqrt{\pi a}$ for K_1.

2.7. Modification of Theory by Early Experimental Work.

Three different theoretical approaches to the problems of calculating the fracture stresses and the energy needs for fracture in a body have been examined. They all assume the body is a continuum and fully elastic. It now becomes an experimental requirement to investigate the relevance of the formula to real materials and to determine the limitations or changes nesessary in their use.

When crack propagation occurred in brittle materials, it was known from the work of Griffith that an equation of the following form,

$$\sigma_F = \sqrt{\frac{2E.\ Const.}{\pi a}} \qquad \ldots\ldots\ldots(14)$$

could be applied and that the constant was comparable to γ_t. In other less brittle materials a similar form of equation has been found to apply but the constant is very much larger than γ_t. Irwin 1948, Orowan 1950. Irwin and Kies 1954.

This raises again the concept of brittleness and before looking further at the experimental work it is necessary to give a definition of brittle fracture.

2.7.1. Brittle Fracture can be defined as follows,

1) At the commencement of fracture, the crack propagation is unstable. This is similar to saying the failure is catastrophic but recognises the possibility that there may not be sufficient energy available to cause the complete failure of the structure.

2) The applied stress at fracture must be less than the general yield stress of the material. This implies the existence of a crack or other stress raiser in the material.

It will be seen later that a crack can form and extend in a yielding or ductile fashion until a critical length is reached, at which it becomes unstable and the crack takes on the characteristic of brittle fracture. This critical length necessary for fracture may well be considered as a criterion of the 'brittleness' of the material. It can vary from say a few microns in silicon nitride, to a few hundred microns in clay bodied ceramics to as much as a metre in a mild steel plate - (small mild steel test pieces show ductile failures).

2.7.2. Surface Energies Returing to equation (14)

$$\sigma_F = \sqrt{\frac{2E\ Const.}{\pi a}}$$

this was re-written by Orowan and Irwin in the form

$$\sigma_F = \sqrt{\frac{E(2\gamma_E + \gamma_P)}{\pi a}} \qquad \text{.....(15)}$$

where γ_P takes account of all the other energy absorbing processes such as plastic flow at the crack tip, heat

and noise generation and mechanical friction. In other words, it is being said on experimental grounds that fracture will occur if one chooses the correct surface energy term for the initiation of fracture. Once fracture has commenced, the conditions at the crack tip will have altered and the surface energy term associated with the continuance of crack propagation will be different.

Two further surface energies can be defined and are usually referred to as γ_i and γ_f

1) γ_i is the surface energy for the initiation of fracture and in terms of equation (15) $2\gamma_i \equiv 2\gamma_e + \gamma_p$

2) γ_F is the surface energy associated with the complete work of fracture of the material.

If on experimental grounds equation (15) can now be taken to describe the critical situation at which unstable crack propagation just commences, the stress intensity factor measured in that situation would be K CRITICAL or for the opening mode used in this thesis K_{Ic}. However unless $\gamma_p << \gamma_e$, in which case the equation reverts to the theoretical form, the values obtained for K_{Ic} are unlikely to be consistent. The methods developed in recent years for measuring K_{Ic} (one of which is discussed later), are specifically designed to ensure that the size of any plastic zone at the crack tip is small in relation to the crack length. When the test criteria have been met, consistent K_{Ic} values can be obtained and such measurements are known as valid K_{Ic} determinations.

If a consistent value of K_{1c} and of E can be obtained for a material, it is reasonable to look again at equations (12) and (13) rewriting (13) for example as

$$G_{1c} = \frac{K_{1c}^2}{E}$$

where $G_{1c} = 2\gamma_i \equiv (2\gamma_t + \gamma_p)$

There is no theoretical basis for this step but it is intended to show later* that for clay bodied ceramics under certain conditions, it is a permissible step.

Substituting K_{1c}^2 for $E(2\gamma_t + \gamma_p)$ in equation (15)

$$\sigma_F = \sqrt{\frac{K_{1c}^2}{\pi a}}$$

or, for the more general case applicable to different crack geometries

$$\sigma_F = \frac{1}{Y}\sqrt{\frac{K_{1c}^2}{C}} = \frac{1}{Y}\sqrt{\frac{2E\gamma_i}{C}} \quad .....(16)$$

where C is the crack length

and Y is a geometrical constant.

In the case of an edge crack in a semi-infinite sheet $K_1 = 1.12\,\sigma\sqrt{\pi C}$ which gives $Y = 1.98$

or $$\sigma_F = \frac{1}{1.98}\sqrt{\frac{K_{1c}^2}{C}} \quad .....(17)$$

In equation (16) we have an empirical equation with apparently obvious connections with a theoretical background. The next section will consider some of the work and ideas that evolved in the years between about 1950 - 1970 and this will be followed by a section dealing with more recent ideas.

*p. 133

2.8. Developments during 1950 - 1970 - Grain size and Porosity.

If one considers a generalised form of Griffith equation $\sigma_F = \frac{1}{Y}\sqrt{\frac{2E\gamma_i}{c}}$ it is reasonable to assume for a uniform material that E and γ_i will be constant and that the equation can be reduced to $\sigma_F = K c^{-1/2}$, where K is some constant of the material and the geometry, the actual value of which will depend on the units used. A number of works have endeavoured to determine the significance of C - assumed to be the Griffith crack dimension, in relation to a physical parameter of the material.

In 1949, Orowan suggested that for a brittle polycrystalline metal, C is equal to the Mean grain diameter D

i.e. $\sigma_F = KD^{-\frac{1}{2}}$ .....(18)

He made the assumption that the fracture originated at some flaw within a grain and propagated through it to the grain boundary. The grain boundary acted as an energy barrier to further crack extension and fracture ceased until the applied stress had reached a value capable of crossing the barrier into the next grain. At this point, the stress would be in excess of that required to fracture the second grain and crack growth would continue, usually in a catastrophic fashion. The grain diameter thus represented the Griffith crack dimension.

A modification to Orowan's equation was suggested by Petch 1953 in which allowance was made for possible

yielding of the material prior to fracture.

$$\sigma_F = \sigma_Y + KD^{-\frac{1}{2}} \quad \ldots\ldots\ldots\ldots\ldots\ldots(19)$$

The generality of the Orowan and the Petch equations was later examined by Knudsen 1959 using data obtained from a literature survey. He found that two out of the five sets of results available did not conform to the Orowan equation, but that all conformed to the Petch equation. However, it was also found that the results could all be represented by an equation of the form

$$\sigma_F = KD^{-a} \quad \ldots\ldots\ldots\ldots\ldots\ldots\ldots\ldots(20)$$

where 'a' is a constant with values ranging from 0.2 to 0.9. The implication of this Knudsen argues is that the propagation of a crack across a grain boundary may not be more difficult than the propagation of a crack within a grain. Thus for those cases where 'a' is not equal to 0.5,

1) the strength of a brittle body depends on the size of the flaw or crack at which the fracture originates and 2) the size of these so called Griffith flaws increases with increasing grain size in a manner which can be represented by the formula,

$L = kD^{-2a}$, where L is the Griffith flaw size.

In two major papers Carniglia 1965 and 1966 has reviewed existing published work and drawn a number of conclusions. With regards to the Petch and Orowan equation, he finds that though for large grain sizes the Orowan equation can be applied, for small grain sizes a yield condition exists and the Petch equation is needed. In his second paper dealing with results on MgO, Al_2O_3 and BeO he goes on to conclude that some yielding must always

take place prior to fracture. He points out that although previous workers such as Orowan have obtained mathematically satisfactory fits to the Griffith's equation, they have not been able to make any physical interpretation of the 'critical crack'.

Carniglia finds evidence that minute traces of impurities along grain boundaries are responsible for a considerable drop in the fracture strength of the materials. He considers the observed fracture, behaviour conditioned by these impurities, may be extrinsic to the material as a whole. This finding serves to emphasise the view taken in this thesis that all real materials are polyphase and that it is unreasonable to talk about the fracture behaviour of, say, pure Alumina without accepting the limitation of the word 'pure'.

Carniglia's papers have provoked a number of comments. Rice 1972 does not agree that the strength/grain size curve shows the branching indicative of a change from the Orowan to the Petch relationship. The figure overleaf shows both his and Carniglia's plot of the same data. Rice considers that an error in plotting by Carniglia of the two fine grain size points considerable emphasises the branching of the curve. He also considers that the data used by Carniglia was not the most suitable as the grain sizes were inferred from the firing temperatures rather than measured directly. Earlier data in which grain sizes were measured directly are also plotted and show no signs of branching.

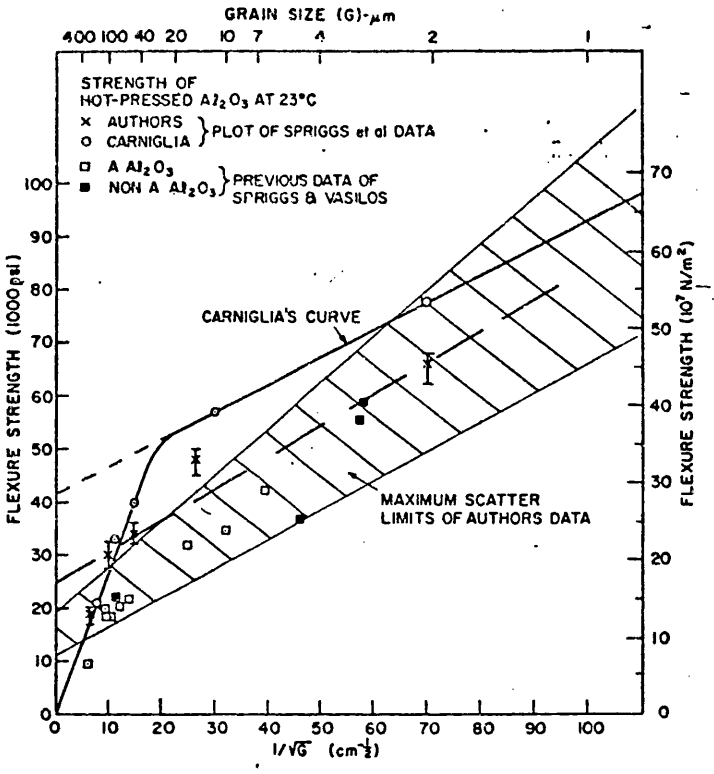

FIGURE 2
Comparison of Carniglia's and the author's analysis of Al_2O_3 flexure-strength at 23°C.

from Rice 1972 Proc Br Ceram Soc 20 p209.

Evans and Tappin 1972 consider the non-linearity of the strength/grain size curve is because there is no direct correlation between grain size and flaw size. They specifically refute any suggestion of plastic flow at the smaller grain sizes in alumina at room temperatures.

The effect of Porosity on σ_F was investigated concurrently with grain size. It is to be expected that pores will act as stress raisers or areas of weakness in the material and thus tend to lower the value of σ_F. However, Davidge 1969 has pointed out, pores in pure polycrystalline ceramics are typically only about $\frac{1}{10}$ of the grain diameter and should have less of an effect. Ryshkewitch 1953 investigated the compression strength of porous sintered alumina and zirconia. He was able to

introduce up to 60% porosity in finely divided pores and his graphs gave a straight line for a log. plot of strength against porosity. Duckworth 1953 commenting on the results showed the data for both the alumina and the zirconia fitted the expression

$$\sigma = \sigma_o e^{-bP}$$

where σ = strength of porous body

σ_o = strength of non porous body

P = porosity expressed as a fraction

and b $\sim$ 7 for both materials.

Cutler 1957 measured the fracture stress σ_F by 4 point bend of sintered aluminas of different compositions and bulk density. He found σ_F varied with bulk density but the relationship was almost linear and he was of the opinion that his pores, much smaller than those introduced artificially by Ryshkewitch may have been the cause of the difference. He was not able to assess the interaction of different grain sizes in the alumina. In the same paper in which he discussed grain size Knudsen considered the argument that porosity by reducing the load bearing area, reduced the strength. He was able to show theoretically that for idealised cubic and rhombohedral specimens with up to 10% porosity, an expression of the form $\sigma = \sigma_o e^{-bP}$ would be expected to apply and 'b' would lie between 6 and 9. An analysis of published work on steel and aluminas showed good qualitative agreement. Knudsen therefore proposed a single equation to combine both the effects of grain size and porosity.

$$\sigma_F = KD^{-a}e^{-bP} \quad \ldots\ldots\ldots\ldots\ldots\ldots\ldots\ldots(21)$$

Experimental work he carried out on Thoria fired at different temperatures, and fractured at temperatures up to 1000°C, showed the formula was accurate to within about 10%.

In a major paper, Passmore, Spriggs and Vasilos 1962 published work on alumina aimed at distinguishing between the effects of grain size and porosity on strength. They considered a relationship of the Knudsen type could be fortuitous because decreasing porosity with increasing grain size is a normal processing effect. They worked initially within the range 3% to 6% porosity and measured the fracture stress at 25°C and 1200°C - even at this temperature they saw no evidence of plastic deformation. With a formula of the form $\sigma_F = KD^{-a}$, 'a' varied from 0.5 to 0.4 for 3% and 6% porosity respectively. This is thought to reflect a reduced grain size dependency for the more porous alumina. For the effect of porosity on strength, the porosity range was extended down to 0.2% and the following relationship wer found.

at 25°C $\quad \sigma_F = 142{,}500\ G^{(-0.60 + 3.33P)} . e^{-11.83P}$

at 1250°C $\quad \sigma_F = 73{,}000\ G^{(-0.60 + 3.33P)} . e^{-11.33P}$

Confirmation was thus obtained of an interaction between grain size and porosity.

A theoretical treatment carried out based on surface energy consideration gave good agreement with the experimental results and supported a Griffith type of crack propagation. But it appeared that unknown factors associated with fracture mechanics, may have given rise to above average strengths at large grain size and high porosity, and in this case, the critical crack size may not

be controlled by a simple Griffith mechanism with a constant initiation energy γ_i.

Most of the published work concerns pure polycrystalline materials but Dinsdale and Wilkinson 1966 investigated the effect of porosity on the strength of earthenware and whiteware bodies. They found a figure of 3.9. for b with an equation $\sigma_F = 17,700\ e^{-3.9P}$ They also draw attention to the work of Lundin1959 in which he recorded that crystals of increasing grain size (in this case mullite) formed in situ,behaved differently to large grains added to the starting material. This comment appears to have gone unnoticed but the present work confirms it.

2.9. Developments since 1970 - Crack shape and Flaw Linking.

Some of the papers written towards the end of the 1960's were clearly indicating the unsatisfactory nature of the Knudsen type analysis, in that, it bore no direct connection to the structure of the material concerned and was very much in the nature of a curve fitting exercise. This is not to say it had no value, it showed,albeit for reasons not clearly understood, that a careful choice of grain size and a minimum of porosity would yield higher strength materials.

It was also becoming apparent that small traces of impurities would lodge in the grain boundaries and cause a disporportionately large drop in strength. Very high purity materials or possibly neutron radiated materials-

Sambell and Bradley 1963, were considered a possible way to obtain maximum strength from materials such as polycrystalline alumina and magnesia. Excepting for a few specialised uses, this seems to be very much a case of diminishing returns and out of the question for the vast bulk of ceramic materials. Indeed, it seems to emphasise the point that all polycrystalline materials are polyphase and one might hope that the effects observed in the relatively pure materials will be similar in type, if not in scale to those observed in the intentionally polyphase materials.

2.9.1. Modulus of Elasticity E No mention has yet been made of the effects of grain size or porosity on E. Since it is a material parameter and used in the determination of the surface energy γ_i, this omission should be rectified. Unlike the fracture stress, the elastic modulus is not concerned with the ultimate strength or fracture of a material. Ideally a measurement of E involves no change in the test material with no rupture of any bonds or inelastic straining.

(note.- Noise measurements usually indicate some material damage and this is the case for this work on clay ceramics)

It is not surprising, therefore to find that E is affected rather differently to σ_f by changes in the grain size and pore size. Bailey and Hill 1970 found that the elatic modulus was insensitive to the grain size, but that it varied markedly with the proportion of the different phases present and with the porosity. An equation of

the form $E = E_o e^{-bP}$ fitted the results where P is apparently the porosity. The same finding is mentioned in a review paper by Davidge and Evans 1970 and by Penty, Hasselman and Spriggs 1972.

The results on two aluminas with porosities of 0.2% and 1.5% studied by Swanson 1972 do not however appear to agree. The differences in findings are probably related to pore shape and distribution. Rossi 1968 in a paper on the prediction of the elastic moduli of composites, considers the effect of the shape of the included phase as well as the elastic moduli of the individual phases. In the case where the included phase is porosity, for a composite with a Poisson's ratio of 0.2 and containing pores described as orientated spheroids he quotes,

$$E = E_o \left(1 - \left(\frac{5a}{4c} + \frac{3}{4}\right)P\right)$$ where 'c' is the length of the unique axis parallel to the stress vector and 'a' is the length of the axis in the perpendicular plane. Thus when $c \gg a$, $E \simeq E_o\left(1 - \frac{3}{4}P\right)$ and the effect of the porosity is a minimum. This corresponds to tubular shaped cavities lying in the direction of the stress.

Rice 1975 extends this analysis and points out that even with a knowledge of the pore shape, the average porosity is not a satisfactory measure. Inhomogeneity of pore size or spacing will give rise to variations in the measured elastic properties, excepting for the case of tubular or laminar pores orientated in line with the direction of stress. Here Rossi's equation shows E to be dependent only on the volume of the pores.

2.9.2. Surface Energy Meaurements - the Equivalent Elastic Crack C_E

A group of workers, Evans, Davidge et al have concentrated on surface energy type measurements rather than on fracture stress. The surface energy it will be remembered is much more a material parameter than is the fracture stress. The approach has generally been to determine K_{Ic} by means of a notched bar test in 3 or 4 point bending and relate this to γ_i by the expression $K_{Ic}^2 = 2E\gamma_i$. Davidge and Tappin 1970 introduce a method for determining the Griffth flaw size or the Equivalent Elastic Crack C_E. A measurement of σ_F was made using unnotched bars and a further measurement using notched bars gave K_{Ic}. When for a semi-infinite sheet from equation (17)

$$\sigma_F = \frac{1}{1.98}\sqrt{\frac{K_{Ic}^2}{C_E}}$$

or for a test bar quoted by Davidge and Tappin

$$\sigma_F = \frac{1}{1.92}\sqrt{\frac{K_{Ic}^2}{C_E}} \qquad \text{.....(22)}$$

where C_E is the depth of a sharp surface crack, which on the Griffith theory would have initiated the fracture. It should be noted that in isolation, there are no grounds for saying such a crack ever existed prior to fracture. For instance, the fracture may have originated at a much deeper but blunt crack or from some flaw below the surface. Nevertheless, the approach has been used extensively in this thesis and the variations in C_E have been measured for a number of different materials.

Clarke, Tattersall and Tappin (1966) proposed a toughness parameter related to E and γ_F the work of

fracture which need not concern us, but in the course of their work theyshowed that γ_F for polycrystalline magnesia had a maximum with the grain size in the range 7 - 100μm. Evans and Davidge 1969 found that for γ_i however, there did not appear to be a maximum related to the grain size. They did observe that for shallow notches γ_i was related to the notch depth.

γ_i = 4-6 Jm^{-2} for notches $\sim$ 2 grain diameters.

γ_i = 14 Jm^{-2} for notches $>$ 10 grain diameters.

Flaw linking.

An investigation of the effect of the grain size on the appearance of the fracture surface was carried out by Evans and Tappin. Aluminas made with three different grain sizes were used in γ_i measurements and the fractured surface examined with the following findings.

1) Fine grain alumina ($\sim$3μm) gave a number of relatively large pull outs about 40μm deep and 40μm diameter. In the region from which the fracture was initiated, there was at least one pair of flaws between 10 and 25μm apart.

2) Coarse grain alumina ($\sim$100μ) gave a surface in which it was difficult to detect the point of initiation, but examination prior to fracture showed a high density of surface cracks but with none larger than the grain size

3) Intermediate grain size ($\sim$30μ) gave a small number of pull outs larger than the grain size ($\sim$90μm deep) and a high density of grain sized pull outs.

It thus appears that in structures where there are no

large flaws present, the linking together of smaller flaws occurs prior to failure of the material. This view has been increasingly substantiated since by a number of authors.

Glucklich 1970 considered in detail the implication of the weak link theory - the Weibull analysis approach mentioned in connection with the 4 point bend rig. He points out that if a single flaw is present, the size of the test piece will have no effect on the stress at which fracture will occur. i.e. $G = \left(\frac{c\sigma^2}{E}\right)$ and is independent of the test pieces dimension.

With a population of crack nuclei however, the specimen size will affect the stress at which the first crack will begin to grow - on a statistical basis, the larger the sample the greater the likelihood of a deep crack. But this applies to the initiation of fracture and not to total fracture. Total fracture follows a period of crack growth to which flaw statistics do not apply. He quotes the case of concrete in which cracking commences at 30% of the ultimate failure load.

Meredith and Pratt 1974 chose three grades of alumina with different grain sizes and set out first to establish that fracture toughness (K_{Ic}) measurements made using test pieces of different shapes gave the same result. The shapes chosen, for which accepted K calibrations are available, were Single Edged Notch Bend, Compact Tension and Double Cantilever Beam. They found agreement on the K_{Ic} values within 5%. Fracture samples which were broken by 3 point bend testing were examined to determine the point of origin of the fracture.

In the three cases reported, the origin proved to be a collection of flaws which linked prior to the final failure of the test piece. Using the measured values of K_{Ic} and theoretical stress analysis on the geometry of the particular flaws, the ultimate failure stress was predicted to within 10% of that actually measured. Meredith and Pratt considered the agreement suggested that the measurements of K_{Ic} in their work were acceptably accurate.

Two points emerged in the discussion on the paper. Firstly the samples with 'atomically sharp' cracks gave consistent values for K_{Ic}, whilst sawn notches did not. This is contrary to the findings of Davidge and Evans 1968 who found a sawn notch in alumina was equivalent to within 5% of an 'atomically sharp' crack. Meredith and Pratt suggested that perhaps they were sawing their own notches too carefully.

It must also be presumed that the flaw density in alumina was insufficient for there to be a high probability of a starting flaw at the base of a smoothly sawn notch.

Secondly, only in one case, which was studied in detail, was a single inherent defect comparable to the critical crack size observed. In all other cases flaw linking was necessary.

Kirchener, Gruver and Sotter 1976 fractured specimens of alumina, silicon nitride and silicon carbide in a four point bend rig at different temperatures and loading rates. They were able to identify four different types of flaw responsible for fracture, the proportion of each type varied significantly with the type of material and thus

indicated a material characteristic. Their sample sizes were not large enough to detect variations in fracture type due to loading rates or to temperature.

The four types of fracture were classified as 1) large crystal, 2) pore 3) stepped flaw found close to the surface and subject to flaw linking, 4) penetration flaw or deep cracks extending from the surface and due to surface damage.

Theoretical calculations of the fracture stress from K_{Ic} determinations, when related to the measured values were in good agreement for fracture from large crystals and fracture from pores, providing sub critical crack growth was assumed. Less agreement was obtained in the cases of stepped flaws and penetration flaws for which some possible reasons were offered.

2.9.3. Critical Strain ϵ_c The discussion so far has dealt with the stress but not the strain at which a brittle material fractures. This strain designated the 'critical' strain was considered by Astbury 1966. He pointed out that the stress at fracture could range from a few thousand p.s.i. to a few hundred thousand p.s.i. a range of more than 100:1. The strain at fracture however always lay around the region 10^{-3} or 1 millistrain, the variation being perhaps from 0.5 to 2 millistrains. This feature applied to any brittle material so far measured whether it was silicon nitride, earthenware or salt, Stokes 1966. No explanation was offered for this phenomonen and there still does not seem to have been a published reason.

In the same paper Astbury considered the question of creep in a ceramic by means of a visco elastic model in which he proposed a brittle phase of elastic particles embedded in a highly viscous phase. If an external stress is applied, it will initially be born by the material as a whole, the viscous phase however will creep and relax, raising the stress concentration in strain in the elastic phase possibly leading to delayed fracture. The paper concludes that the model which bears some resemblance to a conventional ceramic (brittle particles in glass) does not adequately describe all the effects observed in real materials.

The allied question of crack velocity in relation to the observed fracture stress was considered by Shand1961, who showed that whilst in air the fracture stress of glass varied with the crack tip velocity, this did not apply in vacuum over the range $10^{-2}\mu m$/sec to $10^{4}\mu m$/sec. It must be concluded some form of stress corrosion takes place in air. The effect has usually been ignored by most workers in ceramics and cross head speeds in a tensile machine of 0.1, to 0.5 mm/sec give rise to rapid crack velocities and are generally accepted as suitable for bend testing.

2.10. Three Point Bend Tensile Testing.

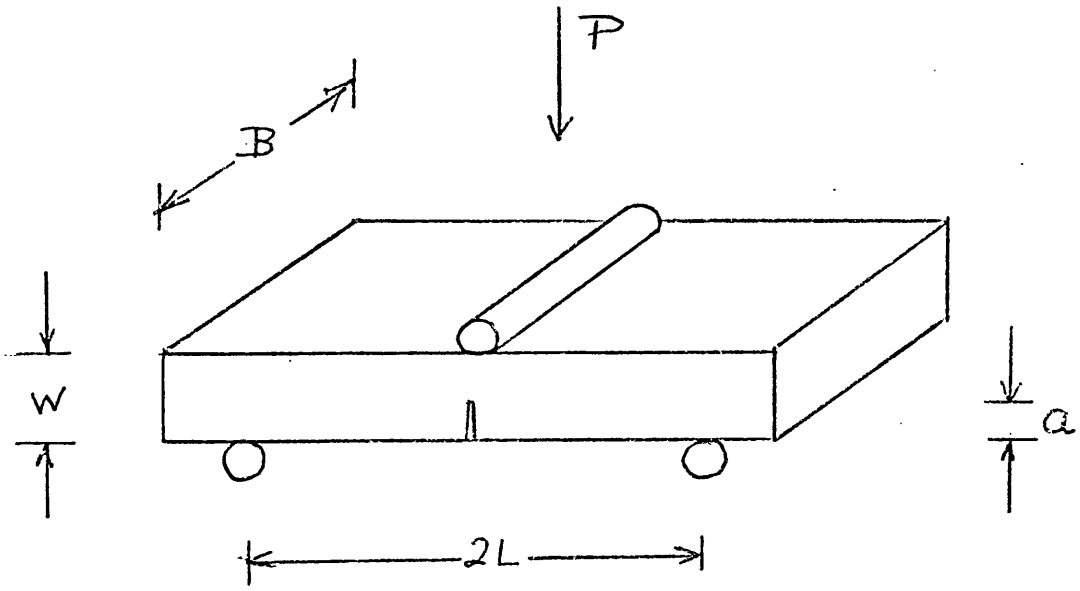

The standard tensile test of gripping the ends of a test piece in a pair of jaws and pulling is not satisfactory with brittle materials such as ceramics. Unless very considerable care is taken in the alignment of the test piece, it tends to break close to the jaws due to localised stresses not representative of the over all stress. This problem in overcome by bend testing in either 3 point or 4 point bend testing rigs.

The 4 point rig has the advantage that the applied stress, a maximum on the surface, is essentially constant over the length between the two inner supports. Whereas the stress in the 3 point rig is a maximum on the surface immediately opposite the single central support, falling lineally to zero at the end supports. Thus a greater area of uniform stress in obtained in the 4 point rig and if one is looking for the 'worst flaw' there is a greater probability of finding it than on the 3 point rig.

This is in line with the Weibull type statistical analysis according to which large samples should be weaker than small samples due to the greater chance of a really bad flaw causing fracture. -see section 4.1.1 page 90.

Clay bodied ceramics are likely to have two types of flaw. Those due to the intrinsic nature of the material which are expected to be numerous, and those due to manufacturing faults which are larger but hopefully much fewer in number. Under these circumstances, there is an advantage to limiting the area of maximum stress with a view to reducing those occassions on which a manufacturing flaw is responsible for the fracture. On these grounds it was decided to adopt the 3 point bend test rig.

The sketch at the beginning of this section details the relevant dimensions. For σ_F and E, the test pieces do not contain the slit of depth 'a' which is required for the K_{Ic} measurements.

2.10.1. Fracture Stress σ_F and Elastic Modulus E

The formula for the Fracture Stress σ_F and the Modulus of Elasticity E are well known.

$$\sigma_F = \frac{3PL}{BW^2} \quad \text{in } MNm^{-2} \qquad \ldots\ldots\ldots\ldots(23)$$

$$E = \frac{2L^3}{BW^3} \times (\text{Slope of the Stress-Strain curve}) \quad \text{in } GNm^{-2} \qquad \ldots\ldots\ldots\ldots(24)$$

2.10.2. Stress Intensity Factor K_{Ic}

The formula for K_{Ic} is less well known and requires some discussion. As already mentioned K calibrations

are now obtained by numerical method solutions to stress analysis. Previously however, Irwin G.R. and Kies 1954 pioneered a compliance method of obtaining K calibrations. The procedure is to measure and plot the compliance C of the test piece for a number of different crack lengths 'a'. The value of K being given by the formula

$$K_1 = P\left(\frac{\partial C}{\partial a} \cdot \frac{E}{2B}\right)^{\frac{1}{2}}$$

where P is the applied load at crack depth 'a'

The advantage of compliance methods is that they give a direct measurement of K for the shape of the test piece concerned. Whilst they have obvious limitations in the size and shape of the testpieces to which they can be applied, they provide a necessary check on the accuracy of computed K calibrations.

The requirement to provide engineers with reliable and relevant information on the toughness of materials (steels in particular) has been the driving force behind the evaluation and application of K calibrations. Brown and Srawley J.E. 1965 and 1966 under the sponsorship of the American Society for Testing Materials have produced a number of K calibrations for differently shaped test pieces. The calibrations have been refined and checked experimentally and the currently accepted calibration for the 3 point bend configuration - referred to as the 'Single-edge-notched'(S.E.N.) is given in S.T.P. 410. This calibration is also now embodied in the British Standard (BS. 5447:1977.) and given overleaf.

$$K_1 = \frac{3PL}{BW^2}\left[1.93\left(\frac{a}{W}\right)^{\frac{1}{2}} - 3.07\left(\frac{a}{W}\right)^{3/2} + 14.53\left(\frac{a}{W}\right)^{5/2} - 25.11\left(\frac{a}{W}\right)^{7/2} + 25.80\left(\frac{a}{W}\right)^{9/2}\right] \quad \text{.....(25)}$$

where $0.4 \leqslant \frac{a}{W} \leqslant 0.6$

As would be expected substituting $\sigma = \frac{3PL}{BW^2}$, the formula reduces to $K_1 = \sigma \sqrt{a}\, F\left(\frac{a}{W}\right)$.

The stress intensity analysis for the K calibration is 2 dimensional and it was the usual practice to adjust this more closely to fit the actual 3 dimensional test by multiplying by $(1 - \nu^2)^{-\frac{1}{2}}$ where ν is Poisson's ratio. This practice was followed in the earlier STP 381 but has currently been dropped on two grounds

1) it is considered the correct factor may be less than $(1 - \nu^2)^{-\frac{1}{2}}$

2) if ν is taken as say 0.3, the correction is less than 5% and from the point of view of the engineer is on the safe side.

The use of the formula involves some limitations on the specimen dimensions. The requirement that $0.4 \leqslant \frac{a}{W} \leqslant 0.6$ is general to all materials and follows from the constraints of the stress analysis. Three other limitations involve choosing a test piece sufficiently large to ensure that failure is by brittle fracture and not by general yielding. When the failure of the test piece is abrupt,- as in the case of the ceramics

used in this thesis, the view taken in STP 410 is that the conditions will have been met. Evenso, it is worth looking at the nature of the limitations and checking the validity of the test pieces used.

1) The crack length 'a' must be large compared with the radius ρ of the plastic zone at the crack tip and an arbitrary figure of $0.02\,a > \rho$ is assumed. For SEN specimens this causes and over estimation of K_1 of 6%.

2) The width W or more exactly the width of the ligament (W - a) below the crack tip must also be large compared to the size of the plastic zone to permit the development of the stress field. If it is assumed W = 2a (the centre of the region $0.4 \leq \frac{a}{W} \leq 0.6$) and if $0.02\,a > \rho$, then the error involved in K_1 is found to be less than 0.5%.

3) The thickness B must be sufficient to ensure conditions of plane strain operate at the crack tip. From experimental results on metals, it is found that B should be $\geqslant 2.5 \left(\frac{K_{1c}}{\sigma_y}\right)^2$. In terms of the plastic zone this gives $B \geqslant 47\rho$ or approximately equal to 'a'. (For comparison in the case of ceramics if one substitutes the equivalent elastic crack C_E for ρ, equation (22) gives $B \geqslant 9.3 C_E$)

Combining conditions (1), (2) and (3) together gives,

$$B \geqslant a = (W-a) \geqslant 2.5 \left(\frac{K_{1c}}{\sigma_y}\right)^2$$

For the clay based ceramics used in this thesis, inserting typical values gives,

$$B = 12 \geqslant a = (W-a) = 6 \geqslant 2.5 \frac{K_{1c}^2}{\sigma_F^2} = 2.5$$

For truly brittle materials the claim is made that

the formula calculates K_1 correct to within 1%.

Hartline et al 1973 criticise the formula on the grounds that it appears to be sensitive to the value of $\frac{a}{W}$ although values of $\frac{a}{W}$ as high as 0.8 lie on a correction curve. However, it is not part of this work to investigate the accuracy of K calibrations or the applicability of its transfer from the metal to the ceramic field. It is sufficient that it gives reasonable figures for the value of K_1 and that the figures should be comparable with others obtained in the same way using the same size of test pieces.

2.10.3 Work of Fracture γ_F The work of fracture can be measured by making use of notched test pieces, Davidge and Tappin 1968, Nakayama 1965.

The area under the stress-strain curve when the test piece fractures is a measure of the work done by the tensile test machine.

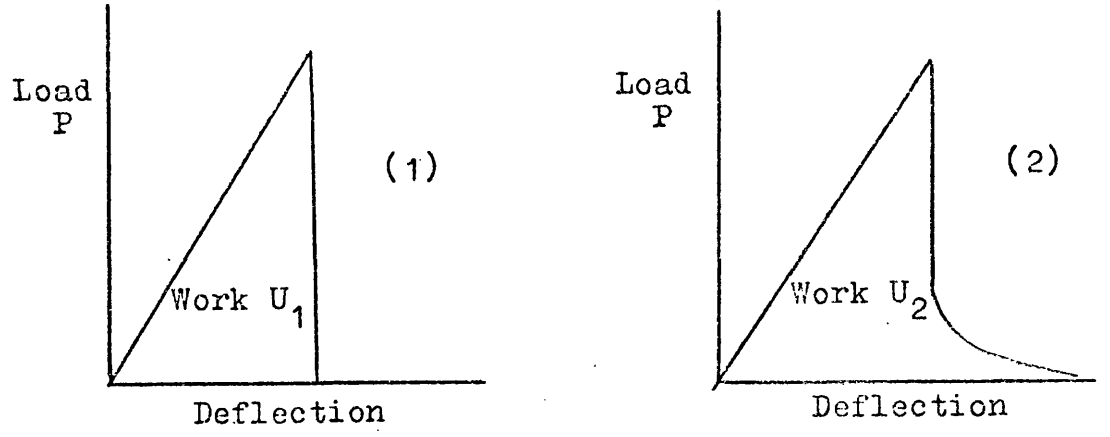

The sketches indicate two modes of fracture for brittle test pieces. In (1) when fracture occurs the stored energy in the system is all released and an unknown

quantity is lost in the form of kinetic energy imparted to the test piece. In (2) the stored energy is not quite sufficient to fracture the sample completely and this is continued in a controlled way by the test machine, allowing the measurement of the energy absorbed by the sample.

Ceramic test pieces designed for the measurement of σ_F always fail in mode (1) as tensile test machines are not stiff enough - i.e. there is too much elastic energy stored in the machine. However if a deep notch is cut in the test piece, it can easily raise the stress at the bottom of the notch by a factor of 10 over the applied stress and under these conditions the stored energy can be less than that required for complete fracture and mode (2) applies.

Whence $$\gamma_F = \frac{U_2}{2B(W-a)} \quad \text{in } Jm^{-2}$$

From work carried out by Coppola and Hasselman 1973 it appears that friction at the knife edge supports (5 thou. radius) of the 3 point bend rig can absorb up to 30% of the energy available at fracture when compared against $\frac{3}{8}$" diameter rods in roller bearings.

Measurement of the work of fracture was not pursued in this thesis. It is considered that although the area under the curve represents the work done by the system to fracture the test piece, the amount that appears on the new and possibly rough surface as surface energy is not determinable. - see virtual surface energy section 5.2 page 128.

2.11. The Source and Firing Reactions of Clay

2.11.1. Sources of Clay Two types of clay are in common use in the pottery industry; China clay or Kaolinite and Ball clay.

Deposits of kaolinite are found in many parts of the world but principally in England, the United States of America, Czechoslovakia and East and West Germany. The clays can be either primary or secondary residual. That is clays which are found at their site of origin are primary residual, those which have been transported in rivers and re-deposited elsewhere are secondary residual. English clays are of the primary residual type.

Kaolinites are of high purity, particularly those found in Devon and Cornwall where the term 'China Clay' is applied. The refined clay consists of lamellar crystals or platelets, sometimes referred to as booklets, of fine particle size. Typically kaolinite particles are of the order of 2 microns. Quality control by the suppliers during the extraction and processing of the clay provides a consistent refined product available in bulk to a carefully controlled specification. The properties of the clay can be tailored to meet the different requirements of industries, diverse as pottery and papermaking.

Deposits of ball clay are more common than of Kaolinite and are always secondary residual. The clays vary in composition but consist basically of differing proportions of kaolinite and silica with other mineral impurities. The particle size is about a factor of ten less than that of kaolinite giving the green or unfired material a higher

modulus of rupture. Unfortunately ball clays cannot be readily refined and their specifications are less controlleable than those of kaolinite.

The reactions of kaolinite and ball clay during firing are broadly similar with those for kaolinite being more fully researched. The chief effect of the impurities, particularly the basic oxides or felspars in commercial clays is to lower their firing temperature and reduce their firing range. This effect is of particular importance to industry allowing the production of pottery at furnace temperatures around 1300°C some 200-300 degrees less than would otherwise be the case.

When fully fired or fluxed, clay ceramics are the most brittle materials in common use. Although views have been expressed on the possibility of plastic flow at the crack tip, there is little evidence for such a view at temperatures under 50% of the absolute melting temperature of the ceramic — Groves 1970, Evans 1970. From the point of view of the work carried out in this thesis kaolinite provides a convenient raw material for the production of fracture test pieces. Also it will be seen that by varying the firing temperature or by the controlled addition of other materials, a series of different brittle structures can be obtained. The particular grade of kaolinite used throughout the work was 'Meledor' china clay and its specification is given in Appendix 1.

2.11.2. Firing Reactions of Clays In its pure form kaolinite is a mineral with the formula $Al_2O_3.2SiO_2.2H_2O$

and thus one is considering the SiO_2 - Al_2O_3 system and the phase diagram is given below.

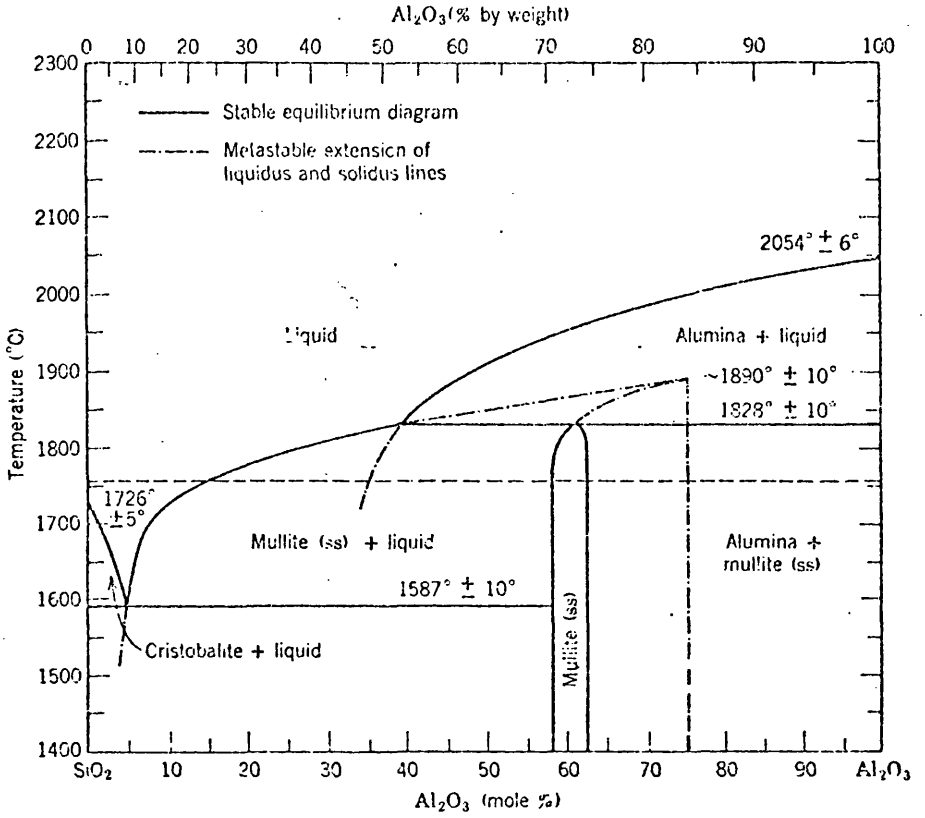

Fig. 7.28. The binary system Al_2O_3-SiO_2. From Aksay and Pask, *Science*, 183, 69 (1974).

from Kingery Bowen and Uhlmann 1976 Introduction to Ceramics. John Wiley and Sons, New York.

The diagram shows that no liquid is produced until about 1587°C although mullite ($3Al_2O_3.2SiO_2$) is formed in solid solution with silica or cristobalite at temperatures below this. Ghote, Hasselman and Spriggs 1973 synthesising high purity mullite from fine grain γ alumina and amorphous silica found that Xray analysis showed the presence of mullite at 1200°C although a minimum of twenty hours firing at 1400°C was needed for the complete reaction. They reported that Lohne and Arbon had observed that spherical or globular aggregates resulted from solid state reactions, but the presence of the slightest trace of any

liquid phases (silica)promoted the characteristic needle formation of mullite.

The phase diagram also shows the proportion of mullite in the final product can be increased by the addition of alumina to the mix until at about 73% alumina, the mix will fire to 100% mullite. This feature has been used to vary the properties of the experimental test pieces.

It has already been mentioned that the presence of impurities in kaolinite reduces its firing temperature and there is still some uncertainty about the chain of reactions leading from kaolinite to mullite. The main reactions are quoted by Hamano and Lee 1972 as,

1) $Al_2O_3 \cdot 2SiO_2 \cdot 2H_2O \longrightarrow Al_2O_3 \cdot 2SiO_2 + 2H_2O$ ca 500°C

2) $2(Al_2O_3 \cdot 2SiO_2) \longrightarrow 2Al_2O_3 \cdot 3SiO_2 + SiO_2$ ca 950° C

3) $3(2Al_2O_3 \cdot 3SiO_2) \longrightarrow 2(3Al_2O_3 \cdot 2SiO_2) + 5SiO_2$ ca 1200°C-1400°C

The overall reaction being

4) $3(Al_2O_3 \cdot 2SiO_2 \cdot 2H_2O) \longrightarrow 3Al_2O_3 \cdot 2SiO_2 + 4SiO_2 + 6H_2O$

The disagreement centres around the exothermic reaction shown by D.T.A. to be taking place in the region 900-1000°C. Richardson and Wilde 1952, Brindley and Nakahira 1959 and others considered the metakaolin first splits to γ alumina and amorphous silica which at a somewhat higher temperature forms mullite with the excess silica converting to the crystalline form cristoballite.

Glass 1954, Roy, Roy and Francis1955, Comer 1960, 1961 and others considered that at least some mullite was formed in the initial reaction and evidence for this was found by X-ray diffraction. More recent work by Percival and Duncan 1974 working with an infra- red spectroscope gave evidence for both views. They found that metakaolin formed by reaction (1) at 500°C gradually decomposed as the temperature was raised into γ alumina and amorphous silica. At 900°C reaction(2) produced poorly formed mullite and probably some spinel. At 1100°C the bulk of the secondary mullite formed and excess silica crystallised out as cristobalite. These findings are in line with the current findings of other workers though a temperature of 1100°C for secondary mullite is lower than usual.

It is generally agreed that mullite formation is observed first by X-ray diffraction spectrography at about 1000°C and that it is not visible in the S.E.M. until a temperature in excess of 1200°C is reached, Rue and Ott 1972, Lach 1972, Hamano and Lee 1973. Lach sees the development of mullite in three stages and for the purpose of this thesis they form a sufficient guide for the understanding of the results obtained during the firing of test pieces.

1) isometric small crystals
2) growth of these crystals } 1000°C
3) well formed mullite $\sim$ 1400°C

Stages (1) and (2) correspond to Primary or Scaly mullite forming in the kaolinite stacks and not visible in the

S.E.M.. Stage 3 is the recrystallisation of secondary mullite from the glassy phase giving the familiar well defined structure of mullite which is clearly visible in the S.E.M. - plates (5) and (8).

Although the secondary mullite recrystallises out of the glass phase, Comer 1960 and Lach maintain its size and orientation is governed by the original size of the kaolinite crystals. This finding has not been confirmed by the observations made in the course of this work and Lundin 1959 suggests that the mullite crystals are random in the kaolinite phase although of a different nature to those orientated in felspar relicts.

The formation of cristobalite over a short range of firing temperature is observed by X-ray diffraction by Lach, Hamano and Lee and others and was confirmed by the author.

The exact temperatures at which reactions take place are obviously dependent on the source and purity of the clay. Sequit and Anderson 1971 report the S.E.M. examination of two clays. In the purer sample they could not observe mullite until a temperature of 1300°C was reached whilst in the less pure material which fluxed at a lower temperature, mullite was observed at 1200°C. This is in line with the finding that a liquid phase is nesessary for the development of well defined mullite crystals. On thermodynamic considerations, Soliman and Hammad 1970 have found mullite to be the most stable product over the whole firing range to 1500°C.

It is not of course the purpose of this thesis to investigate the reactions of kaolinite on firing. The

reactions which have occurred at any given part of the material will be determined by local variations in that part of the mix and by impurities. Thus although the samples for this thesis were fired for 20 hours and allowed to cool slowly, small local variations will exist and these variations will affect the stress field.

3. Experimental Procedures.

3.1 Test Piece Preparation

Clay the starting material for all test pieces is conveniently available as a dry powder. For most of the work a grade known as 'Meledor China Clay' was used and to this was added the necessary other components as required by the formulation being studied. The specification of the clays and other components are gathered together in Appendix 1 and the details of the formulations are given in Appendix 11.

During the course of the work, two separate deliveries of Meledor clay were purchased at over twelve month intervals. Repeat trials on the second delivery were indistinguishable from those from the first and no distinction has been made elsewhere in this thesis. In the case of the other components such as sand, felspar and alumina, sufficient material for the whole programme was obtained in one delivery.

The production of test pieces entailed the following stages.

1) Mix the dry components and wet out to obtain a moulding dough.
2) Mould the dough into blocks.
3) Cut the blocks to test size and insert notch for K_{IC} test pieces.
4) Dry and fire the test pieces.

3.1.1. Powder mixing and wetting. A Hobart commercial

food mixer with a bowl capable of holding 5 kg of dry powder was used for mixing and wetting. The weighed powders were first mixed for one hour using a spade type paddle. At the end of this time, there was no obvious inhomogeneity in the mix and the paddle was changed to the dough hook. Water was added over a period of about five minutes until a soft dough judged suitable for moulding was obtained. It was usually necessary to scrape the sides of the bowl to assist the mixing and it was found worthwhile to leave the dough in the bowl for about half an hour before using to ensure uniform wetting. Dough in excess of immediate needs was stored in plastic sacks until required.

The water content of the dough was not critical in relation to the properties of the finished test pieces. In relation to the stiffness of the dough some care was needed to get the water content about right if an easily handleable dough was to be obtained. As a rough guide, about 30% water by weight on the weight of the clay was satisfactory.

In the early stages of the work an additional operation was carried out. This was the pug milling of the dough with a view to obtaining a more intimate mix of the compoments. At that time, the dough was made with less water to give the stiffer mix required for pug milling. Comparative testing of pieces made by the two processes was unable to distinguish between them and the pug mull operation was dropped.

3.1.2. Moulding

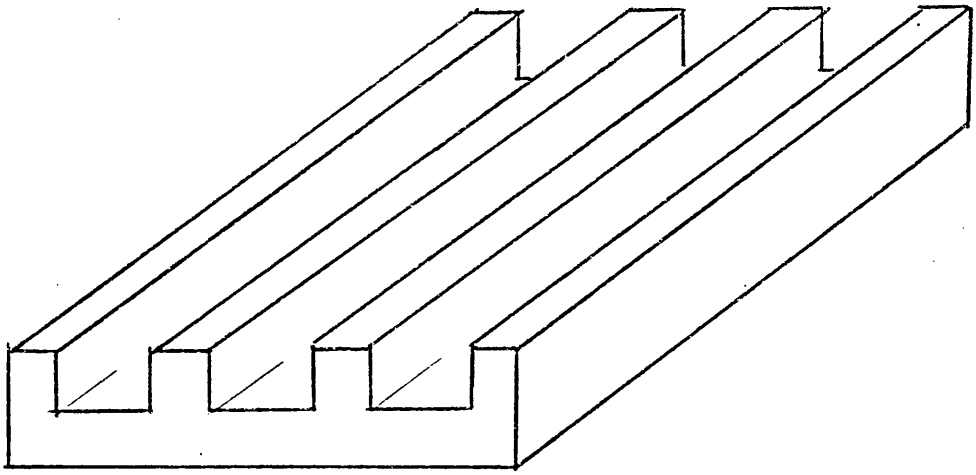

A simple wooden mould with three open ended cavities sketched above, was used to mould the dough into blocks for subsequent cutting into test piece size. Each block measured about 25 x 5.5 x 1.5cm. Prior to use the mould was sprayed with a silicone furniture spray which acted as a satisfactory release agent for the dried moulding.

The mould was filled by spreading the dough into each cavity with a spatula and removing the excess level with the top surface of the mould. A second spatula held across the end of the cavity served to close it during the filling process. In the case of the stiffer dough obtained from pug milling it was necessary to press the dough into the mould by hand before smoothing with the spatula.

During drying, appreciable shrinkage occurred with those formulations containing only a small volume of filler. To control this, since the finished test pieces would be only half the length of the moulded block, a cut was made across the centre of each block immediately after filling. The position of the drying shrinkage was

thus determined and the formation of shrinkage cracks in the middle of the test piece almost entirely eliminated.

The mould was wrapped in an absorbent paper such as paper rag or kitchen roll to reduce the surface drying rate. It was them allowed to dry naturally for about twenty four hours. At the end of this time the blocks had shrunk away from the sides of the mould and become sufficiently firm to be pushed gently through the open end of the cavities. The stiffness of the block was rather critical with respect to the next operation but experience showed that with a small amount of practice, judging the correct stiffness presented no difficulty.

3.1.3. Cutting to Test Piece Size and Inserting the Notch The half length blocks from stage 2 were cut to a length of not less than 10 cm and divided lengthwise into three giving a total of eighteen test pieces from each moulding. A simple thin bladed kitchen knife guided by a ruler held on the top of the blocks served to cut the test pieces provided the clay was correct. If the clay was too dry, cracks would be produced by the cutting; if too wet, the test pieces would slump.

Each test piece measured about 11 x 1.7 x 1.5 cm No attempt was made to ensure the pieces were more than roughly equal as the relevant dimensions of every piece would eventually be measured at the point of fracture, and the calculations for σ_F etc. made individually.

3.1.3 1. Insertion of Notch for K_{Ic} Measurements The notch was made by pushing a razor blade into the test piece to a depth determined by a couple of stops placed

on either side. This gave a level notch of uniform depth and did not appear to damage the clay or create a line of weakness below the bottom of the notch. The method was tried for test pieces with different degrees of dryness. If too dry - i.e. drier than satisfactory for cutting the block into test pieces, the notching operation split the test piece into two. If too wet, i.e. the test piece had slumped, apart from the occasions when some rejoining of the notch occurred, the test piece fired and fractured satisfactorily.

A discussion of the sharpness of the notch obtained is given in section 3.2.4 - page 67.

3.1.4. Drying and Firing The test pieces were laid flat on a board with a small air gap between each piece and allowed to dry for not less than 48 hours. At the end of this time they had turned from grey to white with further shrinkage. The shrinkage produced some warping in the samples, in the case of the K_{Ic} test pieces it usually tended to open the notch from the top. Occasionally it closed it, but after firing only rarely was any positive rejoining of the two sides of the notch observed.

The dry pieces could be fired immediately or if required be kept for several months without any signs of deterioration. In all cases prior to firing, the pieces were further dried in a hot oven at 100°C for not less than half an hour. This was found necessary to ensure complete dryness and to avoid bursting in the furnace.

An electric furnace with overhead heating elements was used for the firing. The test pieces were loaded flat onto the base of the furnace as close together as

possible. A few further pieces were placed crossways on top of the base layer taking care to use only the stronger unnotched pieces and to place them across the ends of the pieces on the base. In this way 48 test pieces could be fired at once giving four sets of ten with a few spares in case of breakage, bad manufacturing cracks or severe twisting.

The furnace took between two and four hours to reach operating temperature and was then allowed to run at this temperature for 20 hours after which it was allowed to cool naturally for 24 hours before opening. The constancy of the firing temperature was considered from two aspects

1) Repeatability. The temperature control could be set to within two Centigrade degrees of the chosen temperature. The controller maintained this set temperature as indicated by the $\pm 25^{\circ}$ deviation scale to within $\pm$ 3 degrees.

2) Accuracy. The furnace temperature as indicated by the control dial was compared on two occasions at a twelve month interval with an optical pyrometer. Agreement was within 10 degrees each time which is rather better than expected from the quality of the measurements.

It was therefore considered the control setting of the furnace was sufficiently accurate to be taken as the firing temperature.

3.2. Fracture Testing

3.2.1. Test Machine As stated in section 2.10 the test

pieces were fractured in a three point bend rig. For this work the test machine was an Instron model TT - D fitted with either a 500 kg or a 10,000 kg load cell. The three point bend rig was supplied by Instron for the machines and was adjusted to a span 2 L of 70 mm between the supports which were 10 mm diameter bars fixed to substantial pedestals mounted on the base of the Instron.

3.2.2. Correction for Test Machine Compliance Reference to equation 24 will show that the calculation for E involves the slope of the stress-strain curve. Any lack of stiffness in the test machine will reduce the slope of this curve and give rise to a lower value of E. In the case of ceramics, despite the massiveness of the test machine compared with the test piece, a correction is necessary and can be applied by the formula

$$\frac{1}{\text{True test piece slope}} = \frac{1}{\text{Measured test piece slope}} - \frac{1}{\text{Machine Slope}}$$

The slope due to the lack of stiffness in the test machine and load cell was measured by driving the central point of the three point bend test rig against the base of the rig which was bolted to the base of the Instron

10,000 kg load cell slope 24.5 MN/m^{-1}

500 kg load cell (below 30 kg) slope 4.8 MN/m^{-1}

500 kg load cell (above 30 kg) slope 20.0 MN/m^{-1}

The cause of the sharp and repeatable change in stiffness of the 500 kg load cell at 30 kg was not discovered. However, the measurements for E were carried

out on the σ_F test pieces and the slope was measured at values above 30 kg.

In the case of some samples, the correction doubled the calculated value of E.

3.2.3. Fracture of Test Pieces. The test piece was placed in the three point bend rig and the cross head lowered at 0.2 mm/minute. A chart speed of 50 mm/minute was found to be suitable. - see typical charts overleaf.

In the case of K_{IC} pieces the notch side was naturally place downwards resting on the two supports - i.e. facing away from the single point of the three point bend. In the case of the σ_F pieces, either the top or bottom of the moulding was placed down. Visually the top side which had been smoothed by the spatula appeared less cracked but in practise no difference was found in the calculated values of σ_F. It must be assumed the visual roughness of the lower moulded surface was not 'sharp'.

As the load was applied by the cross head, the sample frequently settled or ground down onto the supports in a series of jolts and it might have been thought the sample was beginning to crack. That this was not so was shown by the slope of the stress-strain curve which remained unaltered before and after each jolt - (see sample chart).

With the σ_F test pieces sufficient elastic energy was stored in the machine system to ensure the fracture was complete and the two halves of the test piece flew apart. With the K_{IC} pieces, although the fracture was catastrophic and brittle, the test piece not infrequently stayed in place supporting about 5% of the fracture load.

The charts on the following three pages are all taken with a chart speed of 50mm/min.. Individual details are,

σ_f for Kaolinite + Alumina (3)

100kg full scale, firing temperature 1350°C.

The chart shows the brittle fracture of four test pieces numbered 5-8. A certain amount of settling at the supports is seen in test piece 6.

The straight lines are drawn for the determinition of E.

K_{IC} for Kaolinite + Alumina (3)

20kg full scale, firing temperature 1350°C.

Test pieces 3-6 are shown and it can be seen that test pieces 3 and 5 did not break completely, continuing to support a residual load of about 0.5kg.

The dip at the start of each test is a feature of the Instron. The procedure was to lower the X-head at a higher speed and switch to the test speed as loading commenced.

σ_f for Kaolinite + Felspar

100kg full scale, firing temperature 1450°C.

Note the repeatability of the results even though bloating of the test pieces was sufficient to reduce the general level of the fracture load.

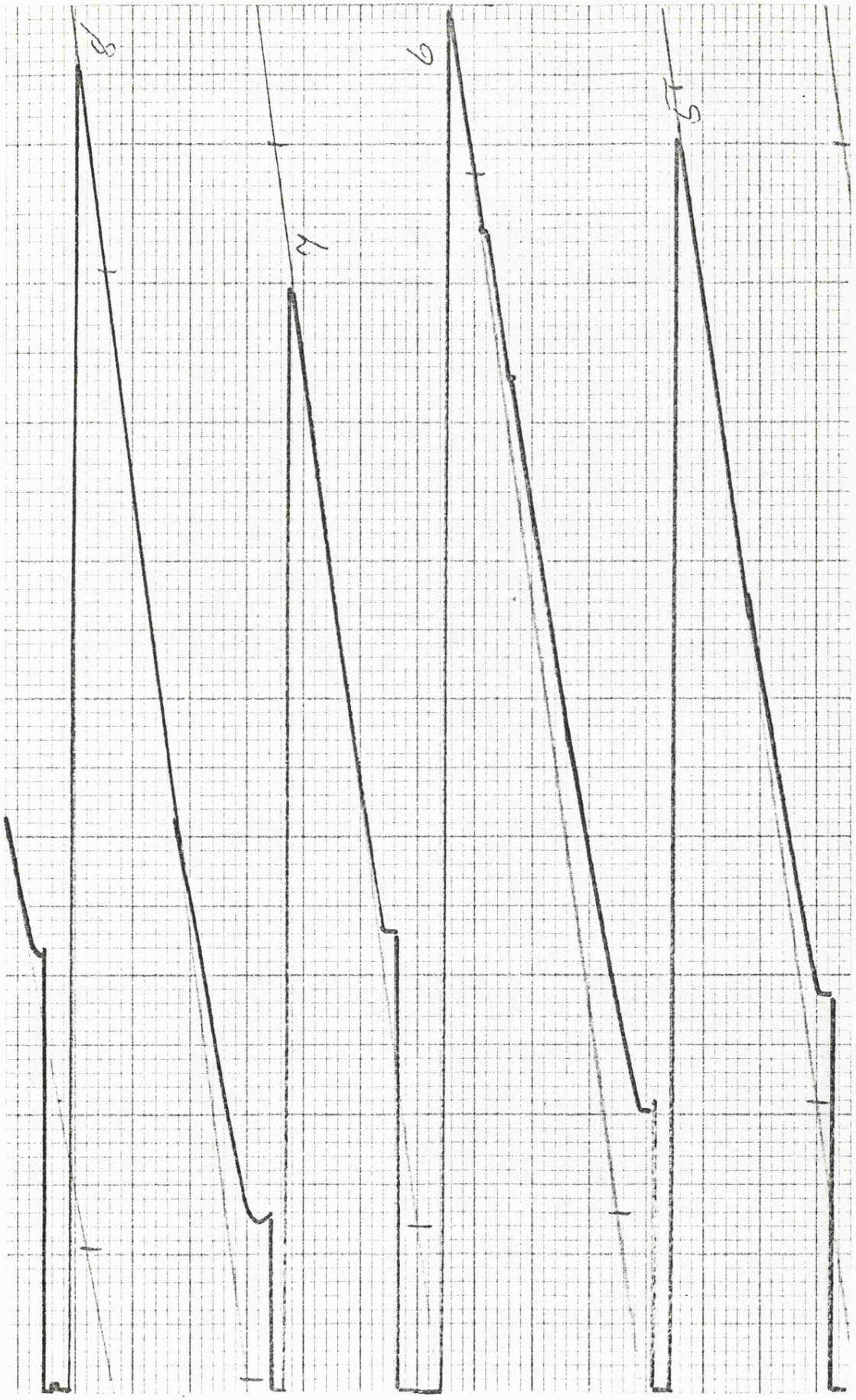

σ_f for Kaolinite + Alumina (3)

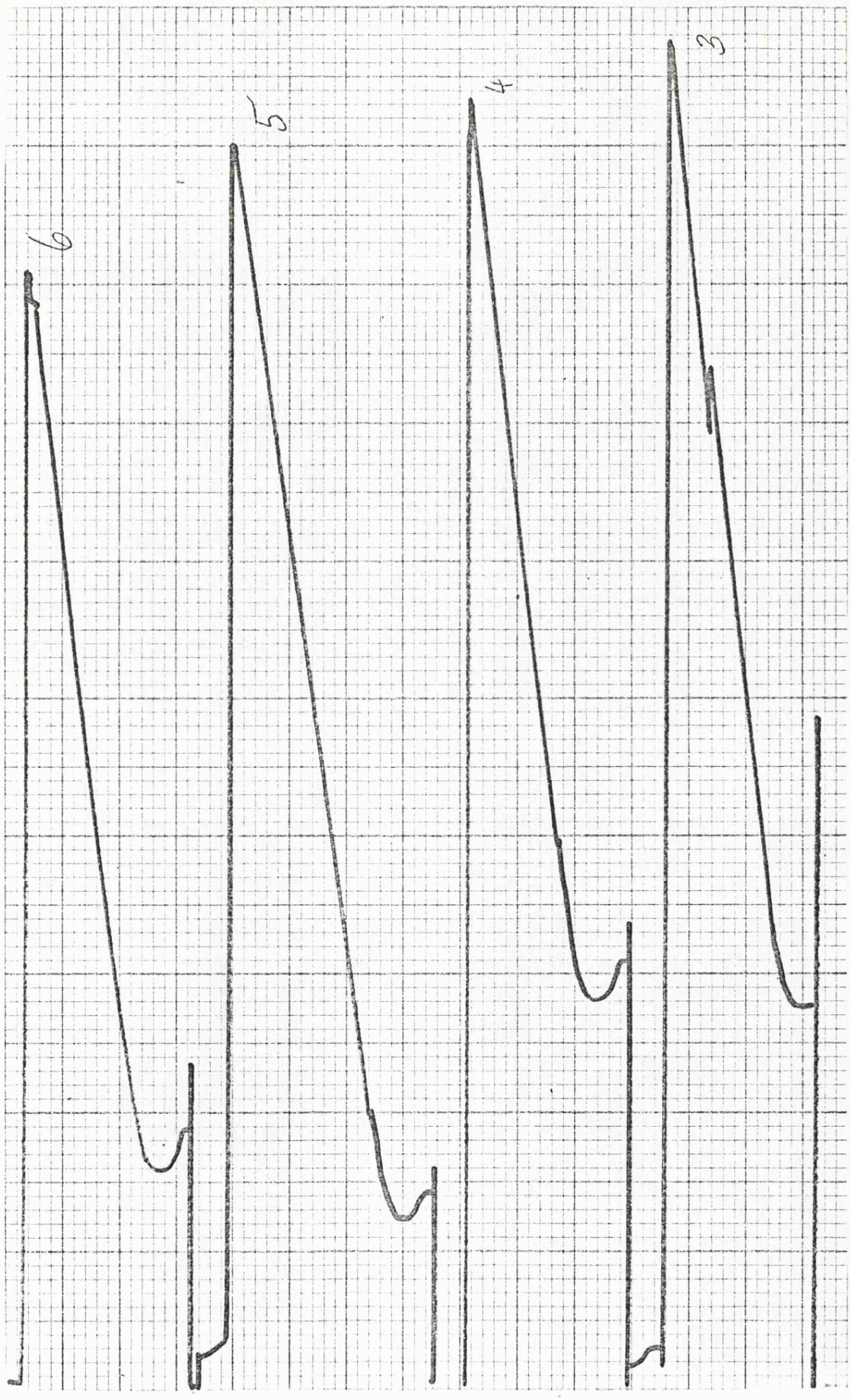

K_{IC} for Kaolinite + Alumina (3)

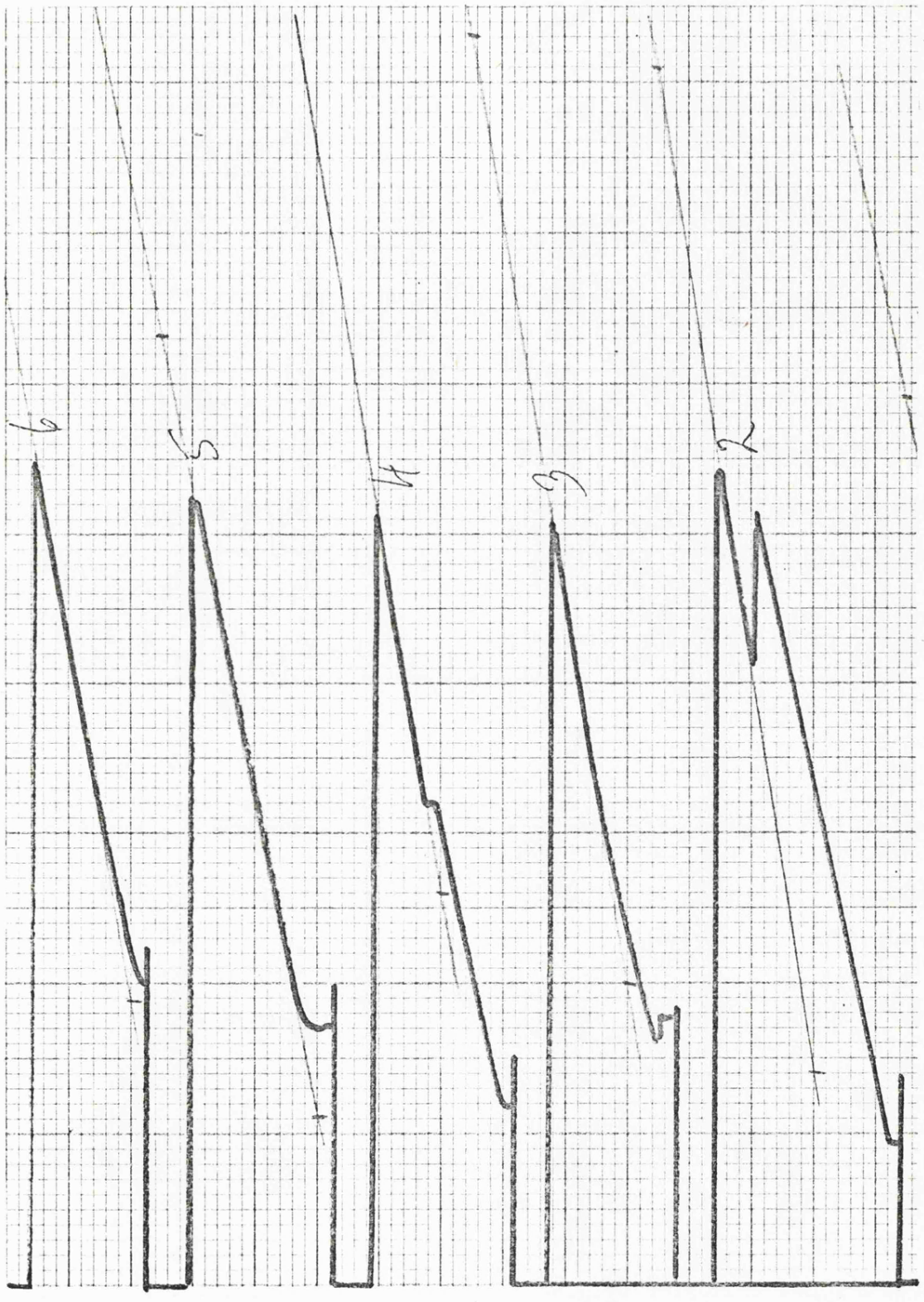

σ_f for Kaolinite + Felspar

3.2.4. Sharpness of K_{Ic} Notch Most reported cases of K_{Ic} measurement are on materials such as alumina which are obtained in a finished form. It is thus necessary to cut a notch into a solid piece of material and this is usually done by sawing. Opinions vary as to whether or not this produces a 'sharp' notch - Davidge and Evans 1968, Meredith and Pratt 1974. In a paper setting out to compare directly the differences between a sawn notch and a genuine crack, Simpson 1974 concludes that for a valid K_{Ic} determination the sawn notch should have at its root a crack of the dimensions shown.

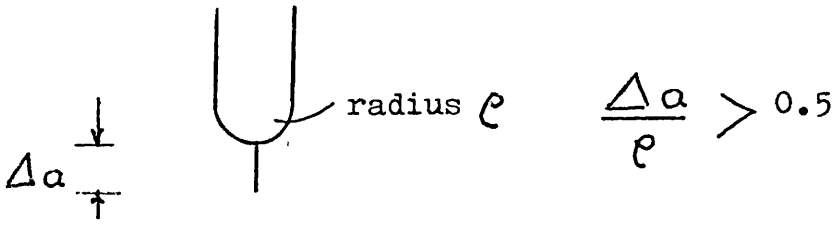

The insertion of a notch prior to firing provides a different situation and relies on thermal stresses during cooling to cause the formation of sharp cracks at the base of the notch. The presence of these cracks was investigated with a dye penetrant.

The procedure was to spray the fired test piece liberally with penetrant in the region of the notch and then to dry it thoroughly. The excess penetrant was removed with absorbent paper and the drying completed by ten minutes in a hot air oven at 100°C. This ensured that there was no liquid penetrant left at the bottom of the notch capable of running onto the fractured surface. The test piece was then broken in the normal way and the

fracture surface examined.

In materials where glass formation had commenced, short cracks extending from the root of the notch were clearly visible. In the minority of cases with no glass formation, the materials were porous to the dye penetrant and no conclusion could be reached. It was felt however for these cases that the porosity exhibited was indicative of the presence of connected pores and cracks.

An attempt was also made to produce some samples with shallow notches and to extend these prior to fracture by driving a wedge into the notch. This proved difficult to control but those cases in which dye penetrant indicated a satisfactory crack had been propagated, gave results in agreement with the standard test pieces.

3.2.5. Measurement and Examination of the Fractured Test Pieces. A simple hand magnifier with a graticule calibrated in 0.1 mm divisions was used to measure the dimensions of the test piece at its point of fracture - (i.e. referring to section 2.10, B,W and a). Distortion during drying and firing made the fracture cross section irregular and some judgement was needed in deciding on the values of B,W and a. At the start of the work both sides of the fracture were assessed independently but since agreement was found to be within 0.1 mm the practice was discontinued. The judgement of the values is obviously subjective but all the measurements were carried out by the author and repeat measurements on test pieces at several months interval indicated a constant standard.

At the same time that the test pieces were measured

any gross defects in the fracture plane such as large air holes or manufacturing cracks were noted.

3.2.6. Calculation and Assessment of Results. Programmes were written for the solution of the equations for σ_F, E and K_{Ic} (No's 23, 24 and 25) on a 'Compucord Scientific' calculator and the individual values for every test piece worked out.

Test pieces were rejected for any one of the following reasons but in the normal course of events the rejection rate was less than 10% - i.e. less than one test piece per set. See also section 4.1.1. page 92.

1) When a hole or an 'odd' break had been noted against a test piece, if its fracture value was low (greater than one standard deviation), the result was rejected.

2) When the calculated value was more than two standard deviations from the mean (usually but not always low), the result was also rejected even if there was nothing obviously wrong with the test piece.

3) The occasional set of test pieces had a rejection rate of 50% or more and in this case a repeat firing was carried out to check, a) that it was a material characteristic and not a manufacturing fault

and b) to obtain a greater number of 'satisfactory' test pieces.

3.3. Scanning Electron Micrographs.

These were taken as a matter of routine from every set of test pieces in order to build up a library of

of photographs for comparison with the fracture values.

3.3.1. Preparation of Samples. The samples were taken from K_{Ic} test pieces by slicing off the fracture surface in a section about 2 mm thick. This was a simple operation with a water cooled diamond slitting saw (approx 0.5 mm thick) and two samples were cut from each set of test pieces.

It was usually necessary to trim the sample to fit the S.E.M. stub and care was taken to ensure that the start of the crack, as indicated by the base of the notch, was always left in the sample. This allowed positive identification of the direction of travel of the crack in the subsequent S.E.M. examination. All the photographs in this thesis are mounted with the crack travelling from the bottom to the top of the print.

3.3.1.1. Etching the Samples. One from each of the two samples cut was etched. The reason for the etching of the sample is readily apparent from a brief look at some of the prints. The aim of the etch is to dissolve out some of the amorphous glass phase without affecting the crystalline phase - usually mullite.

In practice this proved straight forward. A few trials were carried out with different etching times in a 15% HF solution at room temperature. For the particular glasses formed, times between about 30 and 120 seconds were satisfactory and a time of 60 seconds was chosen as standard. With more than 120 seconds some rounding off and degradation of the crystalline structure became apparent. With less than 30 seconds the etch was shallow.

(Note: Even the shallowest of etching showed the outline of the mullite. This verified that even though in an unetched print there could be no evidence of mullite in the fracture surface, it was nevertheless present.)

3.3.1.2. Mounting and Coating the Sample. Clay ceramics are poor conductors and to overcome charging problems in the S.E.M. a conducting layer has to be vacuum deposited on the surface. It is occasionally necessary to use two different coatings, such as silver on top of carbon, but with the materials used for this thesis, one type of coating was sufficient.

The samples were stuck onto S.E.M. stubs with a conducting paint care being taken to carry the paint up the edge of the samples to ensure good contact with the coating.

The vacuum coating was carried out in the usual way, normally with silver which proved satifactory provided sufficient was applied. The amount required was found to vary quite markedly with the sample. The low fired samples where little or no fluxing of the glass phase had taken place needed the greater amount. The procedure adopted was to coat all the samples once and to recoat those found to require it. This was readily determined by a visual examination of the coated sample, those with insufficient coating appeared dark or even black rather than silver.

3.3.2. S.E.M. Photography . The mounted sample was placed in the S.E.M. at a angle of approximately 40^{o} to

the electron beam and orientated so that the base of the notch corresponded with the bottom of the viewing screen. The fracture surface was then examined at the lowest magnification (20x) and an area free from gross defects close to the start of the crack, say within 0.5mm was chosen. Three photograghs were then taken in this area at nominal magnifications of 5,000x, 1,000x and 100x. No attempt was made to select 'representative' parts of the area for these photographs.

If the sample contained features of special interest, these were searched for and photographed additionally at suitable magnifications.

The films were developed and the negatives proof printed in the usual way.

3.4 X-ray Diffraction Analysis. The changes in clay based materials during firing are discussed in section 2.11.*

One of the points brought out is the difference between results obtained by X-ray diffraction and by S.E.M. The X-ray results invariable show the formation of mullite -referred to as Primary or Scaly mullite, at firing temperatures up to 200°C less than those at which mullite becomes visible in the S.E.M. Because of this it was decided that although the thesis is concerned with the visual appearance of the fracture surfaces, X-ray analysis would provide a useful check that the various formulations were behaving in the usual manner and that no unexpected phases had developed.

3.4.1. Sample Preparation. The sample was prepared by taking a few chippings from a fracture test piece and grinding in an agate pestel and mortar. The grinding was carried out under alcohol to retain the powder formed and continued until all feeling of grittiness had disappeared. On a practical point, it was found helpful to crush the chippings in a vice between filter paper before grinding. The sample was then dried and passed through a 100 mesh (150μ) sieve. Care was taken to ensure that all the sample would pass through the sieve. This avoided any possibility that a harder phase in the material had remained unground.

In view of the plentiful supply of powdered material the X-ray spectrograph was preferred to the powder camera. The sample holder for the spectrograph was back filled by repassing the sample through the sieve and allowing it to

*p. 68

shower down into the holder cavity. Gentle tamping down of the powder gave a smooth and uniform filling.

3.4.2. X-ray Results. The sample was exposed to the $K\alpha$ radiation from a copper target. A spectrographic record was taken for a scan 2θ from 3° to approximately 70° which trials had shown covered all the major lines and the glass flare. The 'd' spacing for the individual lines was calculated from Bragg's law

$$n\lambda = 2d \sin\theta$$

where for Copper K_{α} radiation $\lambda = 1.541819^{\circ}$ and $n = 1$

The substances responsible for the lines were identified from tabulated records in the usual way. To assist identification a comparison chart was drawn up with the positions marked for the major lines of mullite, alumina and cristobalite.

The results obtained were very much as expected and table (2) overleaf gives an indication of the changes occurring during firing. It should be understood that the quantitative assessment of the substances present from the magnitude of the x-ray lines has not been attempted. The figures are simply the number of chart divisions by which the major peak for mullite, cristobalite and alumina stands out from the background noise. The figure for the glass flare is obtained in the same way.

Thus for example in the case of Kaolinite and Alumina (3), the mullite peaks were almost constant from the $1350^{\circ}C$ firing onwards whereas the peak for cristobalite clearly defined at $1250^{\circ}C$ had virtually disappeared by $1450^{\circ}C$. The fact that the cristobalite peak was less than the mullite peak does not necessarily mean there was more

Relative Strengths of X-ray Lines

Kaolinte + Quartz (2)	Mullite	Alumina	Cristobalite	Glass Flare
1265°C	15	17	5	1.5
1350°C	20	15		2.5
1450°C	38	5		3.5
1550°C	50			4.0
Kaolinite + Flint (2)				
1250°C	34		44	4.0
1350°C	34		60	5.0
1450°C	42			8.0
1550°C	43			8.0
Kaolinite				
1050°C	4			2.0
1150°C	18		Trace	3.0
1265°C	22		7.0	4.0
1350°C	26			4.5
1460°C	32			5.0
1550°C	32			5.0
Kaolinite + Alumina (3)				
1265°C	17	4	11	2.5
1350°C	23	5	5	3.0
1450°C	25	5	Trace	4.5
1550°C	26			4.5
Kaolinite + Alumina (4)				
1250°C	11	37		1.0
1350°C	19	28		1.5
1450°C	39	17		1.0
1550°C	48	7		1.0
Kaolinite + Alumina (5)				
1250°C	10	36	Trace	1.5
1350°C	15	35		1.0
1450°C	25	29		0.5
1550°C	40	16		0.5

Table 2

mullite. The cristobalite may be less 'efficient' in diffracting the copper $K\alpha$ X-ray beam. At the same time as the lines increased in length they sharpened indicating a better defined structure to the crystal.

Although not shown on table (2), in the case of kaolinite, there was a suggestion from the line spacings that a sillimanite phase ($Al_2O_3.SiO_2$) formed at 1350°C and 1450°C. This would be in agreement with the findings of Percival and Duncan 1974 and Soliman and Hammad 1970. However the 'd' spacings for sillimanite and mullite are so similar that it was not possible to be certain on this point and it has been assumed that the mullite phase (the more stable) is always dominant over the sillimanite.

A feature of the X-ray charts - see example overleaf, was the virtual absence of impurities. Whilst this is to be expected from the kaolinite analysis in Appendix 1, it provided confirmation of the high intrinsic purity of the china clay deposits and the quality control exercised in the production of a commercial product. When for comparison a sample of 'pure' kaolinite was obtained from the British Drug Houses, only a slight reduction in the extraneous X-ray peaks was found.

The appearance of a cristobalite phase on the X-ray spectrograph was very marked and short lived. It was never observed in firings below 1150°C and had essentially broken down at just over 1350°C by which temperature a glass layer was becoming visible in the S.E.M.

The alumina phase behaves as expected disappearing as it combines with the silica to form mullite. The X-ray

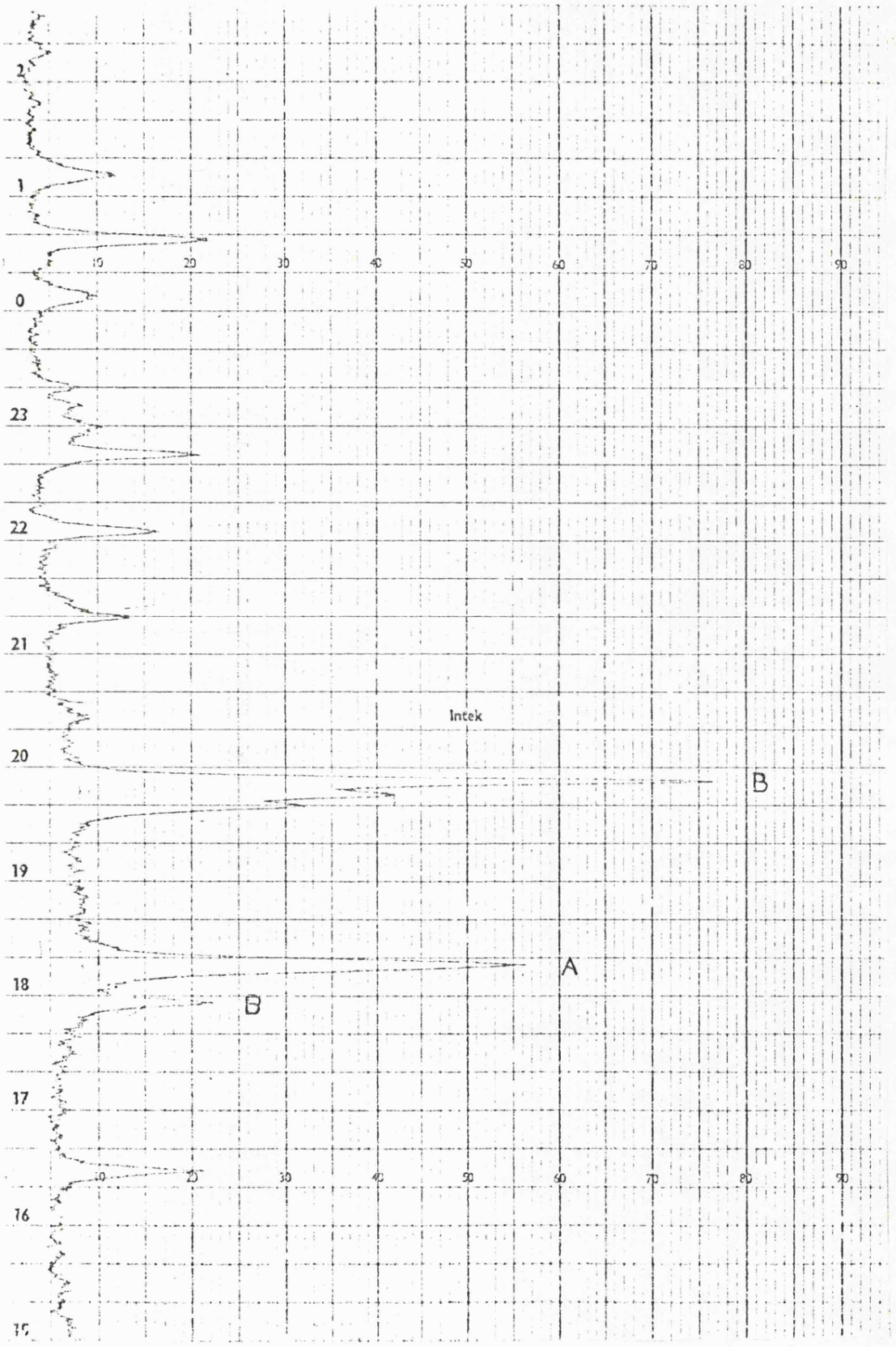

Peak A -Cristobalite, B -Lime felspar, all others -Mullite

X-ray trace of Kaolinite + Flint fired at 1250°C

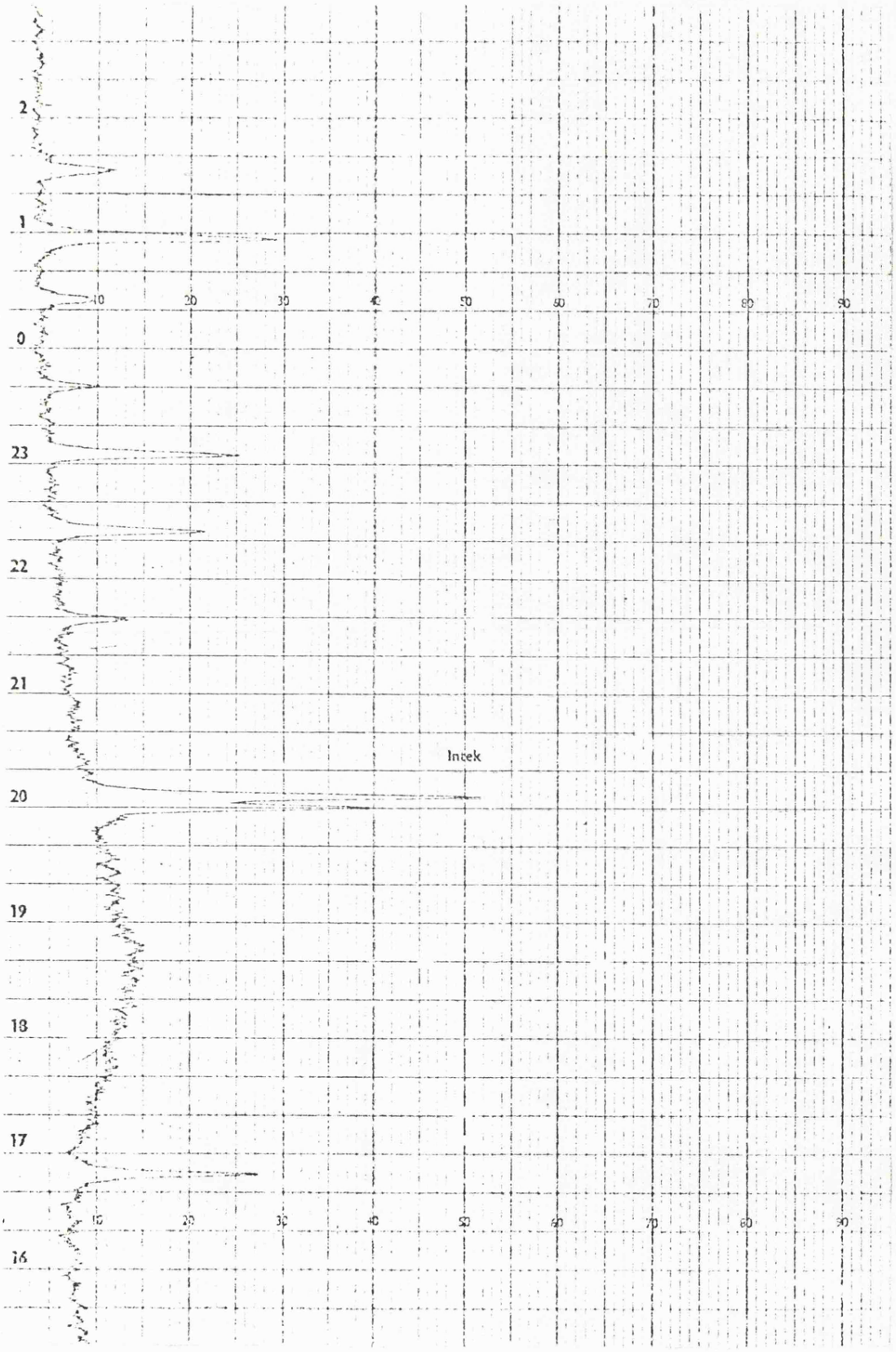

All peaks -Mullite

X-ray trace of Kaolinite + Flint fired at 1550°C

results show the calculation for the formulations Kaolinite + Alumina (4) was about right with most of the added alumina being used up. Had the firing time been extended beyond 20 hours at 1550°C, it is possible that no trace of alumina would have been left on the x-ray chart. In the same way Kaolinite + Alumina (5) has an excess of alumina.

The reason for the alumina appearing in the X-ray trace for Kaolinite + Quartz (2) is not understood. It can be seen that as a phase it is persistent over a firing range of 200°C and it may have played a part in producing at 1450°C the unusual structure shown by the S.E.M. plate (10) which is discussed later. The correspohding traces for Kaolinite + Flint (2) do not show the presence of alumina and the S.E.M. samples do not show the broken structure at 1450°C.

Mullite begins to appear in firings of kaolinite, either pure B.D.H. or commercial Meledor china clay at temperatures of 1050°C. By 1250°C firings its presence is well established though the peaks are still relatively broad indicating a weak (ill defined) crystal structure. As the firing temperature is increased the peaks sharpen and increase in height until by the 1550°C firing they are almost the only feature apart from the glass flare left on the X-ray chart. The usual assumption made by other workers is that secondary mullite with a well defined crystal structure is produced by recrystallisation from the liquid phase formed at the higher temperature - Rue and Ott 1974. This would certainly seem to be born out by the S.E.M. photographs. Plate (5) which shows only

mullite and glass (silica) at 1450°C and 1550°C is in complete agreement with the X-ray results.

However, in the case of Kaolinite + Alumina (4) and (5) the X-ray data and the S.E.M. photographs are less obviously compatible. The X-ray results show a clear and sharp increase in the mullite content and crystal structure at temperatures of 1450°C and 1550°C. This in the normal way would be assumed to be the recrystallisation from the glassy phase but the glass flare shown by the X-ray is considerably reduced and the S.E.M. photographs plate (9) show no sign of any glass phase. The fracture results also suggest that the structure has remained 'point bonded' throughout.

Thus one must conclude that when steps are taken deliberately to reduce or prevent the formation of an overall glassy phase, this does not prevent the growth and refinement of the mullite crystal. It does however confine it to within the original particles and the S.E.M. does not detect it. Whether in these circumstances it is secondary mullite is open to doubt.

3.5. Measurement of Acoustic Emission During Fracture.

It will be seen later in the thesis that flaw linking as a form of subcritical crack growth is considered a normal feature of ceramic fracture. In the case of clay bodied ceramics, it is also considered that a large number of essentially similar subcritical paths exist, one of which will ultimately give rise to catastrophic failure.

A few measurements were made of the noise emitted by test peices during loading to determine whether any supporting evidence for flaw linking over a multiplicity of subcritical paths, was available.

3.5.1. Method The test pieces were fractured in the usual way in the three point bend rig in the Instron. An acoustic transducer was clamped to one end of the test piece by a rubber band. The end of the test piece was not machined flat as it was found that with a liberal amount of silicon grease on the end of the transducer, a satisfactory pick up was obtained. It was immediately apparent from the trace if insufficient grease was used.

The three supports of the bend rig were covered with rubber tubing to reduce the point loading which it was found gave rise to noise due to local crushing of the test piece.

The outputs from the acoustic emission equipment and the Instron were fed onto a two pen recorder and a sample chart is shown overleaf. The curvature on the load trace is due to the rubber on the supports.

Typical Noise Chart.

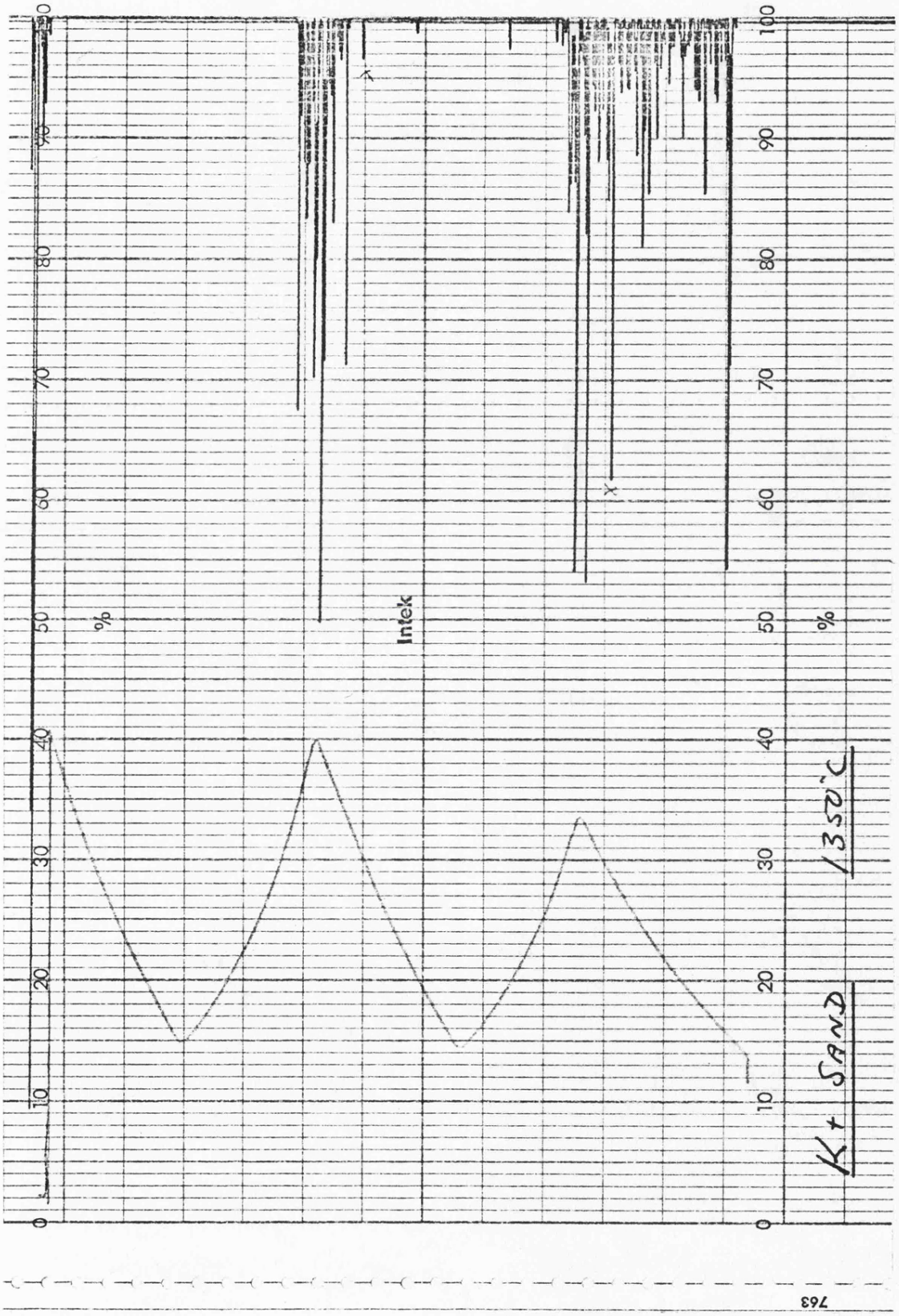

Shows cessation of noise events during the cycling of the load until the previous maximum is reached.

The calibration details for the noise chart are:-

Load trace	100 kg full scale
Noise trace	1 second integration time
Chart speed	20 mm/minute
Instron X-head	0.5 mm/minute

3.5.2. Acoustic Emission Results. Measurements were made on several different test piece formulations to determine whether or not there was a difference in the noise pattern. Apart from a possible increase in counts from the stronger test pieces such as Kaolinites or Kaolinite + Quartz compared with the weaker such as Kaolinite + Sand, there was no marked difference. In the same way, the fracture of a σ_F test piece was not obviously different to that of a K_{IC} test piece. The chart for a σ_F fracture of Kaolinite + Sand test piece can be taken as representative.

It shows, when allowance is made for the pen overlap that noise signals had commenced by the time a load of 14 kg had been reached. The indications from the other records was that the first noise signals occured in the 10-15 kg region irrespective of the ultimate failure load. This suggests a similarity in the events giving rise to noise from one formulation to the next.

The noise output then remained relatively constant and continuous until close to the point of ultimate fracture when an appreciable increase occurred.

Cycling the load clearly shows that one loading is sufficient to cause all the subcritical damage to the test piece up to that load. Further damage does not occur

until the previous load is reached. Strictly speaking the chart shows acoustic emission recommenced when the load returned to within 5 kg of the previous maximum. Even when the load is cycled very close to that necessary for fracture, 40 and 41 kg respectively on the chart, it is possible to unload and reload without further damage. The lack of change in the shape of the loading curve shows the overall compliance of the test piece is virtually unaffected and indicated that the events giving rise to the noise must be small in relation to the sample as a whole.

Thus the results show that subcritical events commence at quite low stresses with no large difference between materials or σ_F and K_{Ic} test pieces. Glucklich 1970 gives 30% of the ultimate failure load as the commencing point for subcritical events in concrete.

It is not possible to determine the number of subcritical events occuring prior to failure. The total count from the equipment is dependent on a number of factors such as the coupling of the transducer to the test piece and the multiple reflection or ringing of any noise signal within the test piece. However with an integration time of one second it is reasonable to assume that each line on the chart represents at least one subcritical event. Subcritical events are therefore numerous and support the view that failure occurs from one of several almost equally likely fracture paths formed by flaw linking during the loading of the test piece.

4. Discussion of Results.

The chapter is divided into three sections.

1. A general review of the experimental results with the aim of showing that changes in the measured values of σ_F and K_{Ic} can be related to changes in the structure of the material as shown by S.E.M. photographs of the fracture surface.

2. An examination of the relationship $\sigma_F = \frac{1}{1.92}\sqrt{\frac{K_{Ic}^2}{C_G}}$ to determine if any physical significance can be attached to the equivalent elastic crack. There is inevitably some repetition between this and the previous section and general comments on both are written jointly at the end of this section.

3. A discussion of the variations found in the values of E and the critical strain ϵ_c

4.1. Comparison of Micrograph with Fracture Results.

(note - rather than interleave the S.E.M. plates (1 - 13) and the fracture graphs (1 - 14) immediately adjacent to the discussion, which would have caused difficulties later in the thesis, they are collected together at the end of this section 4. following page 121.)

The scanning electron micrographs shown in plates (1 - 13) are representative of the total library of prints and selected to illustrate various points. They are all taken from K_{Ic} samples and the direction of

traverse of the crack is from the bottom of the print to the top. In most cases the area of the fracture surface chosen is close to, but does not include the start of the crack as defined by the razor blade notch. The reasons for this choice of area are two.

The first is practical, in that the bottom of the notch is rough, plate (1) and it has so far proved impossible to identify with any certainty the section of the notch from which the catastrophic crack propagation started. In plate (1) three distinct areas can be seen. At the top of the print is area A - the path taken by the propagating crack through the material. The ridge B in the centre is the bottom of the notch and C is one face of the slit cut by the razor blade. It can be seen that in addition to its roughness, the bottom of the crack contains even in this short section at least one flaw which may have been the site at which catastrophic fracture commenced. It can also be seen that the path of the crack A through the material appears relatively smooth and glossy whereas that cut by the razor blade prior to firing does not. This apparently is due to surface tension drawing the glass phase away from an exposed surface into the body of the material. The effect is visible on all outer surfaces and frequently in pores within the material. The appearance is not unlike that achieved by etching.

The second reason for photographing close to but not actually at the root of the notch, is more fundamental. It is intended to establish that the structure of the material as a whole is a determining factor in the fracture

strength. One is thus not seeking to identify the point from which any particular fracture initiated; rather one is saying that although the fracture will have commenced at some particular point, that point is only one of a number of equally likely points along the root of the notch. The material structure will have governed its growth to critical size.

4.1.1. Kaolinite (Meledor China Clay) The formulations based on kaolinite have provided a variety of different structures. Plates (2 -5) show the structure for kaolinite on its own at four temperatures in the range 1250°C to 1550°C, at two magnifications and with samples both etched and unetched. This set of prints is typical of those obtained for every type of material and it is proposed to deal in some detail with them.

Glass formation is best detected or confirmed by comparing the unetched print with the corresponding etched print particularly at the higher magnifications plates (3) and (5). In this way it can be seen that even at 1265°C some glass has started to form though the phase diagram for pure kaolinite does not give liquid formation till 1587°C. Meledor china clay is of course not pure and its felspathic content is sufficient to cause glass formation at much lower temperatures. The X-ray evidence - table (2)* section 3.4.2., suggests some glass is produced by firings as low as 1050°C but it is not apparent on the S.E.M. until about 1200°C.

Porosity. With increasing firing temperatures and increasing glass formation, the material shrinks causing

* p. 75

the pores to coalesce and forcing some out through the surface of the materials - compare the prints on plate (2). Not all porosity is eliminated and triaxial whiteware bodies normally contain up to 10% porosity. Even when highly fired to produce an impermeable vitreous material the porosity will still be in the region of 5%, Lundin 1959.

A further increase in firing temperature is likely to give rise to bloating, i.e. gas formation within the body of the material usually attributed to the felspathic content of the mix. This is mentioned again in section 4.1.2.

Mullite formation is seen most clearly in the etched prints at the higher magnification - plate (5), and is first visible as secondary mullite in material fired at 1350°C. The X-ray results - table (2)* section 3.4.2., in agreement with those of other workers show mullite, as primary mullite, to have increased steadily from firing at 1050°C upwards, - Comer 1960 and Lach 1974.

At 1450°C and 1550°C the mullite crystals grow in size from the liquid phase which is essentially an alumina - silica solution. If the reaction is complete in the twenty hours firing time, the liquid or glassy phase will be almost pure silica containing only the impurities originally present in the Meledor clay. The X-ray evidence suggests this to be so as there is little increase in mullite formation from 1450°C to 1550°C. For Kaolinite + Alumina (3) and (4), the results also indicate that by 1550°C the speed of the reaction is sufficient to

* p. 75

accept increased amounts of alumina.

Fracture path. On first consideration the path of the crack through the mullite - glass mixture is surprising The rod like nature of the mullite looks to be capable of a reinforcing role in much the same way that steel rods reinforce concrete. Plates (2) and (3) however show that whether the mullite reinforces the glass or not it does not do so by forcing the crack to travel round it. (The aspect ratio of the mullite is of the order of 10:1 -see plate (8). As such, if the crack went round the mullite, a considerable number of mullite rods would stand clear of the surface.) With careful examination, the mullite structure can just be made out in the surface of the 1450°C and 1550°C prints.

The fracture stress of glass and mullite is quoted as 55 MNm^{-2} and 170MNm^{-2} respectively for an arbitrary glass and a hot pressed and sintered mullite. One is thus considering a factor of about 3 to 1 between the fracture stress of glass and mullite. The mullite crystals have grown out of the glass phase and so any tendency for a weak interface between the glass and the mullite will be reduced. The aspect ratio of the mullite crystals (greater than 10:1) is apparently sufficiently high to ensure that the preferential path is through the crystal rather than round it.

Fracture values. It has been explained that the S.E.M. photographs were obtained from test pieces used for K_{Ic} determinations. The K_{Ic} values together with the σ_F and E values corresponding to the prints on plates (2 - 5)

are plotted in graph (1) which is presented in two forms, (1a) and (1b). Graph (1a) has standard error bars drawn on it to give an indication of the accuracy of the points.

The standard errors for the different formulations tested remained reasonably constant and to avoid unnecessary confusion they have been ommitted from all the other graphs. If required it can be assumed that the standard errors are:

K_{ic}	values	4.0%	Being the average of
σ_f	values	5.5%	the deviations for all
E	values	6.5%	the formulations.

(note on the statistics employed. The brittle fracture of a material originates at a flaw which may be intrinsic to the nature of the material or which may be formed during manufacture. The size and position of such flaws will vary from one piece of material to the next or from one test piece to the next however carefully the test pieces are prepared. As a consequence, a form of random variation will be introduced into the measured fracture values.

Historically, it has been assumed that a 'weak link' theory of statistics will apply. That is, somewhere in the test piece will lie a worst flaw, which because of its size, shape and position will be the first flaw to give rise to the critical stress intensity as the applied stress is increased. This point of view was recently maintained by Rice (1973). An effect of a weak link theory is that the measured fracture values are related in some way to the size

of the test piece and the method of testing. For example, the larger the test piece, the greater the likelihood of a dangerous flaw and so the weaker the measured strength. Or, if the dangerous flaws are on the surface, a four point bend test in which a greater area is placed under stress will give lower values than a three point bend test.

Various statistical treatments have been developed for this type of variation of which that by Weibull is the best known and is summarised here. He assumed that the probability of fracture was proportional to some function of the stress σ and to some function of the dimensions of the test piece ℓ, (stressed area or volume depending upon which was the relevant criterion.)

Thus the probability of fracture $P = \int_{\ell} f(\sigma) d\ell$

He further assumed the integration should encompass the whole section under stress and defined

$$f(\sigma) = \left(\frac{\sigma}{\sigma_o}\right)^m$$

where m is a constant related to and increasing with the homogeneity of the material and where σ_o is a 'characteristic strength' determined from the distribution function of the fracture values.

The average strength value is obtained by putting $P = \frac{1}{2}$ when $\sigma_{av} = \left(\frac{1}{2}\right)^{1/m} \sigma_o$

As $m \to 0$, $f(\sigma) \to 1$ and fracture is equally likely at all values.

As $m \to \infty$, $f(\sigma) \to 0$ unless $\sigma = \sigma_0$ and fracture only occurs at a single value of the strength.

An alternative viewpoint expressed by Glucklich (1970) and others maintains that whilst the initiation of fracture can be considered on a weak link basis, this applies only to the start of subcritical crack growth and not to the complete catastrophic fracture. The numerous possibilities for subcritical crack growth effectively nullify the random nature of the original initiation. Only when, as Glucklich puts it 'initiation and termination coincide' do weak link statistics apply.

For the coarse clay bodied structures examined herein, it is considered the alternative viewpoint applies and steps were taken during the experimental work further to ensure this was so. (The thesis is concerned with the effect of <u>structure</u> on σ_F and K_{Ic} values).

1) The three point bend rig was used in preference to the four point rig to reduce the area of maximum stress and hence the likelihood of manufacturing faults affecting the result - see section 2.10.

2) Any fracture which visual examination showed to have originated at a 'non typical' gross defect or any K_{Ic} or σ_F value inexplicably low was rejected - see section 3.2.6. page 69.

The statistics more applicable in these

circumstances are the customary standard deviation and standard error based on a Gaussian distribution. They contain no information regarding the cause of the variation. The standard deviation gives the probability of an individual sample lying within a given value of the mean. The standard error gives the probability of the mean of a set of samples lying within a given value of the mean of the total population of samples.

Therefore, for the purposes of this thesis, since the interest is in the effect of the material on the strength parameters, it can be expected that the standard error will give an indication of the accuracy with which the tests measure the material influence. Sufficient sets of samples have been taken to provide grounds for believing the mean and standard error are a good measure of the population mean for the material concerned.)

Returning to graph (1) and the fracture values. It is proposed to compare for each of the formulations in turn, the material structure as shown by the S.E.M. with the values of K_{Ic} and σ_f. For this purpose, it will generally be as useful to consider the differences in the graphs as the similarities. Also, although later in the

thesis the significance of K_{Ic} will be considered, at this stage for convenience of thought and language, it will be assumed that the fracture toughness K_{Ic} is a measure of the intrinsic strength of the material whereas σ_F is the fracture stress dependent on surface cracks or random flaws.

When kaolinite is fired on its own, the value of K_{Ic} is almost constant over a 300°C firing range, 1250°C to 1550°C. In this respect it differs from the other formulations for which K_{Ic} falls off at the lower end of the range. The S.E.M. prints and the X-ray results show the glassy phase also develops at a lower temperature than usual. It is established by 1250°C and persists through to 1550°C with the usual reduction in porosity and without bloating. The secondary mullite structure which appears at 1350°C and increases at 1450°C and 1550°C does not apparently increase the strength. The slight increase in the K_{Ic} value from 1250°C to 1550°C could equally well be attributed to other causes such as the change in the glass phase.

Thus one can conclude, that the mullite does not play a major reinforcing role; previously it was only possible to conclude the fracture path cleaved it. Additionally one can conclude that the glass phase plays a dominant role in determining the K_{Ic} values.

Lundin (page 12) reports that historically various views have been held regarding the reinforcing effect of mullite but that the current view, based on fracture measurements is the one concluded above, namely the glassy phase is dominant.

The value of the fracture stress σ_F unlike K_{Ic},

rises steadily throughout the firing range increasing by more than 100%. It is reasonable to assume therefore that σ_F is reacting to a different mechanism than K_{Ic} and it is suggested that the increase in σ_F can be attributed to the reduction and change in shape of the pores, plate (2). This suggestion will be discussed in more detail later in section 4.2.3.* considering the significance of the equivalent elastic crack.

Thus one is saying that, at least in the case of the firing of kaolinite, with the formation of a coherent glassy phase the intrinsic strength of the material as measured by K_{Ic} is essentially determined. The fracture stress σ_F however has continued to increase due to the elimination of pores or surface cracks.

4.1.2. Kaolinite + Potash Felspar. Many of the comments made in section 4.1.1. regarding porosity, mullite formation and etc. will apply to this and to the other formulations. Plates (6 - 8) have features in common with plated (2 - 5). However they also have marked differences and these are perhaps most clearly seen by the comparison of the corresponding etched prints in plate (4) and plate (7).

It should be born in mind that felspar is a flux and will thus have reduced by say 100°C, the temperature at which reactions take place. That is, a 1350°C Kaolinite print should be compared with a 1250°C Kaolinite + Felspar print.

The porosity of the felspar formulation is noticeably different in both scale and quantity from thatfor kaolinite. The 1250°C and the 1350°C prints on plate(7) show this

*p. 113

quite clearly and, infact, porosity of this nature is unique to the felspar formulations. Chu 1966 and others have pointed out that felspar can produce gas during firing which is trapped within the material giving rise to this characteristic porosity. Bloating, a more severe form of gassing in which actual cracks can be formed within the material is almost always attributable to the felspar content and overfiring. So, although felspar reduces the fluxing temperature, it also reduces the firing range of the material.

The mullite formation is also rather different in character as a comparison of the higher temperature prints on plates (5) and (8) will show. At 1450°C an exceptionally dense mat of mullite has formed. Additionally felspar relicts are visible in the prints on plate (7) and the mullite is better developed in the relicts than in the mass of the material. It is also orientated in relation to the sides of the original particles. This feature has been reported by many authors working with optical and transmission electron microscopes.

Fracture values. Graph (2) shows the fracture results obtained for Kaolinite + Felspar, and is obviously different from that for Kaolinite. It has infact, more in common with the rest of the graphs; the kaolinite graph is the odd one out due to the low temperature at which a cohesive glass layer formed and the long firing range.

The K_{IC} value rises steadily until the 1250°C firing

at which the glass phase could be considered formed - plate (6). For comparison, the 1250°C print for kaolinite plate (2) has a very similar appearance and a similar value of K_{Ic} is obtained. Above 1250°C with the glassy phase formed the K_{Ic} value levels out. The increase in porosity does not apparently affect the strength of the material sufficiently to cause a fall in the K_{Ic} value.

The fracture stress σ_F, as in the case with kaolinite, rises as the firing temperature is increased and the particles coalesce together. It reaches a maximum at 1250°C and it is probable that at the higher temperatures, the increasing porosity produces surface flaws or cracks which lower the value of σ_F.

4.1.3. Kaolinite + Alumina (4) The object of this formulation was to produce a structure containing little or no glassy phase. Sufficient alumina was added just to use up the silica released when the kaolinite was fired. The resultant material should then if the reaction went to completion, consist only of mullite and a few trace impurities from the kaolinite. Plate (9) shows that in relation to the glass formation, the object has been achieved and the material is a loose looking structure bonded where the individual particles contact each other. The X-ray chart confirms the absence of, or considerable reduction in, the glass phase with a low figure for the glass flare.

With regard to the formation of mullite, it has already been pointed out in section 3.4.2. dealing with the X-ray results, that there is no visual evidence of

secondary mullite formation even though the X-ray analysis - table (2)* section 3.4.2., shows a large increase in mullite during the 1450°C and the 1550°C firings.

The X-ray evidence also shows the alumina content of the material to decrease steadily as the firing temperature is raised until at 1550°C it is nearly all reacted.

Fracture values. The four prints on plate (9) have a very similar appearance. It is known that in terms of chemical reactions changes have taken place within and between the particles and it may well be that the strength of the particles and the bonding between them is greater after the 1550°C firing than after the 1250°C firing. Nevertheless the visual appearance of the structure is unchanged and remains that of a point bonded collection of particles. The fracture values for K_{Ic} and σ_F shown in graph (4) reflect this similarity. They are all low and even though the K_{Ic} values rise by about 70% over the firing range, they are still some 200-300% less than the values obtained for structures in which particles are embedded in a glassy phase.

Similar low values are shown in graph (5) for Kaolinite + Alumina (5) where the alumina addition was in excess of the silica's ability to react it. The X-ray results confirm this excess. Similar low values are also shown on a number of graphs for the lowest firing, at which the glassy phase is not developed. S.E.M. prints of these cases - not included in the thesis, show point structures.

The Kaolinite + Alumina (3) formulation, in which some but not sufficient alumina to use up all the silica, was

* p. 75

added, gave a cohesive glassy phase and a glass flare on the X-ray. Graph (3) shows it to have produced the higher range of fracture values.

4.1.4. Kaolinite + Quartz. The addition of silica to kaolinite in the form of quartz or flint will increase the glass content and thus, with the alumina formulations, provide a range of kaolinite based materials from high silica to high mullite. From the fracture results obtained it was hoped to obtain information on the relative strengths of glass and mullite. This did not prove successful, but a fortuitous reaction mentioned in section 3.4.2. occurred with the quartz which further demonstrated the connection between the observed structure of the material and the measured fracture values - graph (6).

Plate (10) shows the change in structure as the firing temperatures were raised. At 1265°C the open structure had just begun to coalesce with the formation of a glassy phase. At 1350°C the glassy phase had become continous and K_{Ic} and σ_F had risen to values expected for a structure with that appearance. At 1450°C however the glassy phase broke down or agglomerated - the X-ray flare showed it still to be present. The values of K_{Ic} and σ_F dropped and there seems little doubt that the change in structure was the cause. By 1550°C the glassy phase had started to recombine and a marked increase in K_{Ic} resulted. It is this increase which lends significance to the drop at 1450°C. The value of σ_F increased only slightly at 1550°C and it seems likely that the pore structure of the body was still too great to permit a

sharp rise.

The addition of silica in the form of flint rather than quartz does not produce a break down in the structure within the firing range and a cohesive glass phase forms at 1350°C and remains up to 1550°C. Flint and quartz although both forms of silica are known to react differently in pottery bodies - Johnson R. 1976.

For flint, graph (7), the K_{Ic} value also falls at 1450°C by almost the same amount as with quartz but in this case there is no large increase at 1550°C. It is suggested that at 1550°C bloating is beginning to occur but that whereas in the case of quartz, the structure is sufficiently open for the gases to escape, this is not so for flint and incipient cracks are formed.

4.1.5. Kaolinite + Sand. The addition of sand to kaolinite is the addition of silica in a different form, a large particle as opposed to a small. The two prints on plate (11) show that even after firing for twenty hours at 1550°C it is still present as a discreet particle. The material thus remains to a great extent a mixture of sand particles in a background of fired kaolinite - i.e. mullite and glass. Some reaction between the two components has taken place as the higher magnification print shows. Mullite can be seen growing into the solution rim of the sand grain.

Fracture values. As would be expected this type of structure produces very different fracture curves. Bearing in mind that the background material is essentially fired kaolinite, graph (8) for Kaolinite + Sand can usefully be compared tith graph (1) for Kaolinte. Not until

the 1550°C firing does the K_{Ic} value for Kaolinite + Sand approach that for Kaolinte. At the lower firing temperatures the S.E.M. photographs - not included in the thesis, show the sand grain to be poorly bonded into the material. As confirmation if a sample fired at 1250°C or 1350°C is broken some grains will fall out whole. The cause is probably differential contraction during cooling - Kingery 1960 p. 392. At 1550°C however the grain is well bonded into the material with a continuous solution rim of silica. In these circumstances it might be expected that the strength would begin to approach that for Kaolinite.

It should be noted that the core of the sand grains are shown to be shattered in the 1550°C prints. This is not the case for the lower fired materials and the effect of this change will be considered in the section on critical crack sizes - page 110.

The value of the fracture stress σ_F is also low increasing as the bonding of the sand grains improves. The grains are sufficiently large to provide surface cracks capable of initiating catastrophic fracture directly without further substantial crack growth.

4.1.6. Kaolinite + Zircon Flour. The additions to kaolinite so far discussed have been able to react chemically with the kaolinite even though in the case of sand the particle size provided a physical limitation on the amount of reaction possible. Zircon (ZrO_2SiO_2) does not react with kaolinite below 1600°C and thus even fine particles can be expected to remain essentially intact over the firing range 1250°C to 1550°C. (Apart from

furnace capability, bloating of the kaolinite above 1550°C determines the useful upper limit of firing temperature.)

The two photographs on plate (11) present a very different appearance to those previously discussed. The zircon particles are embedded in the firm mullite - glass base obtained when kaolinite is fired - see the corresponding kaolinite prints on plate (5). The adhesion between the zircon and the base appears to be good but the S.E.M. photographs for the lower firing temperatures suggest the adhesion improves as the firing temperature is raised.

The fracture path is rough and has been interrupted by the zircon. The particles have either forced the crack to travel round them or have been cleaved. Which occurred in any particular instance, probably depended on the shape and orietation of the particle in the base material. Comparison with the two other prints on plate (11) where the sand grains are seen to have been sheared flat with the surface, highlight the difference.

Fracture values. Graphs (9) and (10) show the fracture values for Kaolinite + Zircon flour and Kaolinite + Zircon sand. The zircon sand was a fine sand very similar to the zircon flour and the two graphs show no significant differences and can be considered together. The agreement provided a useful confirmation of the repeatability of the experimental technique.

The value of K_{Ic} rises as the firing temperature is increased, when, it has been suggested, the bonding of the zircon particle into the base material improves. The peak value of K_{Ic} at 1450°C exceeds the corresponding

value for kaolinite but falls to a comparable value at 1550°C. A significant gain in strength is not unlikely as the fracture stress of zircon is quoted as 140 MNm^{-2} against say 55 MNm^{-2} for glass.

The values for the fracture stress σ_F also increase with temperature and are surprising in that above 1350°C they exceed the values for kaolinte by a considerable amount. The reason for this is by no means clear. It is possible that a form of crack pinning as described by Lange in 'Composite Materials' is taking place. Pinning is usually discussed in terms of fracture energy but the presence of zircon particles may, by pinning the developing crack front, stop the growth of microcracks until the stress has reached the higher value required to force the crack through or past the zircon. It is necessary to assume that the distribution of zircon particles is such that all microcracks have a high probability of meeting a particle before reaching critical crack length.

4.1.7. Kaolinite + Mullite. Mullite obtained commercially is in the form of chunky paricles available ground and meshed to different sizes. The coarse 22's and the finer 100's were used in this thesis. The particles do not exhibit the open needle structure of mullite recrystallised from a glassy phase. As with the zircon, mullite added to a kaolinite formulation is relatively inert below 1600°C. This is confirmed by the photographs on plate (12) in which it can be seen that little or no reaction has taken place between the mullite and the glassy phase - cf. the solution rim of the sand grain.

Fracture values. Considering first the larger mullite 22's and graph (11). The mullite has affected the fracture path - plate (12) but once the particles are firmly bonded into the base at temperatures above 1350°C, the K_{Ic} strength values are similar to those for kaolinite. With the larger particle added at the same percentage by weight to the formulation, it is relatively widely spaced in the base material. This does not however prevent it from providing sufficient surface cracks to ensure the value of the fracture stress σ_F remaining low.

Turning to the finer mullite 100's, the upper prints on plate (12) show what appears to be a considerable amount of surface debris. Some is also visible in the lower mullite 22's prints. The 'debris' is unique to the mullite formulations and it is not loose. It must be assumed to be mullite that the crack has gone round. This is not unreasonable; mullite particles added to a formulation are likely to be less well bound than those grown in situ and additionally their shape will offer less resistance to the crack passing round them.

The graph (12) has characteristics both for K_{Ic} and σ_F which are very similar to those for zircon. Again σ_F has very high values.

4.1.8. Ball Clay Formulations. In section 2.11.1. it was stated that ball clays were less pure than kaolinites, and of a finer particle size. This feature is apparent from the photograph on plate (13). The upper two prints show ball clay fired on its own at 1350°C. The etched print shows a dense mat of mullite crystals much smaller

in size than those seen in the kaolinite formulations. In the unetched print showing the fracture path, the mullite is also just visible in the sample, either as horizontal crystals or as sharp points where the crystal has been stood vertically and sheared.

The lower two prints show a Kaolinite + Ball clay formulation fired at 1150°C. The structure has already developed a cohesive glassy phase due to the higher felspar content of the ball clay. The etched print however does not show any sign of secondary mullite.

Fracture values. Graph (13) for Ball clay provides further evidence of the lower fluxing temperatures of the clay - (note the change in the temperature scale) with K_{Ic} and σ_F reaching their maximum values at 1050°C.

The value of K_{Ic} is very much in line with that for Kaolinite + Felspar - graph (2) if the appropriate shift is made in the temperature axis. The value of σ_F however is considerably greater with its maximum value at 1050°C equalled only by those formulations containing zircon or mullite particles. In this case, the smaller particle size of the clay and its greater plasticity during moulding is likely to have reduced the surface and internal flaws and thus increased the fracture stress σ_F.

The graph (14) for Kaolinite + Ball clay again shows σ_F to reach a high value but more slowly and without a maximum. The addition of the purer kaolinite effectively reduces the percentage of felspar in the formulation and thus the temperature of glass formation is raised.

The value of K_{Ic} also rises more steadily but to a

lower value.

4.1.9. Comments. The preceeding eight sections have discussed the measured values of the stress intensity factor K_{Ic} and the fracture stress σ_F in relation to the observable features of the fracture surface. Different features have been obtained by varying the firing temperatures and the formulations but it is important to bear in mind that it is the structure that is being investigated. The means by which the different structures are obtained is of secondary importance. Indeed, apart from visual clarity, there is no reason to connect the individual points on the fracture graphs.

(note - the X-ray results and the chemistry of fired clays suggest the fracture values are not likely to contain major discontinuities between the points.)

4.2. The Effect of Structure on σ_F and the Equivalent Elastic Crack C_E.

The concept of the equivalent elastic crack was introduced in section 2.9.2. where it was described as the depth of a hypothetical sharp surface crack which would on the Griffith theory have just initiated fracture at the measured overall applied fracture stress. The calculation for C_E in the case of a test bar is given by the formula

from Davidge et al $$\sigma_F = \frac{1}{1{\cdot}92}\sqrt{\frac{K_{Ic}^2}{C_E}}$$

or

$$C_E = 0{\cdot}27.\ \frac{K_{Ic}^2}{\sigma_F^2}$$

where σ_F is the fracture stress of an unnotched bar and K_{Ic} is a valid determination for the material concerned.

The Stress Intensity Factor was discussed in section 2.6.1.2. where it was shown to embody the overall applied stress σ and the geometry of the system to give a factor characterising the stress at a point just ahead of a crack tip. At the instant of fracture this factor becomes the Critical Stress Intensity Factor K_{Ic}. It was further stated that by careful choice of the geometry, 'valid' determinations could be obtained for K_{Ic}. This is tantamount to saying that without a carefully chosen geometry, the mathematics of the stress function or the measurement of the crack depth is too vague to give repeatable results. It is not saying that the value of K_{Ic} is varying.

The fracture stress σ_F was assumed for many years to be random flaw controlled and to obey Weibull statistics. Rather ambiguously it was, at the same time, equated in an arbitrary fashion to some function of the grain size or the porosity. More recently in denser materials, flaw linking has been shown to occur prior to catastrophic failure.

If one accepts that K_{Ic} provides a measure of the strength of the material structure as a whole and that the preceeding section 4.1. has demonstrated that σ_F is also determined partly or wholly by the material structure then it should also be possible to associate at least qualitatively, the value of the equivalent elastic crack C_E to

features visible on the S.E.M. photographs.

Table 3 lists the values of C_E in microns calculated according to the formula, $C_E = 0{\cdot}27 \frac{K_{1c}^2}{\sigma_F^2}$

The standard error is C_E is of the order of 11% and with an average value of C_E around 200μ, it is convenient to take 50μ as a significant difference between one value of C_E and another.

The histogram below compiled from all the values in the table shows the majority of the values of C_E lie in an area around 200μ with a spread down towards 100μ and an appreciable group in the region of 400μ. The latter group, found to be made up chiefly of materials containing large particles, is the most straight forward and will be considered first.

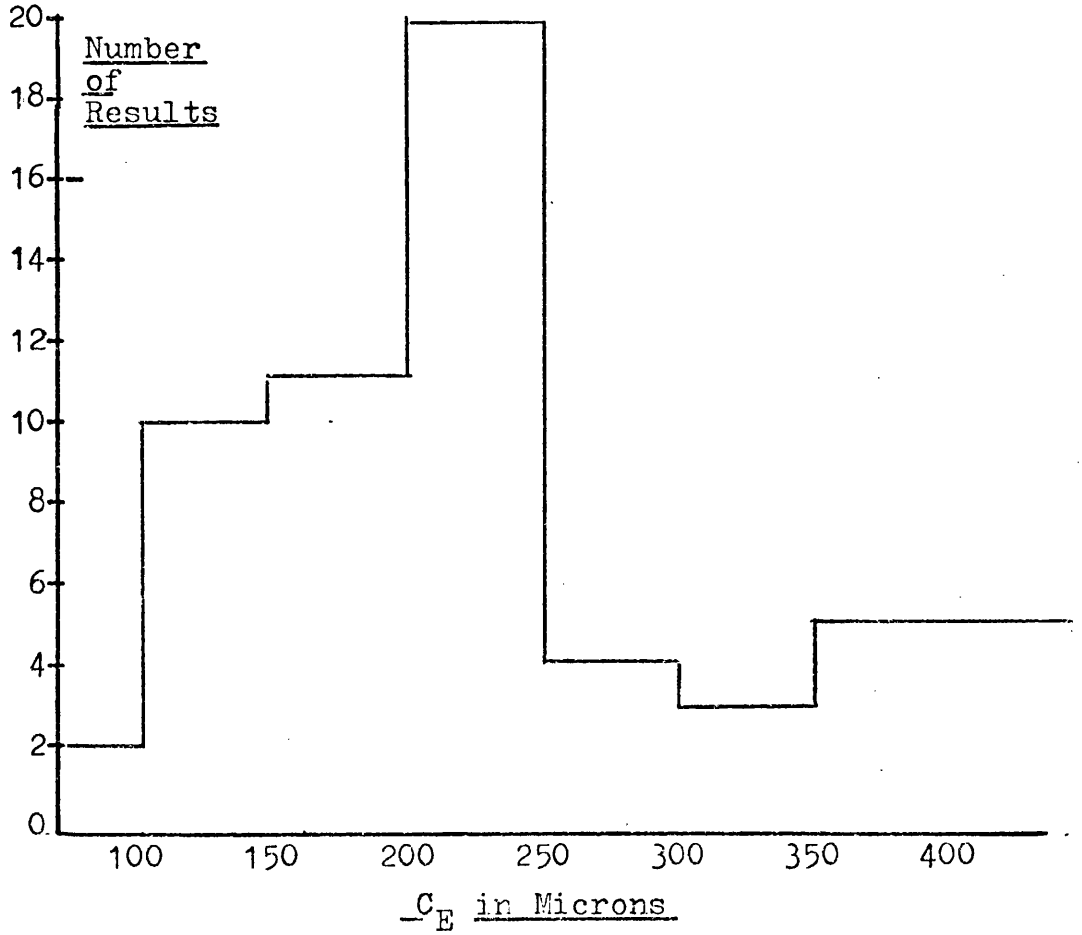

Table of C_E in Microns

Firing Temp °C	950	1050	1150	1250	1350	1450	1550
Kaolinite				394	309	303	207
Kaolinite + Felspar		224	206	145	235	293	
Kaolinite + Alumina (3)				204	248	249	230
Kaolinite + Alumina (4)				197	245	176	225
Kaolinite + Alumina (5)				191	210	362	277
Kaolinite + Quartz				249	201	219	348
Kaolinite + Flint				217	190	144	176
Kaolinite + Sand				489	503	260	480
Kaolinite + Zircon Flour			191	227	227	201	111
Kaolinite + Zircon Sand			188	185	209	260	127
Kaolinite + Mullite (22s)				483	427	383	388
Kaolinite + Mullite (100s)				210	260	194	131
Ball Clay	118	209	157	150	138		
Kaolinite + Ball Clay	81	118	95	110	112		

Standard error of C_E is about 11%

Table 3

4.2.1. Kaolinite + Sand and Kaolinite + Mullite (22's)

The sizes of the sand particles measured on the S.E.M. photographs approach 250μ which is in agreement with the mesh fractions where 77% of the particles were found to lie between 150μ and 300μ. The mullite particles are similar. The sand and the mullite grains are therefore comparable in size with the actual value of C_E found for many of the other formulations. It is expected that they will dominate the value of σ_F though not necessarily the value of K_{Ic} .

The values of C_E suggest the fracture initiating cracks are of the order of 2 grain diameters which is in accordance with the findings of other workers in the simpler structures of alumina.

It is only when particles of this size are used in clay bodied materials, that an 'identifiable particle size' analogous to the grain size in single phase ceramics can be found.

The anomalous figure in the group is the value of $C_E = 260\mu$ for Kaolinite + Sand fired at 1450°C. The difference appears significant and the following explanation is tentatively offered. From an examination of all the prints available it appears that the bonding of the sand grain into the material as a whole might be expected progressively to reduce the value of C_E. However at 1550°C the sand grain cores are shattered - plate (11) due to thermal expansion stresses - Kingery 1960, at 1450°C they are not. It is suggested that the rise in C_E again at 1550°C is due to the shattered core behaving as an

efficient stress raiser.

4.2.2. Ball Clay and Ball Clay + Kaolinite. The lower end of the range of values of C_E shown on the histogram come, to a large extent, from the results obtained with ball clay formulations. Ball clay is a much finer particle sized clay than china clay. English China Clays Ltd. quote:-

Ball clay less than 0.2μ to 1.0μ

China clay less than 2.0μ to 10.0μ

The greater plasticity and improved forming characteristics account for its extensive use in the cheaper mass produced pottery and by the craft potter. It usually contains a considerable proportion of felspar and fires at a lower temperature than china clay.

Plate (13) shows prints which are typical of the appearance of this clay and the immediately obvious difference is the fine scale of the mullite and the relative absence of voids or cracks. There is thus a condition in which the effect of the reduced sensitivity of the K_{Ic} measurement to flaws is minimised resulting in the σ_F values tending to parallel the K_{Ic} values - graphs (13) and (14). Additionally the close flaw free structure might be expected to limit the length or growth of any cracks that do form as the stress is increased, giving a high value for σ_F and a low value for C_E.

The majority of the values of C_E lie in the 200μ range and are less easily explained. The high values could fairly easily be attributed to specific particles,

the lower values for ball clays are reasonable when considered in relation to those for china clay - though no 100μ flaws were detected. Likewise there are no 200μ flaws for the middle range of materials and extensive flaw linking must be assumed.

4.2.3. Kaolinite The values of C_E for kaolinite range from 394μ at the 1265°C firing to 207μ at the 1550°C firing. If the relevant prints are examined on plates (2) and (4) it can be seen that there are no individual flaws anywhere near these sizes. It can also be seen that the size, shape and quantity of the pores changes quite markedly between 1265°C and 1550°C. It is not difficult to imagine the pores in the lower temperature material linking together under stress to form long lines. Those at the higher temperature are more rounded and would appear to offer more resistance.

An attempt can be made to calculate the difference from measures taken of typical flaws on the prints. The equation for the stress at the tip of an ellipse (equation 8, section 2.6.1.1.) gives $\sigma_t = 2\sigma\sqrt{\frac{a}{\ell}}$

If one assumes K_{1c} is a measure of the resistance of the material to crack extension then,

$$\frac{\sigma_{t\,1265}}{\sigma_{t\,1550}} = \frac{K_{1c\,1265}}{K_{1c\,1550}} = \frac{\sigma_{1265}\sqrt{a/\ell_{1265}}}{\sigma_{1550}\sqrt{a/\ell_{1550}}}.$$

Substituting the measured values of K_{1c} and values of $\sqrt{a/\ell}$ estimated from the prints allows the ratio $\frac{\sigma_{1265}}{\sigma_{1550}}$ to be calcutated.

From the measurement of several flaws, taking their

length as 2a and their width as 2ℓ gives

$$\sqrt{a/\ell}_{1265} = 2.9 \quad \text{and} \quad \sqrt{a/\ell}_{1550} = 2.2$$

Whence $$\frac{\sigma_{1265}}{\sigma_{1550}} = \frac{K_{Ic\,1265}}{K_{Ic\,1550}} \cdot \frac{2.2}{2.9} = 0.64$$

It should be remembered that σ_{1265} and σ_{1550} are the overall applied stresses that would be required to extend the surface crack and not the fracture stress at failure when flaw linking has provided a sufficiently deep crack. However, if it is assumed that catastrophic failure follows closely an initial crack extension, then the calculated ratio of $\frac{\sigma_{1265}}{\sigma_{1550}}$ can be compared with the measured value of $\frac{\sigma_{F\,1265}}{\sigma_{F\,1550}} = 0.60$

The close agreement between the two ratios (0.64 and 0.60) is fortuitous and dependent on assumptions and measurements. It is merely an attempt to show that if pore linking takes place, then for the two surfaces depicted in the photographs, a ratio of fracture stresses similar to those actually measured would be expected.

It does not seem possible to attach to the value of C_E a single observable feature. But it must be stressed that the repeatability of the results suggests the features causing failure must be common and uniformly spread throughout the samples, which points again to flaw linking.

4.2.4. Point Bonded Structures. It was stated in

section 4.1. that the absence of a glass phase gave rise to a structure bonded only at the points of contact between individual particles. The example shown was Kaolinite + Alumina (4) - plate (9) and graph (4). The structure was weak both in respect of K_{Ic} and σ_F. The calculation for C_E gives a value in the region of 200μ. Again there is no suggestion that any individual feature has this value. The suggestion is, that before such a material will fail, a crack equivalent to this length will have developed. It can be noted that other point bonded structures - (Kaolinite + Alumina(5), Kaolinite + Felspar 1050°C and 1150°C, Kaolinite + Zircon Flour and Sand 1150°C and Kaolinite and Mullite (100's) 1250°C) give similar values of C_E which suggests the bonding mechanism between the particles is essentially similar and probably due to the small amount of glass formations which it is known would have occurred.

4.2.5. <u>Kaolinite + Quartz - plate (10), graph (6)</u>. This has already been discussed at some length with regard to the break up of the structure at 1450°C which keeps the value of C_E in the 200μ region very similar to that for a point bonded material. At 1550°C the glass is reforming and the K_{Ic} value rises but the photograph shows major cracks which would be expected to affect σ_F and a value for C_E of 348μ is calculated. A similar effect applies in the case of a material such as Kaolinite + Felspar at 1450°C - plate (6) where bloating has started to produce large individual flaws and C_E is calculated as 393μ.

4.2.6. Kaolinite + Zircon Flour and Sand and Kaolinite + Mullite (100's). With these formulation as the firing temperatures are raised to 1550°C the added particles become more securely bonded into the structure and begin to interfere with the propagation of the crack front. The values of both K_{Ic} and σ_F rise and the calculated values of C_E are found to fall to 111μ, 127μ, and 131μ respectively. The low values must, it is considered, be significant and related to the nature of the structure revealed by the fracture surface which the photographs show to be different from those for formulations not containing unreactive particles.

4.2.7. General Comments on Section 4.1. and 4.2. During the course of the experiments some 500 photographs were taken of fracture surfaces. Not all were of value and even less could practically be included in this thesis which contains a selection showing the different type of fracture surface observed.

The points on the graphs represent the breaking of about 1500 test pieces and it has already been stated that the repeatability from month to month was excellent.

Taken together and used in the study of σ_F, K_{Ic} and C_E, it is considered several points emerge.

1) Large particles or major flaws can initiate catastrophic failure giving low values of σ_F. They do not necessarily weaken the micro structure as a whole as evidenced by the ability of K_{Ic} to maintain its value. They result in a high value of C_E for which individual physically observable features can often be considered

responsible.

2) In the absence of large particles or flaws, catastrophic failure is caused by the linking together of minor flaws which are numerous. Thus for any given set of test pieces it is highly probable that similar combinations of flaws will exist which explains why the scatter of σ_F results, here in, are no greater than those for K_{Ic} (or for E).

(note - the same argument applies to the results for larger particles which can also be considered numerous.)

It must be concluded that the σ_F results for clay bodied materials are not random in the sense that failure occurs from unique cracks.

3) The flaws linking to form the critical crack are essentially the same as those within the body of the material. Thus in the absence of major flaws such as those due to sand grains, the values of σ_F and K_{Ic} parallel each other more closely than would be the case if σ_F was random flaw controlled.

4) It is usual to consider that because of the nature of the measurement which reduces the sensitivity of K_{Ic} to minor flaws, K_{Ic} provides a material parameter of strength. For clay bodied ceramics this view is atleast open to question and will be discussed again later. From the point of view of the design engineer there is a lot to be said for the parameter σ_F which 'notices' sand grains compared with K_{Ic} which does not. -sect. 4.1.5. p100.

4.3. The Modulus of Elasticity E and the Critical Strain ϵ_c.

The previous two sections have discussed the effect of the structure of the material on the measured values of σ_F and K_{Ic} and the derived variable C_E.

Historically it has been supposed that the critical stress intensity factor K_{Ic} and the modulus of elasticity E are material parameters, whilst the fracture stress σ_F is a random flaw dependent function. With the increasing evidence of the need for crack extension prior to the development of a critical crack length, Glucklich 1970, Meredith and Pratt 1974, the role seen for the fracture stress has begun to change. The previous two sections 4.1. and 4.2. confirm this change for clay bodied ceramics by demonstrating the effect of material structure on σ_F.

The regarding of the value of E as a material parameter follows naturally from the nature of the measurement which is non-destructive. The present section therefore sets out to examine whether or not the value of E can be related to the material structure as shown by the S.E.M. photographs of the fracture path. In this case however the detailed correspondence between E and the material structure is much less marked and it is not possible to do more than make a few general observations.

4.3.1. High Values of E. An examination of the graphs (1 - 14) shows that the values of E range from under 20 GNm^{-2} to 50 GNm^{-2}. Taking 40 GNm^{-2} as the criterion for a high value of E, the following formulations

are included.

Graph (1)	Kaolinite
Graph (2)	Kaolinite + Felspar
Graph (3)	Kaolinite + Alumina
Graph (9)	Kaolinite + Zircon flour
Graph (10)	Kaolinite + Zircon sand
Graph (13)	Ball Clay
Graph (14)	Kaolinite + Ball Clay ($38GNm^{-2}$)

The materials above reach their high value of E when the glass phase is well formed and free from major flaws. That is the same conditions under which high values are obtained for K_{Ic} and σ_F. It should be noted that the value of E more closely follows the value of σ_F than the value of K_{Ic}. This is particularly apparent in graph(2) for Kaolinite + Felspar where both σ_F and E fall at the higher temperatures when bloating occurs.

4.3.2. Low Values of E. Taking formulations not reaching $25GNm^{-2}$ as the criterion for low values of E gives:

Graph (4)	Kaolinite + Alumina (4)
Graph (5)	Kaolinite + Alumina (5)
Graph (8)	Kaolinite + Sand
Graph (11)	Kaolinite + Mullite (22's)

The materials fall into two groups

1) The point bonded type of material such as Kaolinite + Alumina (4) and to these can be added any formulation fired at a temperature too low to yield a glassy phase.

2) Materials containing large particles capable of acting as major flaws.

Again the conditions giving low values of E are those which give low values of σ_F and usually low values of K_{Ic}

(not necessarily in the second group)

4.3.3. Intermediate Values of E. These are given by;

Graph (6)	Kaolinite + Flint	$28GNm^{-2}$
Graph (7)	Kaolinite + Quartz	$37GNm^{-2}$
Graph (12)	Kaolinite + Mullite (100's)	$32GNm^{-2}$

Little constructive comment can be made regarding these results though it is interesting to see how low the value of E is for Kaolinite + Mullite (100's) compared with the values of σ_F and K_{IC}. In this respect mullite has a very different effect to Zircon on the elastic modulus.

4.3.4. Critical Strain ϵ_c. To avoid any misunderstanding ϵ_c is defined by the equation $\epsilon_c = \frac{\sigma_F}{E}$

where ϵ_c is the strain at fracture. It is usual practice to multiply σ_F/E by 1000 and quote ϵ_c in milli-strain. Astbury - see section 2.9.3.* pointed out that the value of ϵ_c for brittle materials lay between about 0.5 and 2.0. Table (4) giving values for ϵ_c (see overleaf) shows this to be the case for the clay based formulations. Values over 2.0 at the lower end of the firing range can be discounted as not being adequately bonded.

A feature of table (4) compared with table (3) for C_E is the stability of the value for each formulation. With the possible exception of Kaolinite + Sand and Kaolinite + Mullite (22's) and (100's), there is no significant difference between the value when fired at 1250°C and the value at 1550°C.

However, although for example, Kaolinite has the same

*p. 39

Table of ϵ_c in Millistrain

Firing Temp °C	950	1050	1150	1250	1350	1450	1550
Kaolinite				1.1	1.0	1.0	1.0
Kaolinite + Felspar		3.1	1.2	1.1	0.9	1.0	
Kaolinite + Alumina (3)				1.2	1.1	0.9	1.0
Kaolinite + Quartz				1.2	1.4	1.1	1.1
Kaolinite + Sand				1.7	1.4	1.4	1.2
Kaolinite + Zircon Sand			2.2	1.6	1.5	1.3	1.3
Kaolinite + Zircon Flour			2.2	1.5	1.4	1.5	1.7
Kaolinite + Flint				1.9	1.6	1.5	1.7
Kaolinite + Alumina (5)				1.8	1.4	1.6	1.5
Kaolinte + Alumina (4)				1.6	1.6	1.9	1.6
Kaolinite + Mullite (22s)				1.9	1.7	1.8	2.3
Kaolinite + Mullite (100s)				1.6	1.7	2.2	2.2
Ball Clay	2.9	1.8	1.0	1.2	1.4		
Kaolinite + Ball Clay	3.8	2.9	1.4	1.4	1.4		

Standard error of ϵ_c is about 9%

value of ϵ_c irrespective of firing temperature, it does not have the same value as Kaolinite + Flint. An examination of the table suggests it could tentatively be divided into two arbitrary groups by the horizontal line. The mean of all the values of ϵ_c in the upper group is 1.07 and in the lower group 1.64 which is significantly different at the 0.1% level.

Thus a change from a point bonded structure to a glassy structure obtained in a formulation by higher firing temperatures, has significantly less effect than a change in formulation. This is remarkable in that it would have been more expected for similar structures to have similar values of ϵ_c. (i.e., point bonded structures would have one set of values of ϵ_c and glassy structures another set, with the table for ϵ_c tending to divide vertically and not horizontally.)

The reason for this is not known and can at present only be considered a feature of brittle ceramics.

4.3.5. Comments.

1) The value of E can usually be related to the features visible in the structure of the material. An exception is the case of Kaolinite + Mullite (100's).

2) The value of E is sensitive to cracks or flaws in the structure which is in agreement with the findings of other workers (section 2.9.1.)* provided one equates flaws with porosity.

3) The value of E follows the values of σ_F more closely than that of K_{Ic}, indicating the material features important in the determination of E are the same ones important in the determination of σ_F.

*p. 33

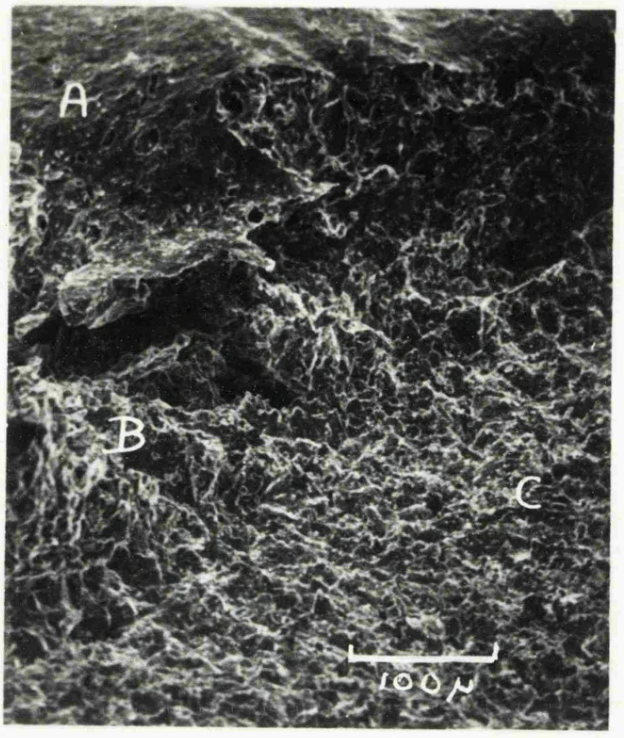

Bottom of Notch

Kaolinite 1450°C

A start of fracture surface with smooth glassy appearance.

B bottom of notch showing possible starting point of fracture.

C cut surface of notch. The glass has drained away into the material exposing the mullite.

Plate 1

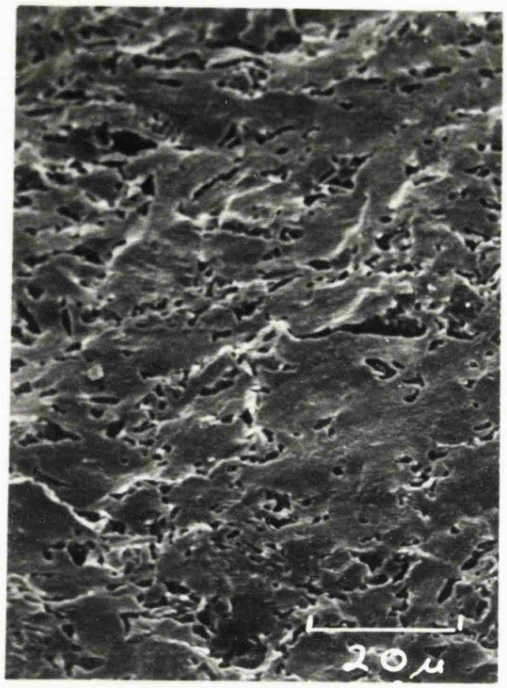

1265°C

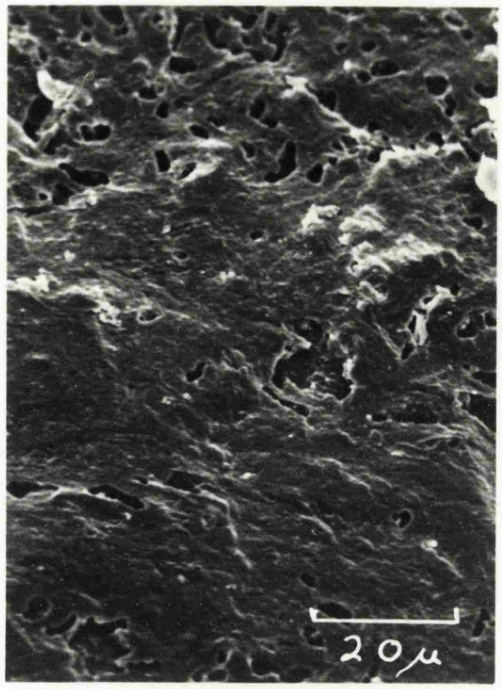

1350°C

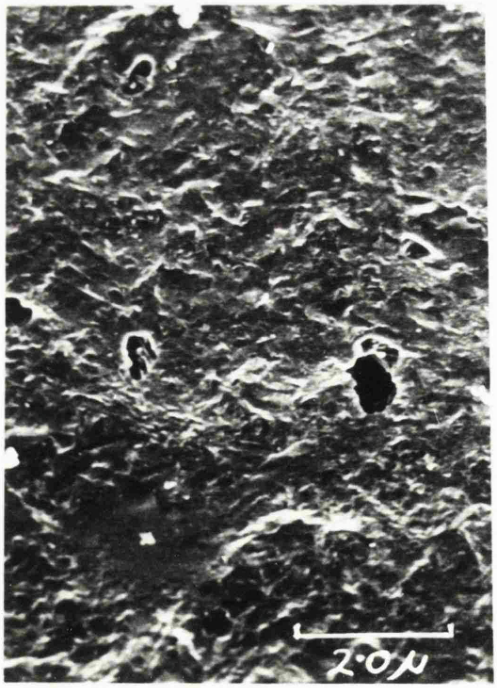

1460°C

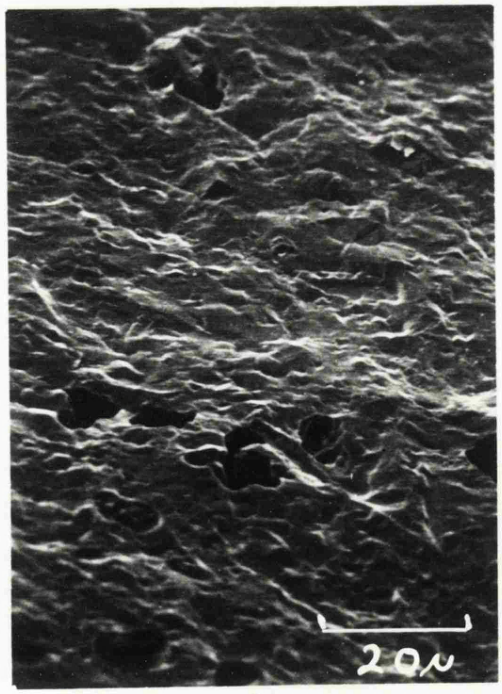

1550°C

Kaolinite

Plate 2

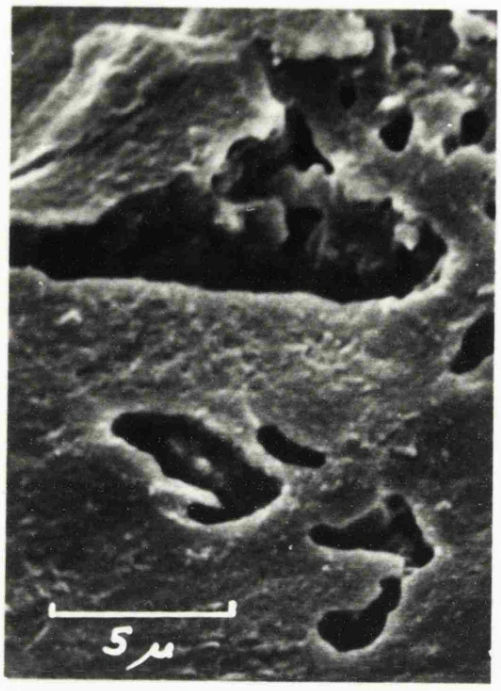

1265°C

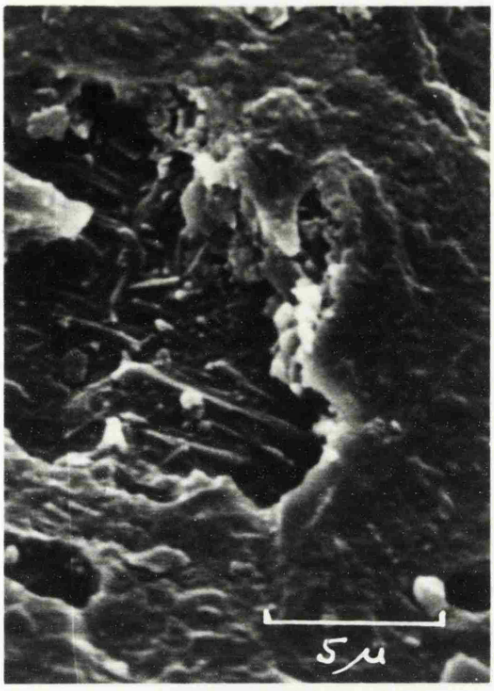

1350°C

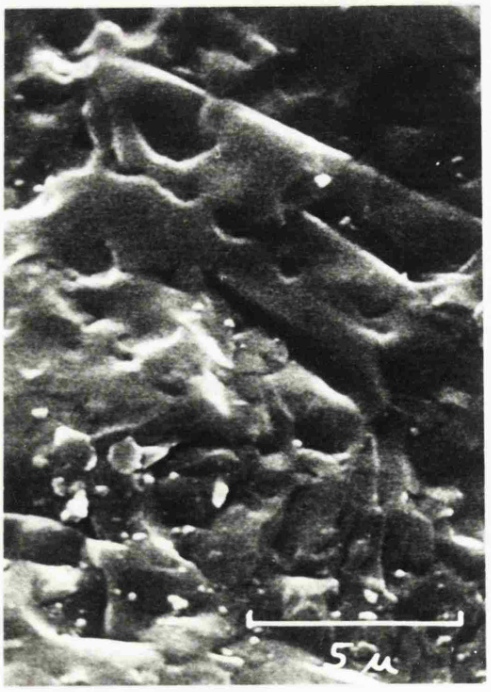

1460°C

1550°C

Kaolinite

Plate 3

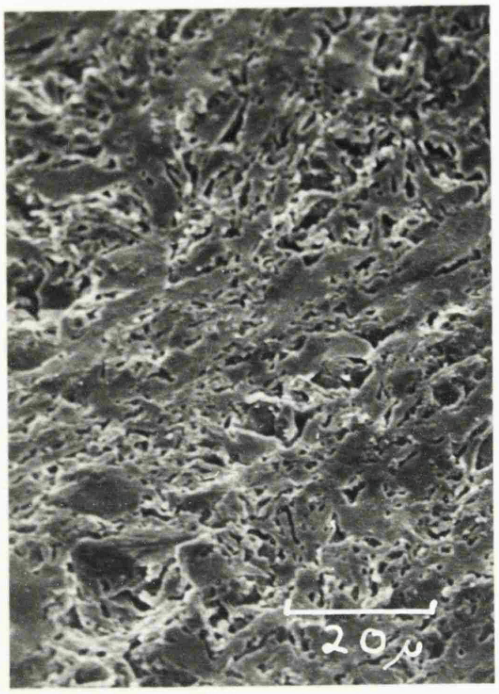

1265°C

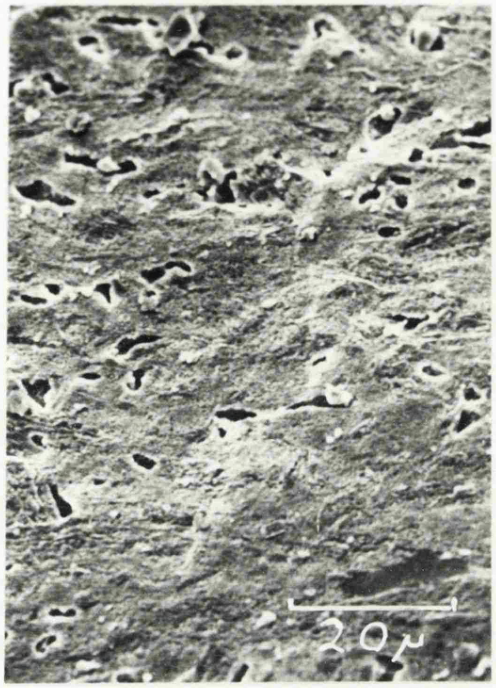

1350°C

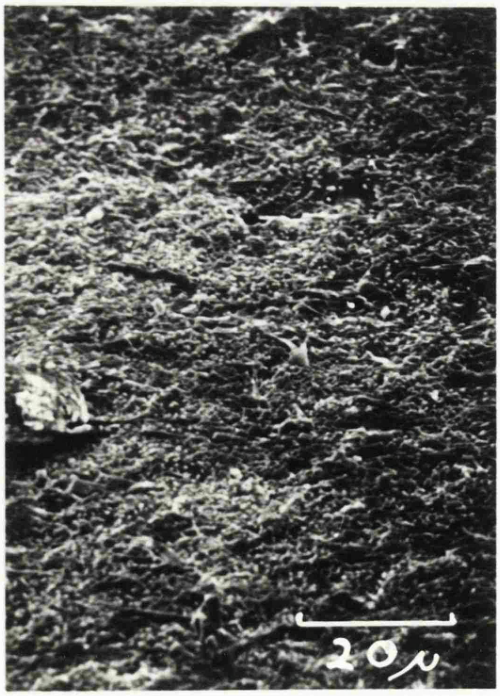

1460°C

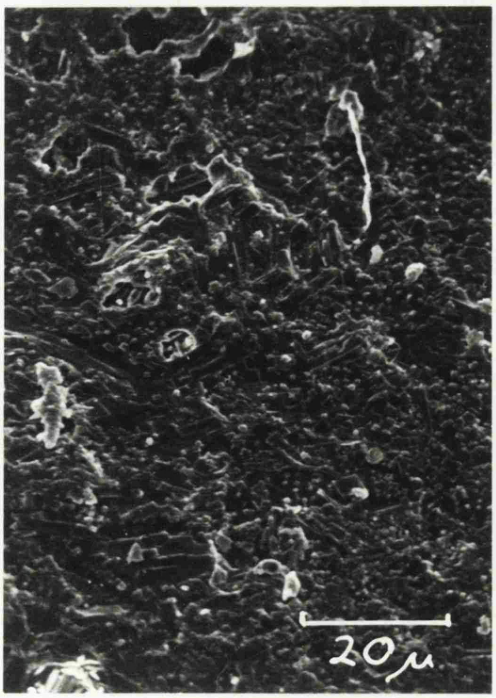

1550°C

Kaolinite

all etched

Plate 4

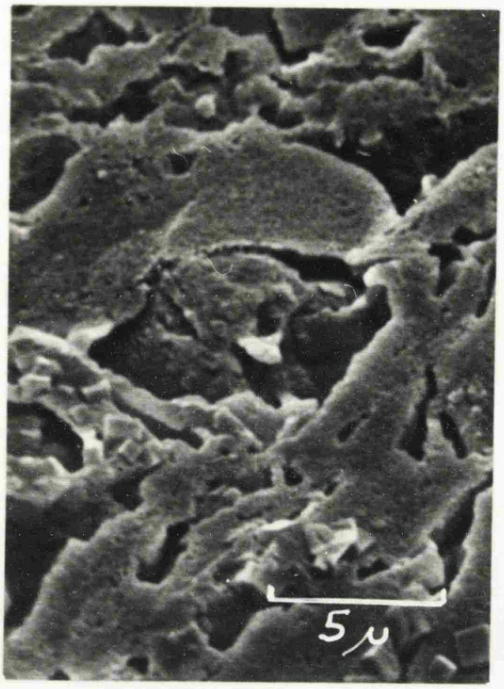

1265°C

1350°C

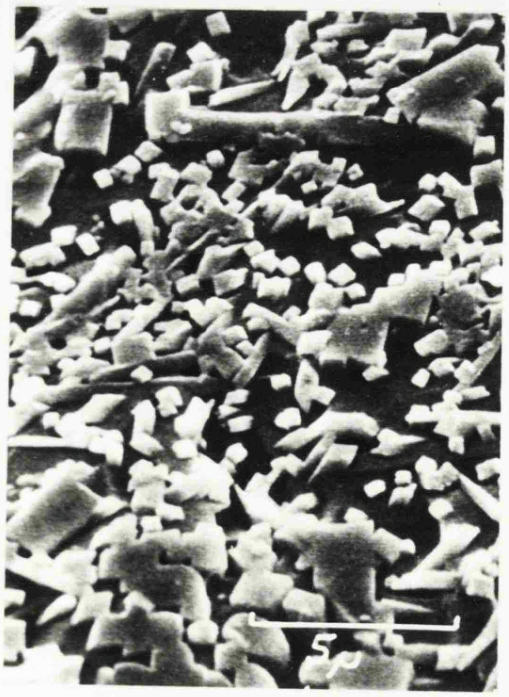

1460°C

1550°C

Kaolinite

all etched

Plate 5

1150°C

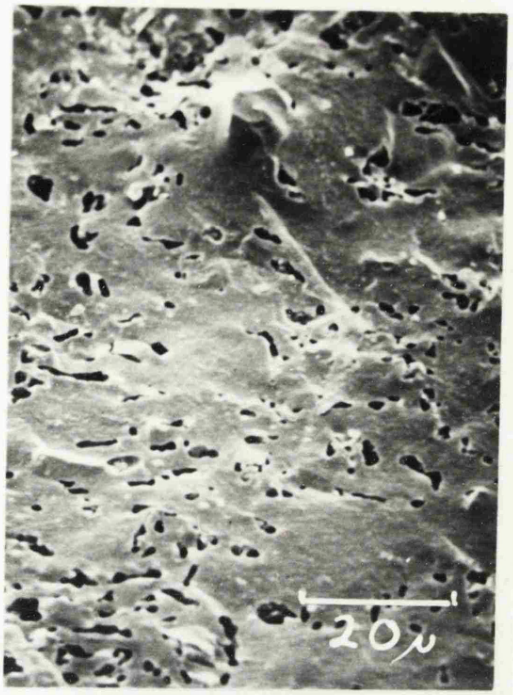

1250°C

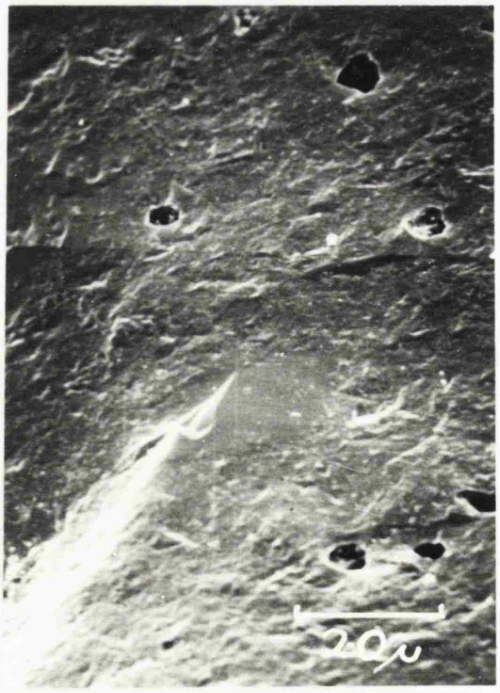

1350°C

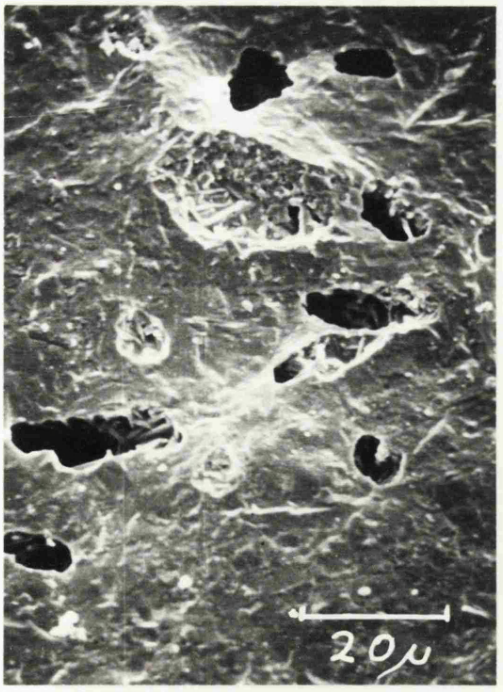

1450°C

Kaolinite + Felspar

Plate 6

1150°C

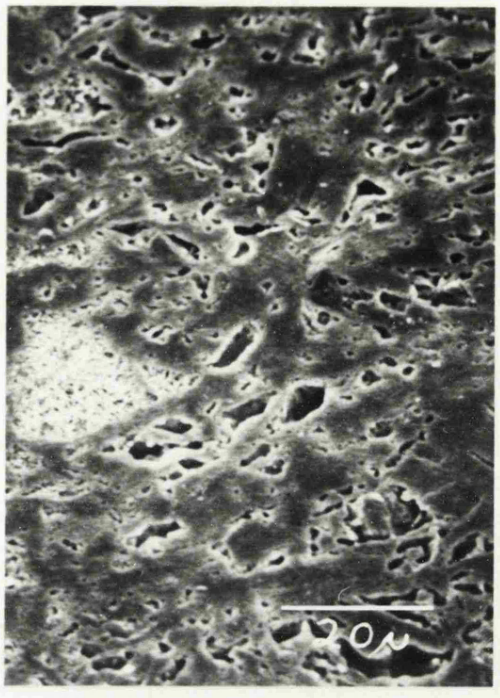

1250°C

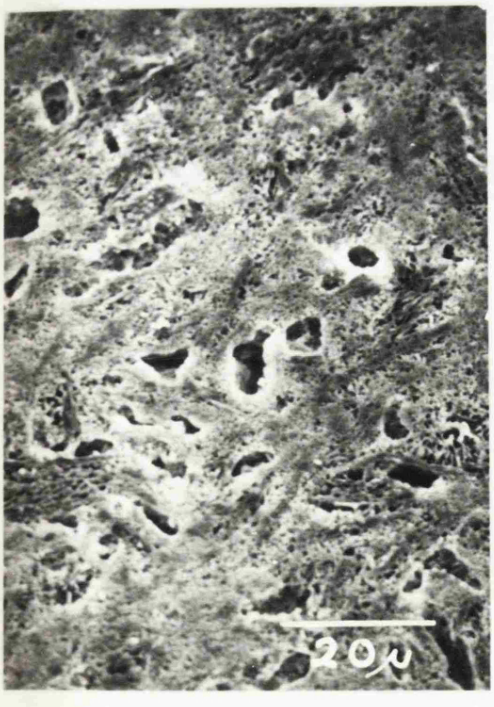

1350°C

1450°C

Kaolinite + Felspar all etched

Plate 7

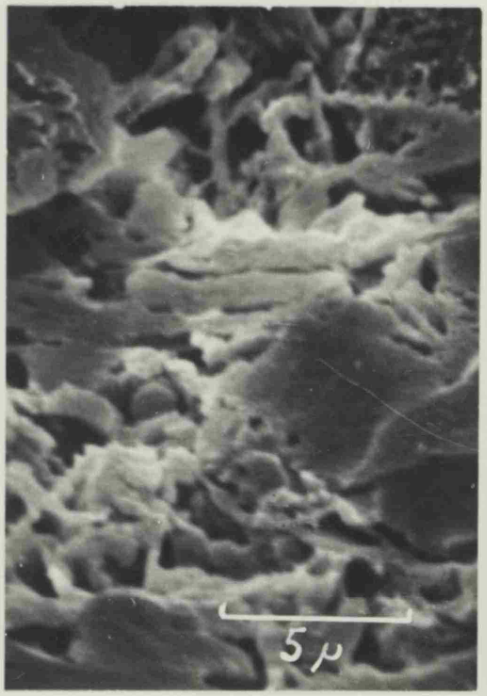

1150°C

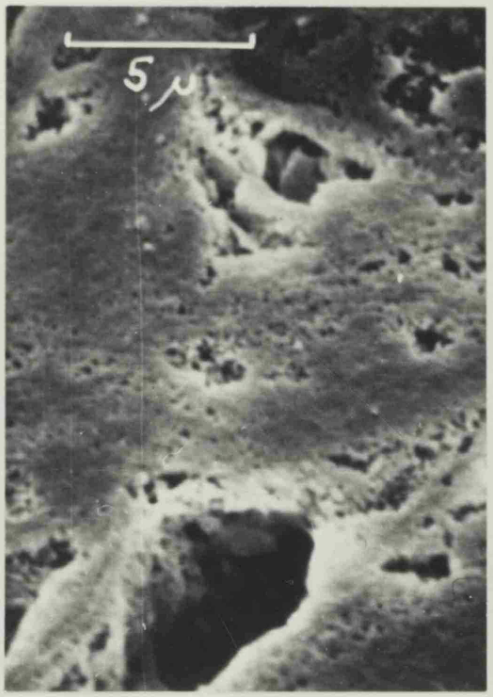

1250°C

1350°C

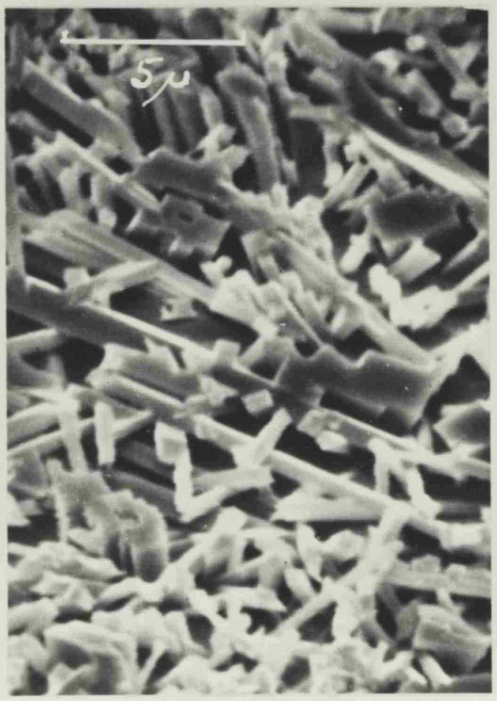

1450°C

Kaolinite + Felspar

all etched

Plate 8

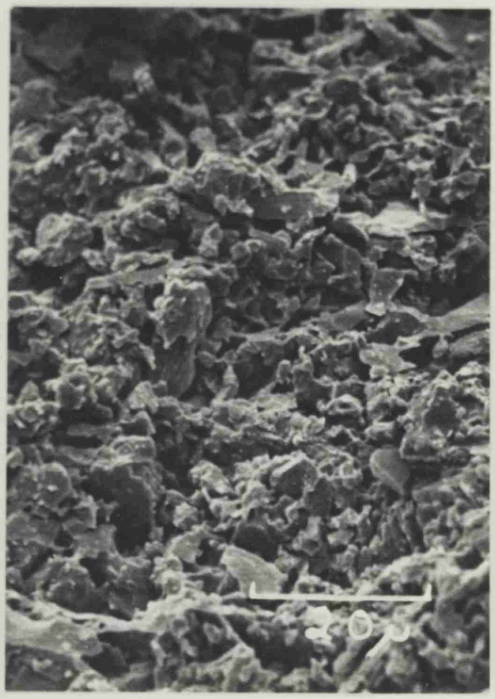

1250°C

1350°C

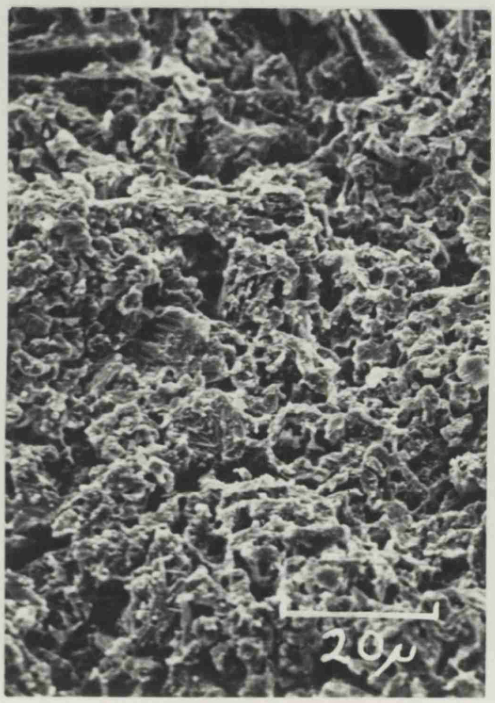

1450°C

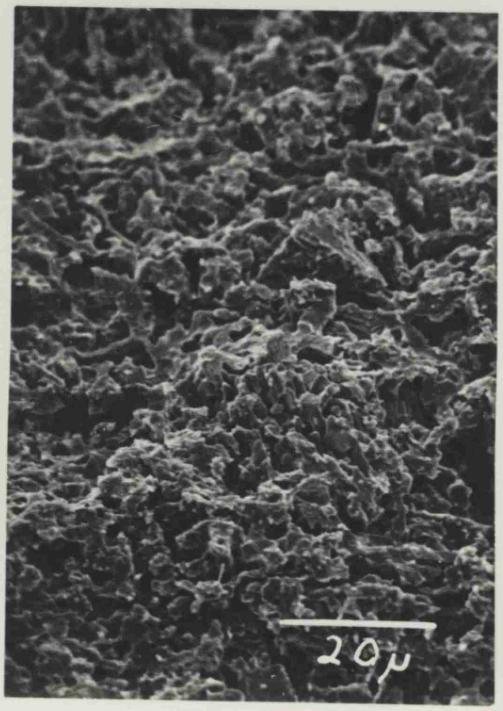

1550°C

Kaolinite + Alumina (4)

Plate 9

1265°C

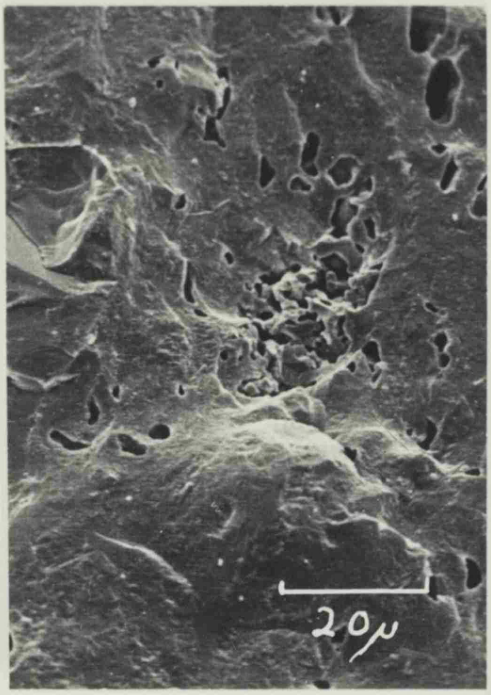

1350°C

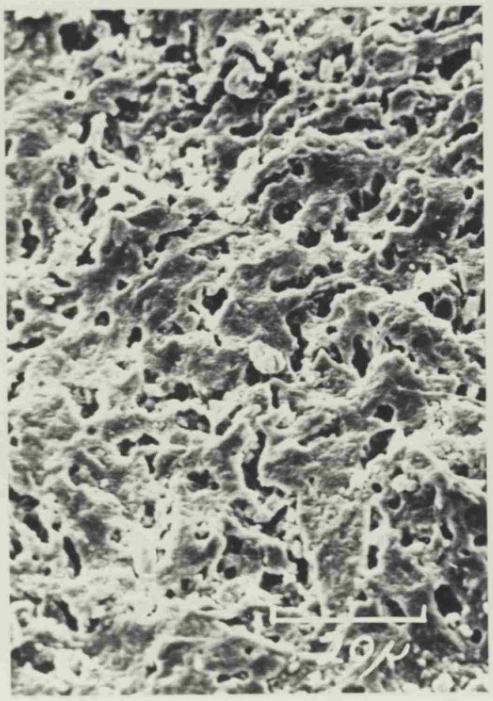

1460°C

1550°C

Kaolinite + Quartz

Plate 10

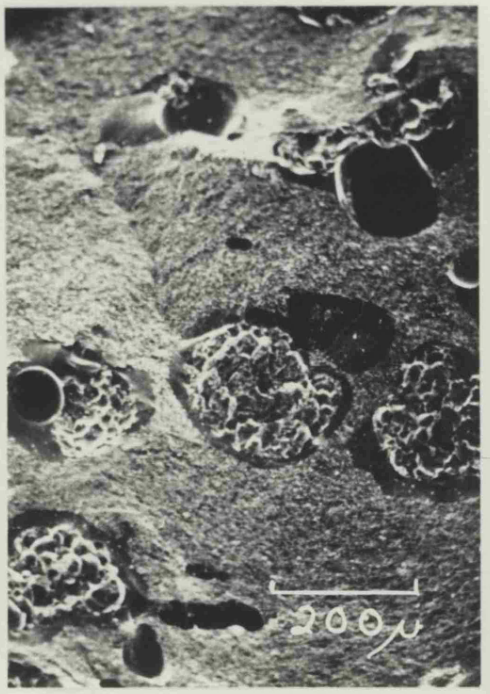

1550°C

Kaolinite + Sand

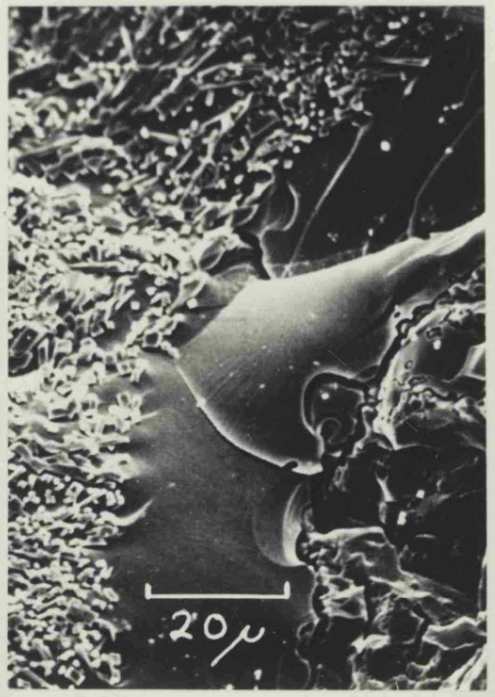

1550°C

both etched

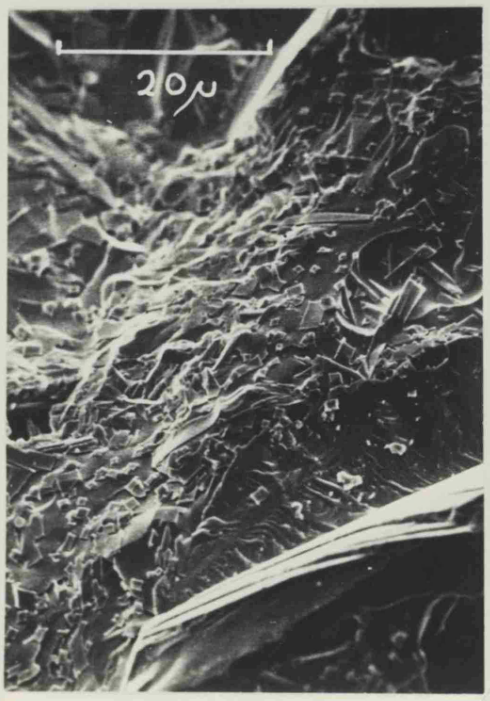

1550°C

Kaolinite + Zircon flour

1550°C

both etched

Plate 11

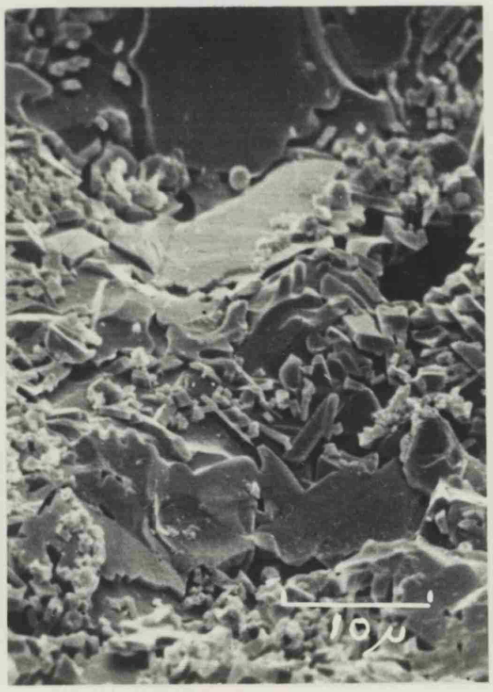

1450°C etched

1550°C

Kaolinite + Mullite (100's)

1450°C

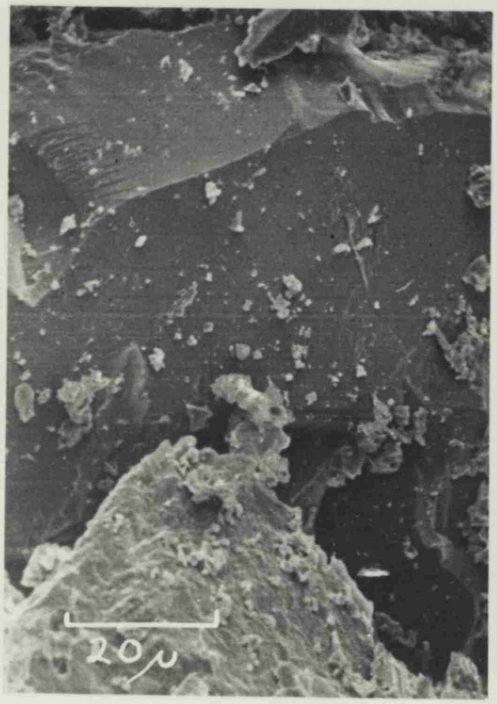

1450°C

Kaolinite + Mullite (22's)

Plate 12

1350°C

Ball clay

1350°C etched

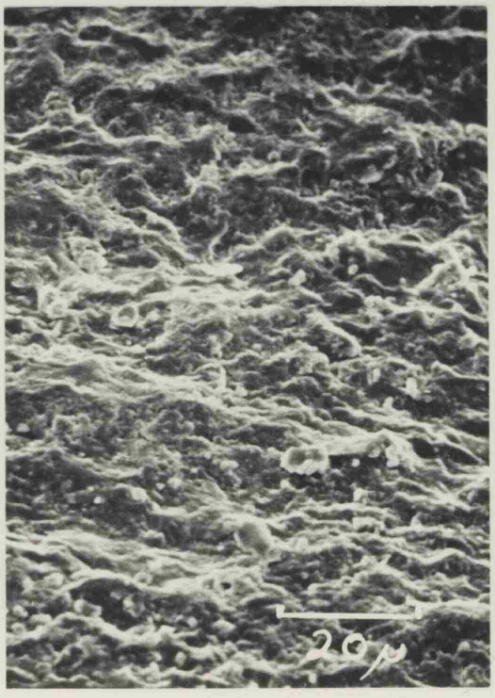

1150°C

Kaolinite + Ball clay

1150°C etched

Plate 13

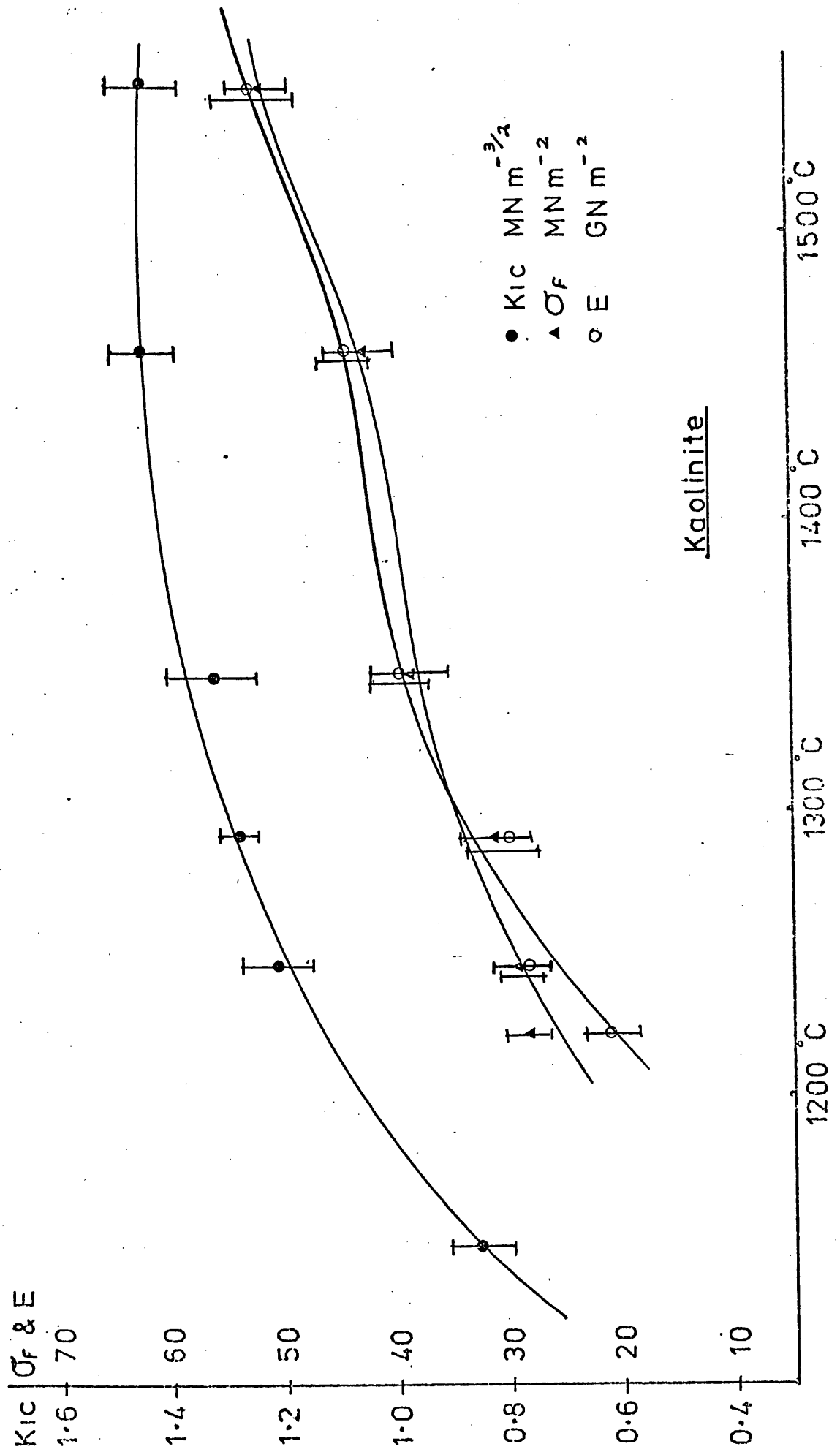
Kaolinite
• K_{IC} MN m$^{-3/2}$
▲ σ_F MN m^{-2}
○ E GN m^{-2}
1200 °C
1300 °C
1400 °C
1500 °C
K_{IC} | σ_F & E
1·6
1·4
1·2
1·0
0·8
0·6
0·4
70
60
50
40
30
20
10

Graph 1a

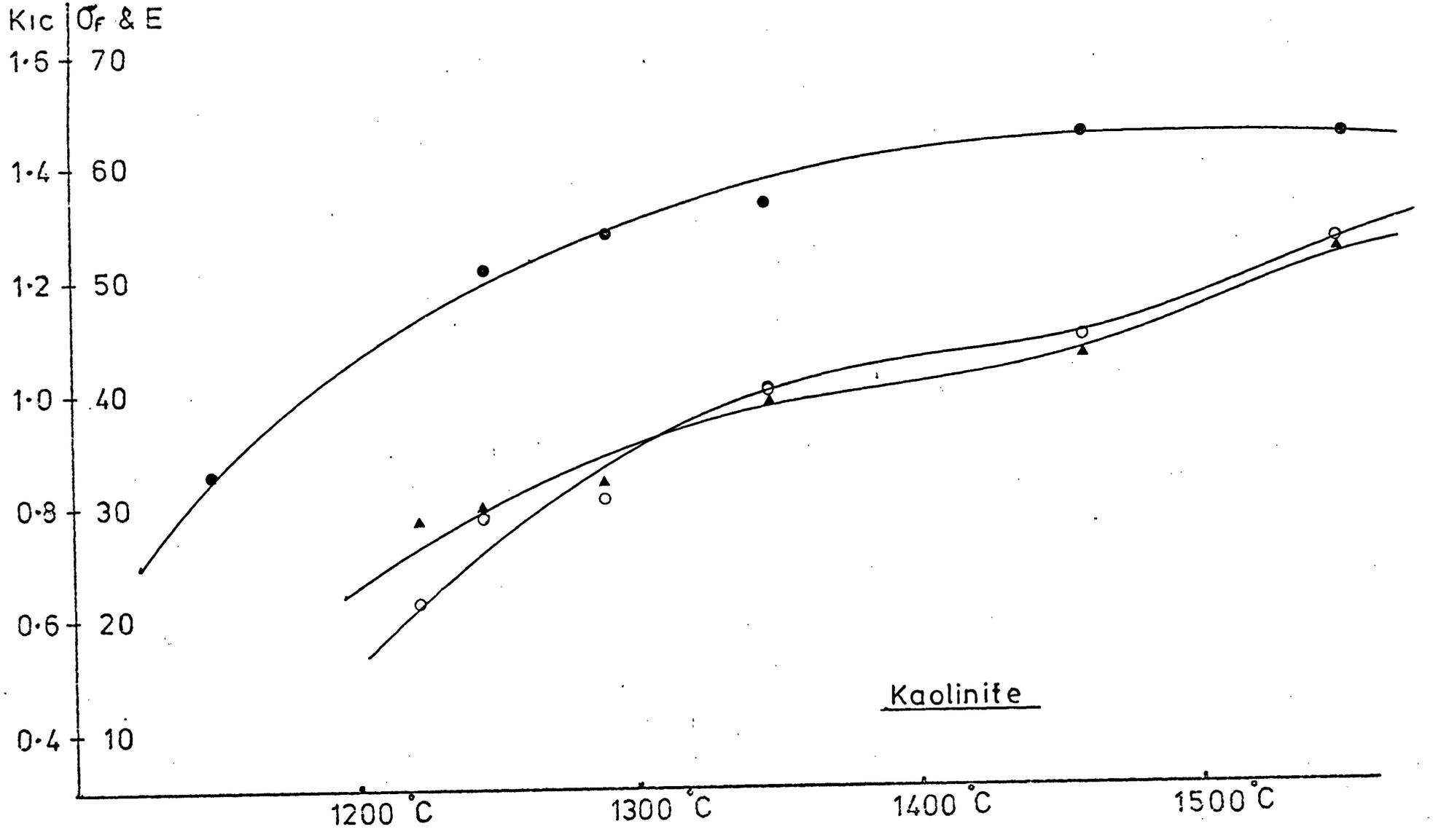
Kic
σ_f & E
1·6
1·4
1·2
1·0
0·8
0·6
0·4
70
60
50
40
30
20
10
1200 °C
1300 °C
1400 °C
1500 °C
Kaolinite

Graph 1b

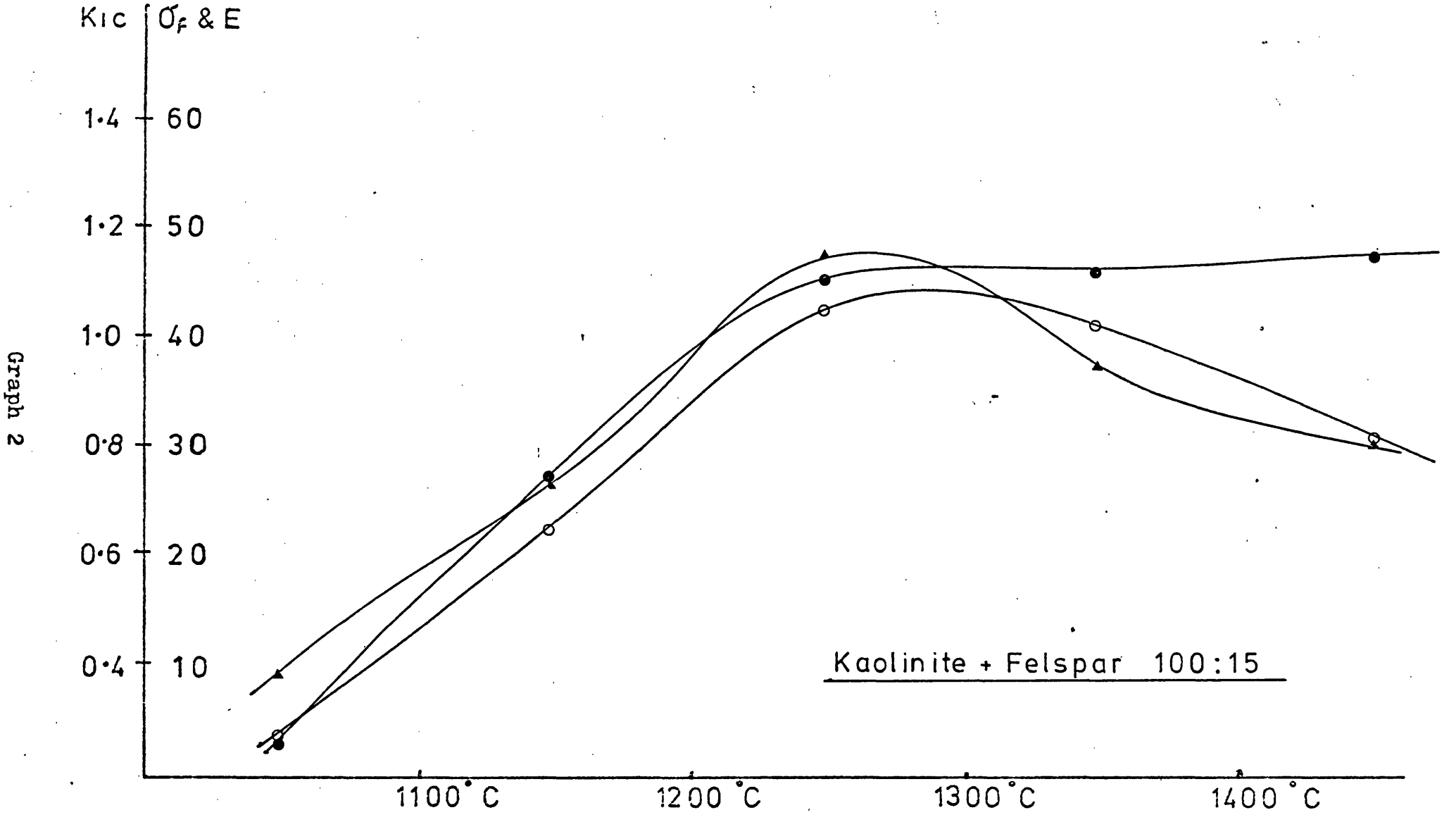
Kic
σ_f & E
1·4
1·2
1·0
0·8
0·6
0·4
60
50
40
30
20
10
1100° C
1200 °C
1300 °C
1400 °C
Kaolinite + Felspar 100:15

Graph 2

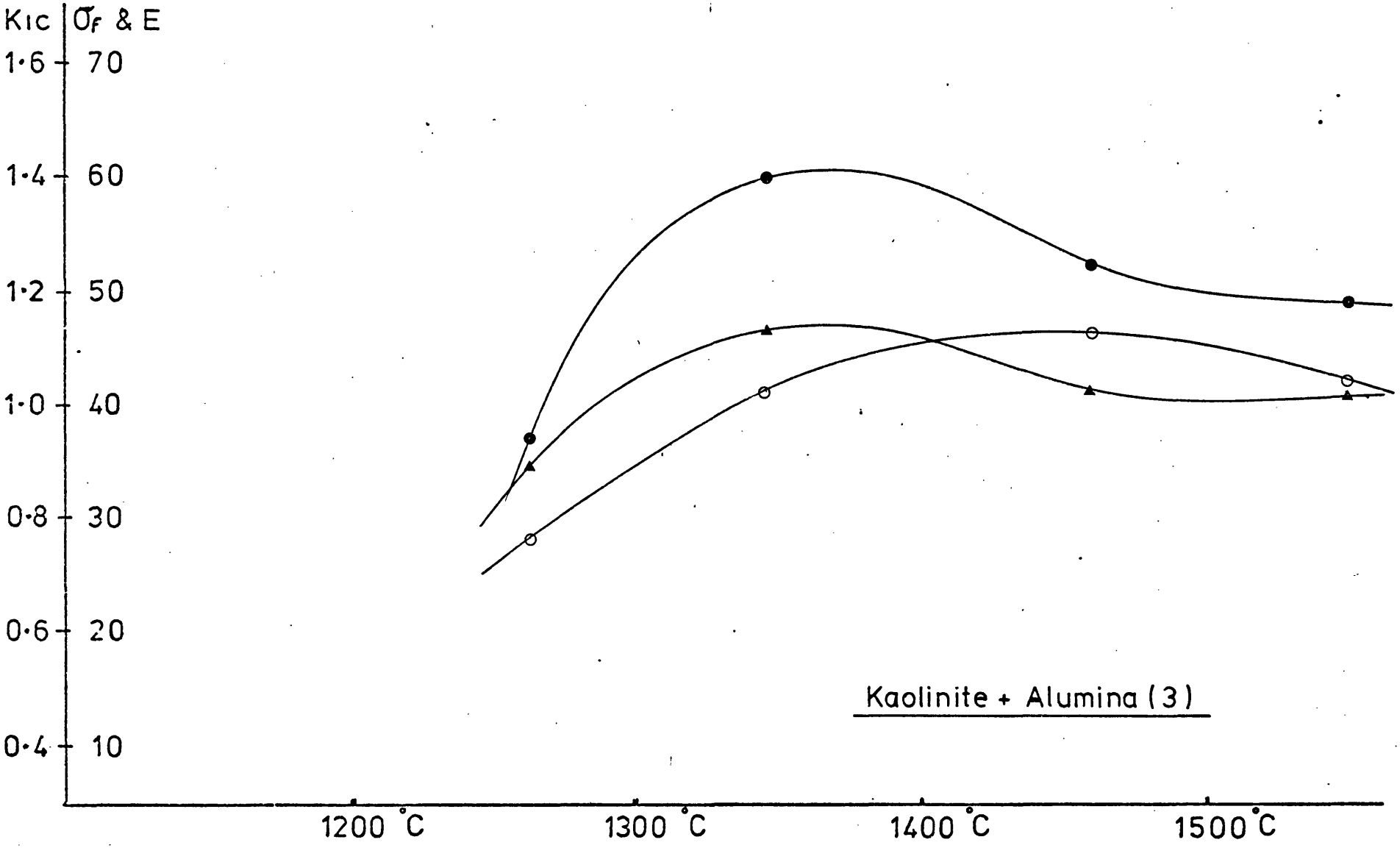
Kic
σ_f & E
1·6
1·4
1·2
1·0
0·8
0·6
0·4
70
60
50
40
30
20
10
1200 °C
1300 °C
1400 °C
1500 °C
Kaolinite + Alumina (3)

Graph 3

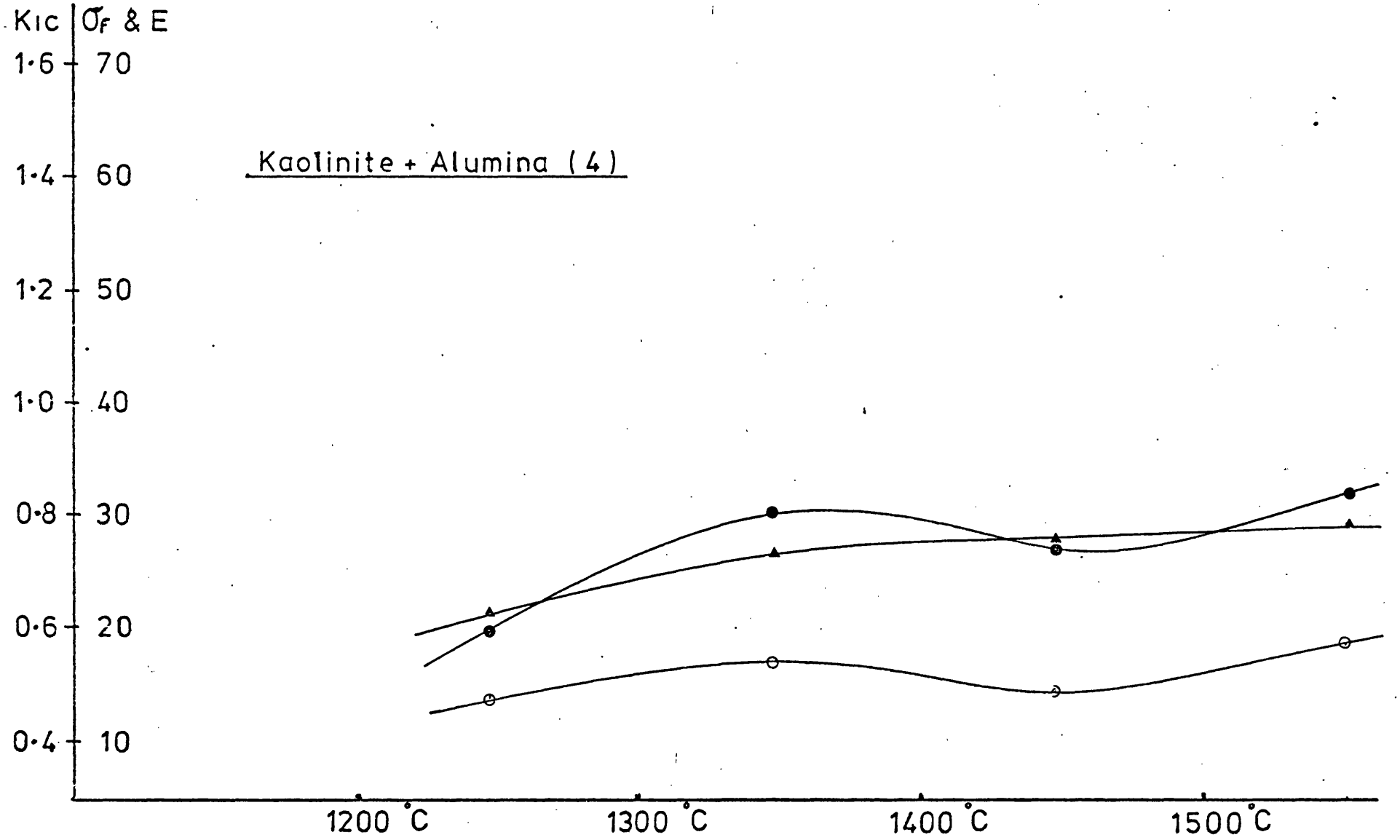
Kaolinite + Alumina (4)
Kic
σ_F & E
1·6
1·4
1·2
1·0
0·8
0·6
0·4
70
60
50
40
30
20
10
1200 °C
1300 °C
1400 °C
1500 °C

Graph 4

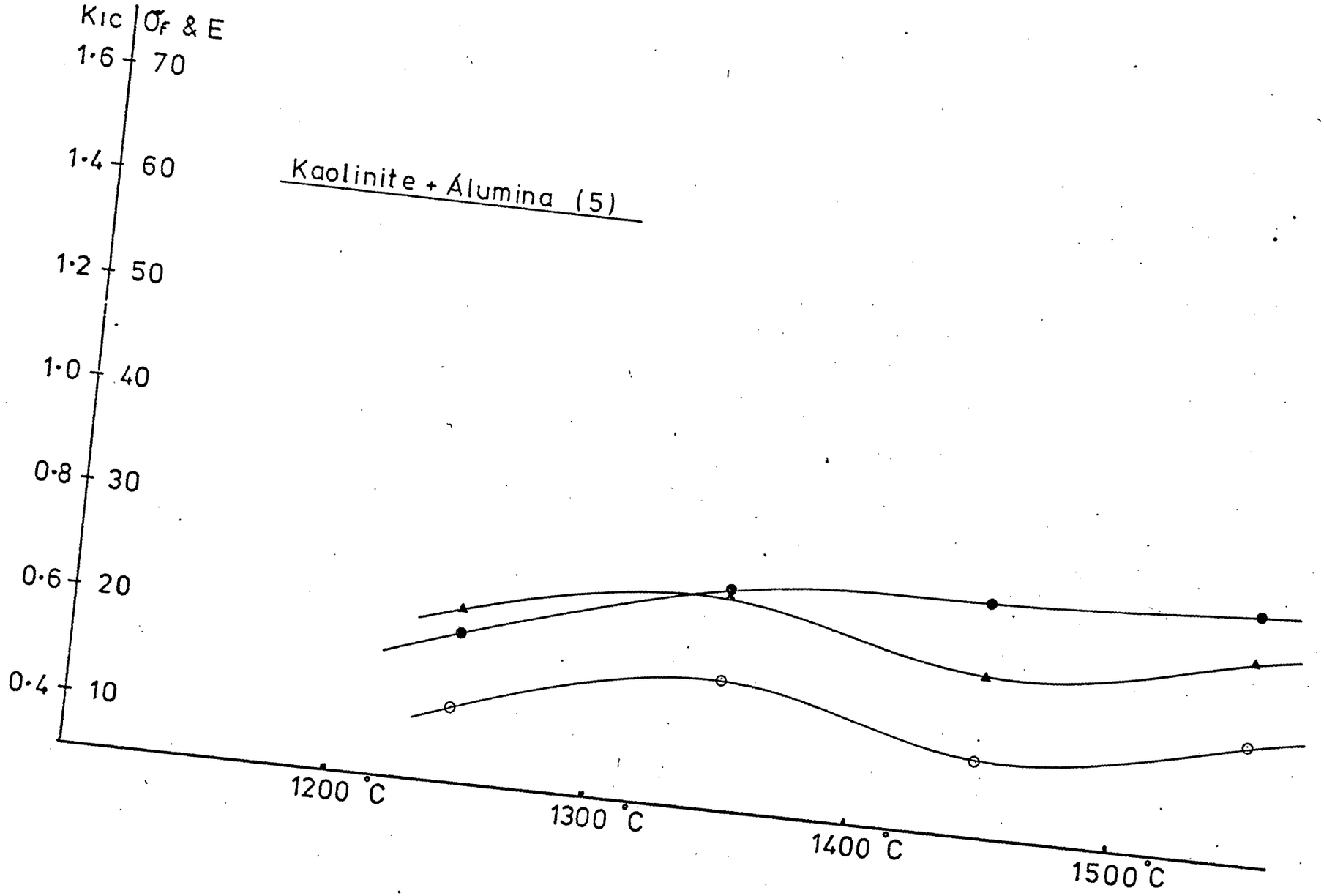
Kaolinite + Alumina (5)
Kic
σ_f & E
1·6
1·4
1·2
1·0
0·8
0·6
0·4
70
60
50
40
30
20
10
1200 °C
1300 °C
1400 °C
1500 °C

Graph 5

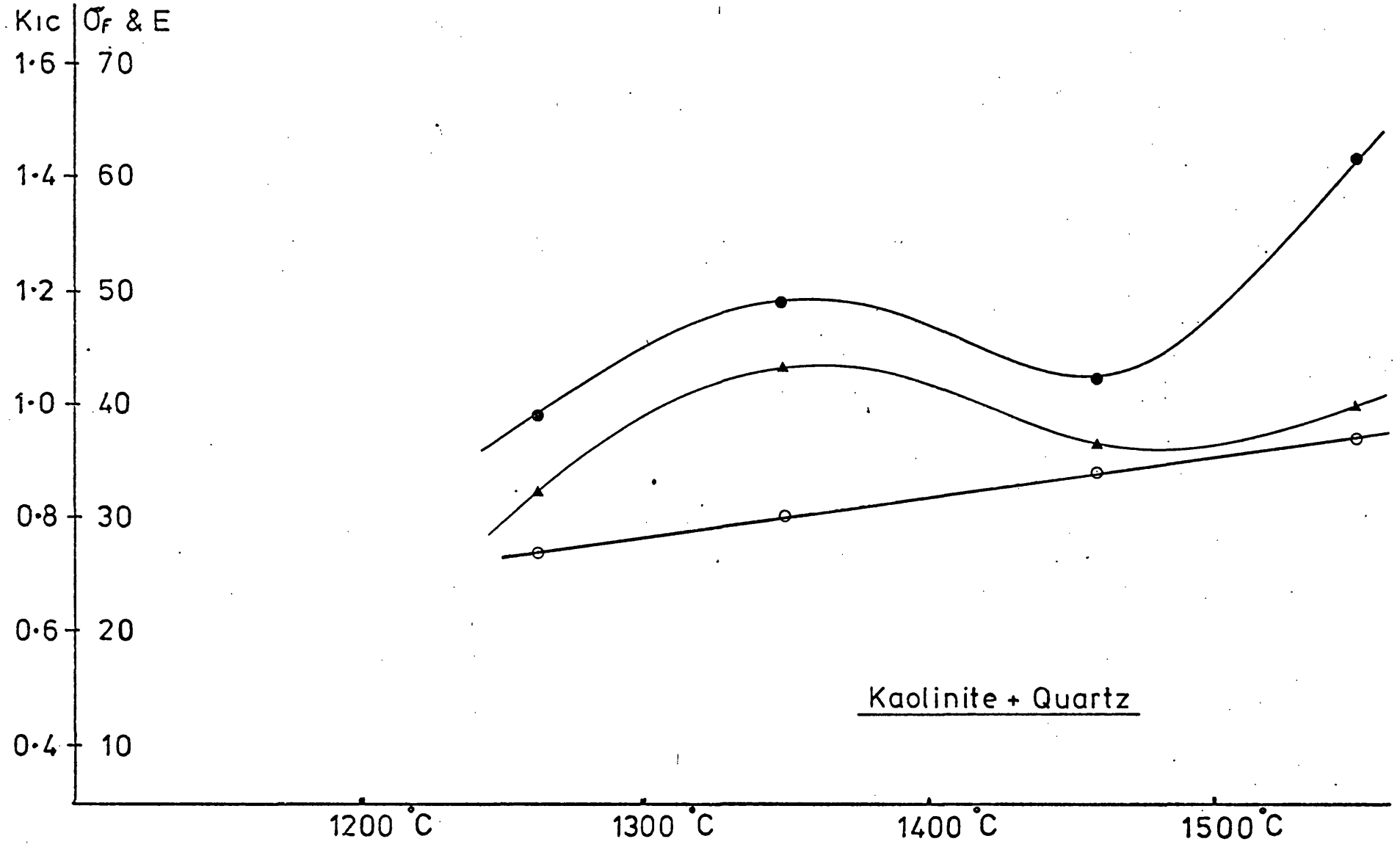
Kic
σ_F & E
1·6
1·4
1·2
1·0
0·8
0·6
0·4
70
60
50
40
30
20
10
1200 °C
1300 °C
1400 °C
1500 °C
Kaolinite + Quartz

Graph 6

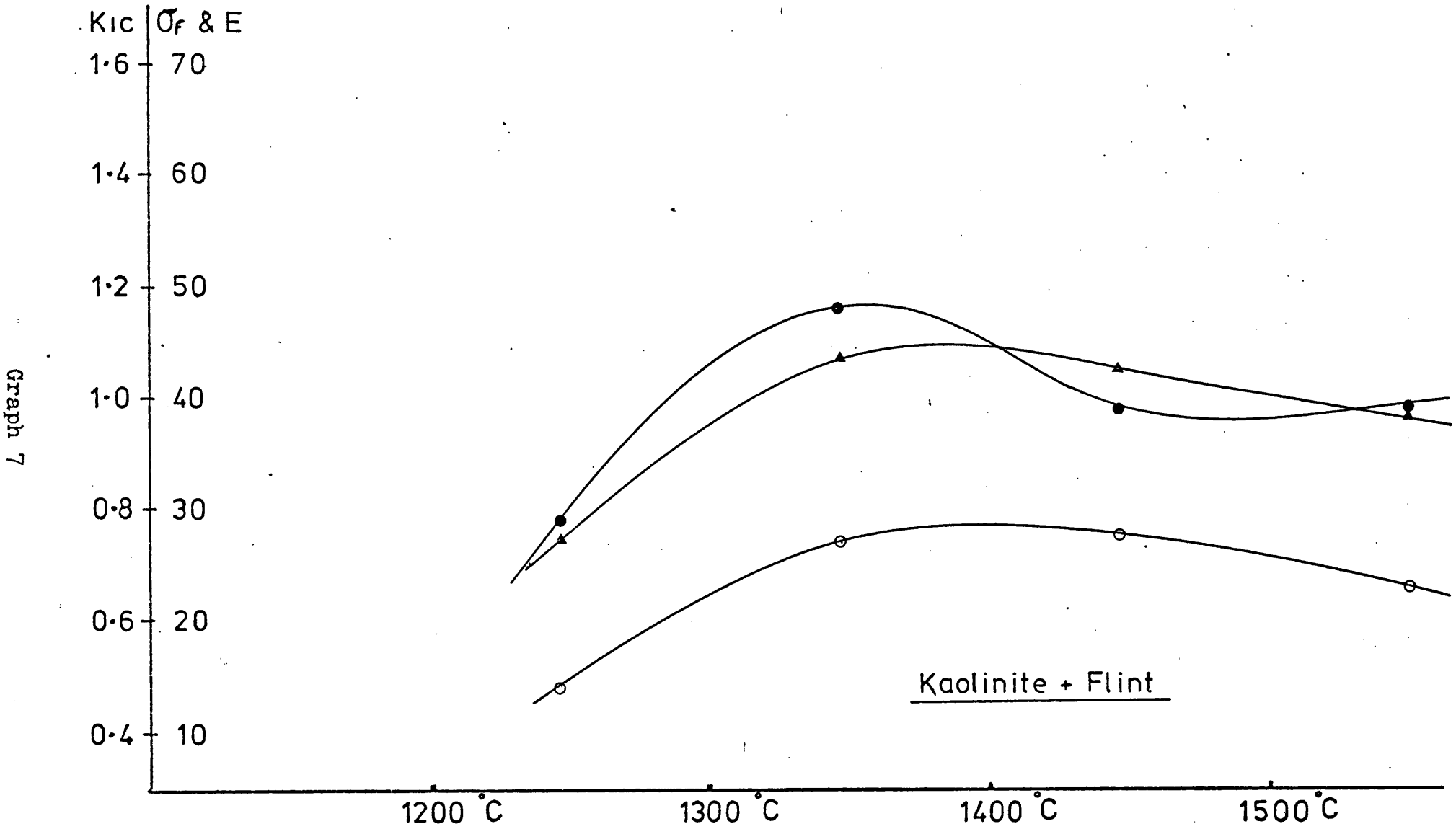
Kic
σ_f & E
1·6
1·4
1·2
1·0
0·8
0·6
0·4
70
60
50
40
30
20
10
1200 °C
1300 °C
1400 °C
1500 °C
Kaolinite + Flint

Graph 7

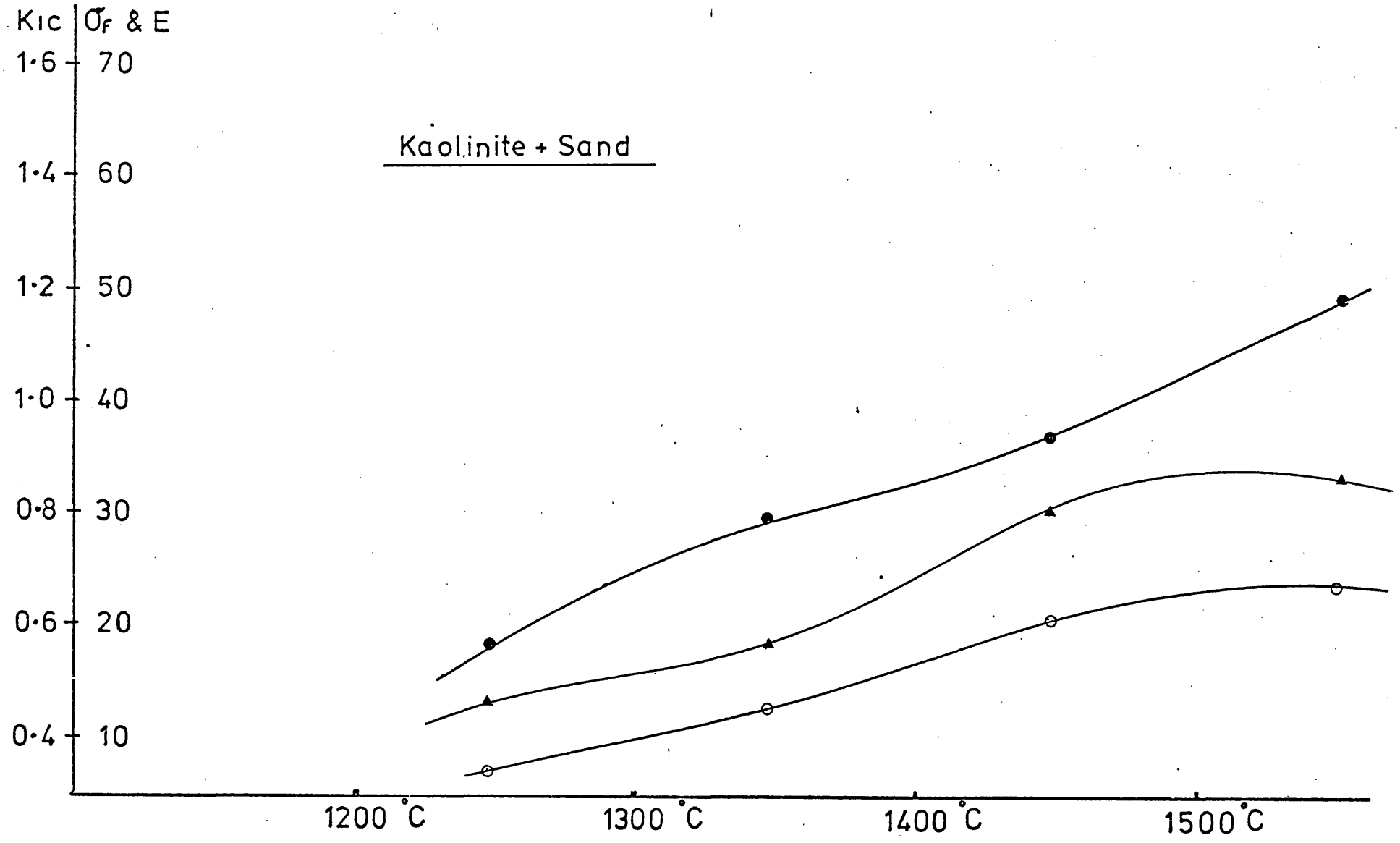
Kaolinite + Sand
Kic
σ_f & E
1·6
1·4
1·2
1·0
0·8
0·6
0·4
70
60
50
40
30
20
10
1200 °C
1300 °C
1400 °C
1500 °C

Graph 8

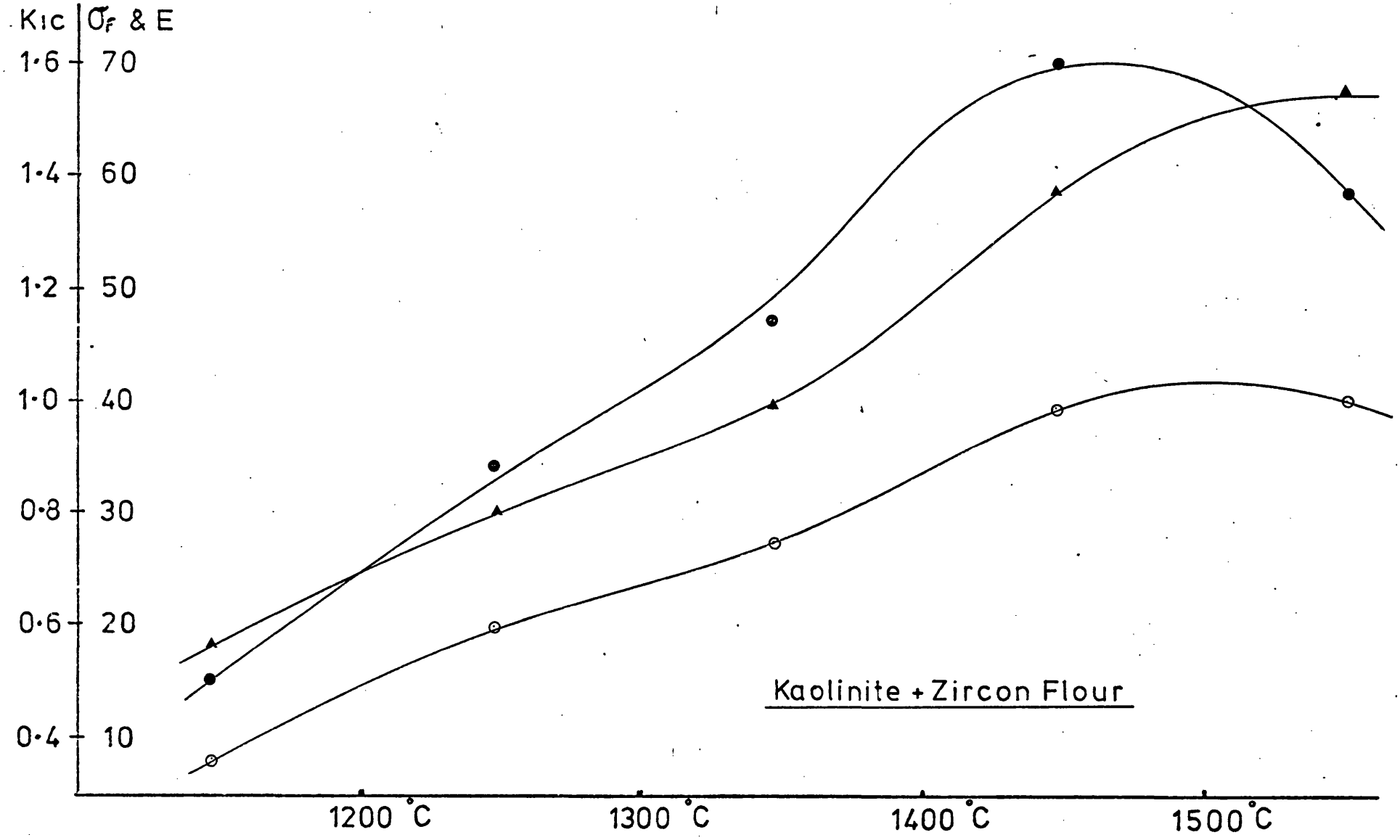
Kic
σ_f & E
1·6
1·4
1·2
1·0
0·8
0·6
0·4
70
60
50
40
30
20
10
1200 °C
1300 °C
1400 °C
1500 °C
Kaolinite + Zircon Flour

Graph 9

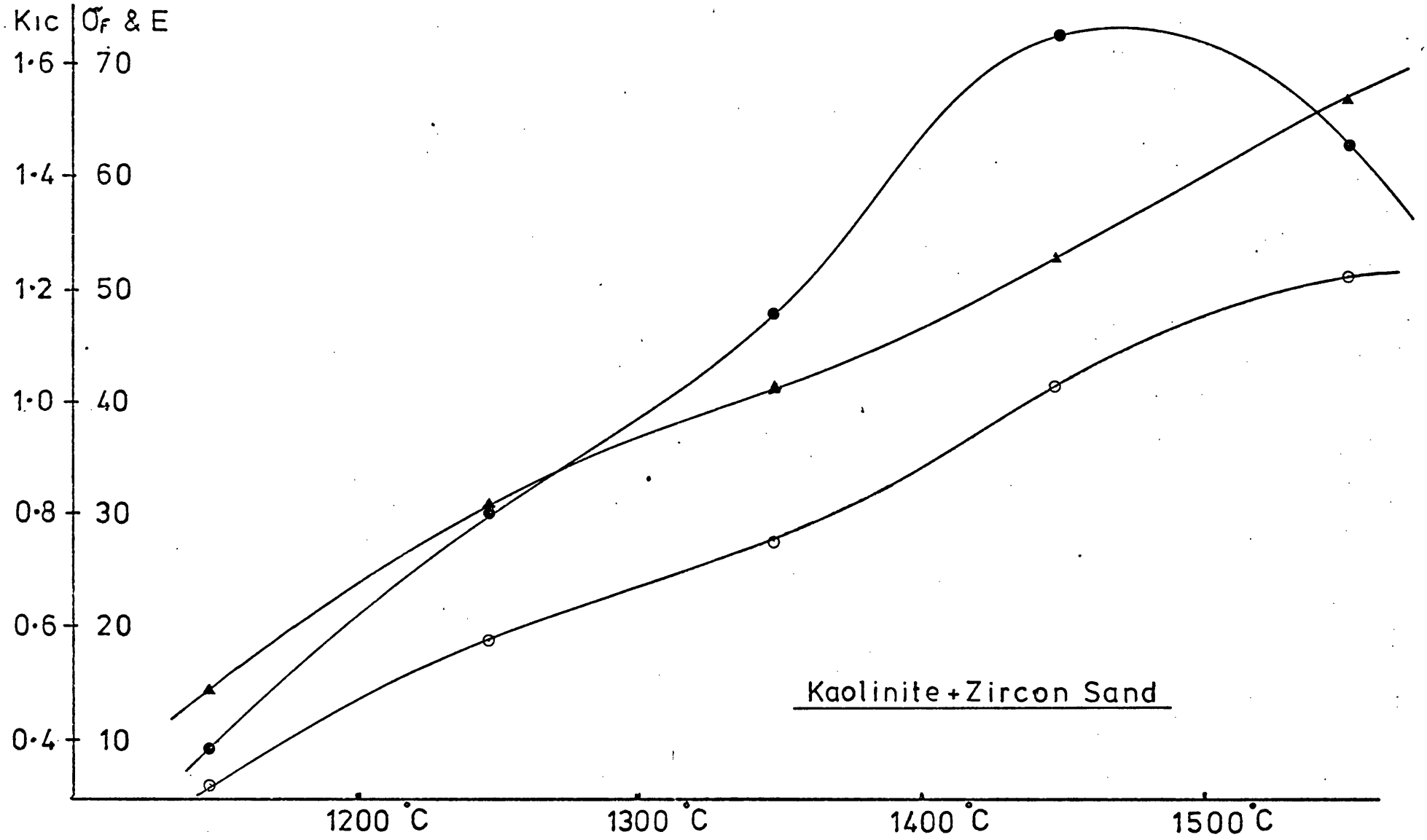
Kic
σ_F & E
1·6
1·4
1·2
1·0
0·8
0·6
0·4
70
60
50
40
30
20
10
1200 °C
1300 °C
1400 °C
1500 °C
Kaolinite + Zircon Sand

Graph 10

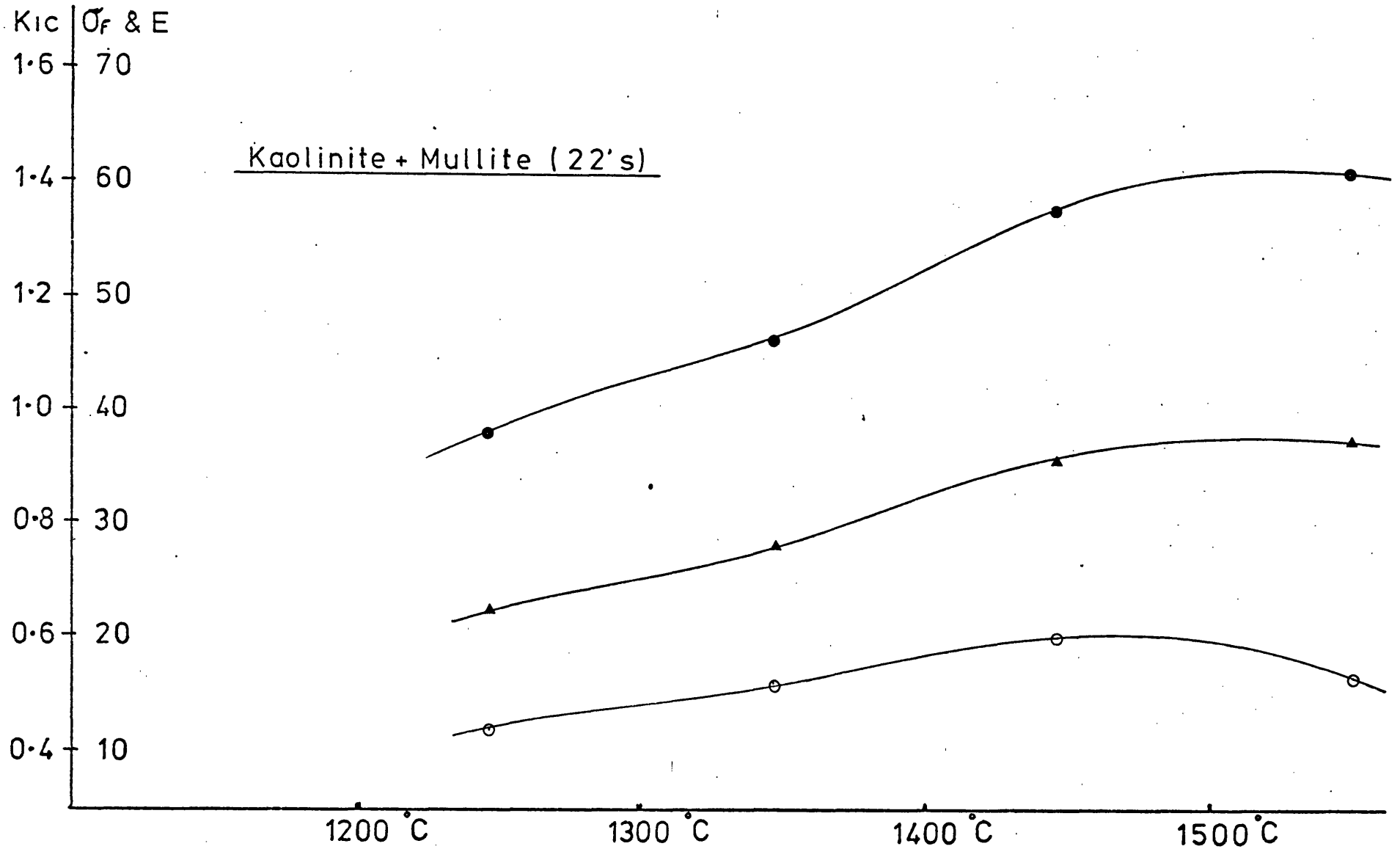
Kic
σ_F & E
1·6
1·4
1·2
1·0
0·8
0·6
0·4
70
60
50
40
30
20
10
Kaolinite + Mullite (22's)
1200 °C
1300 °C
1400 °C
1500 °C

Graph 11

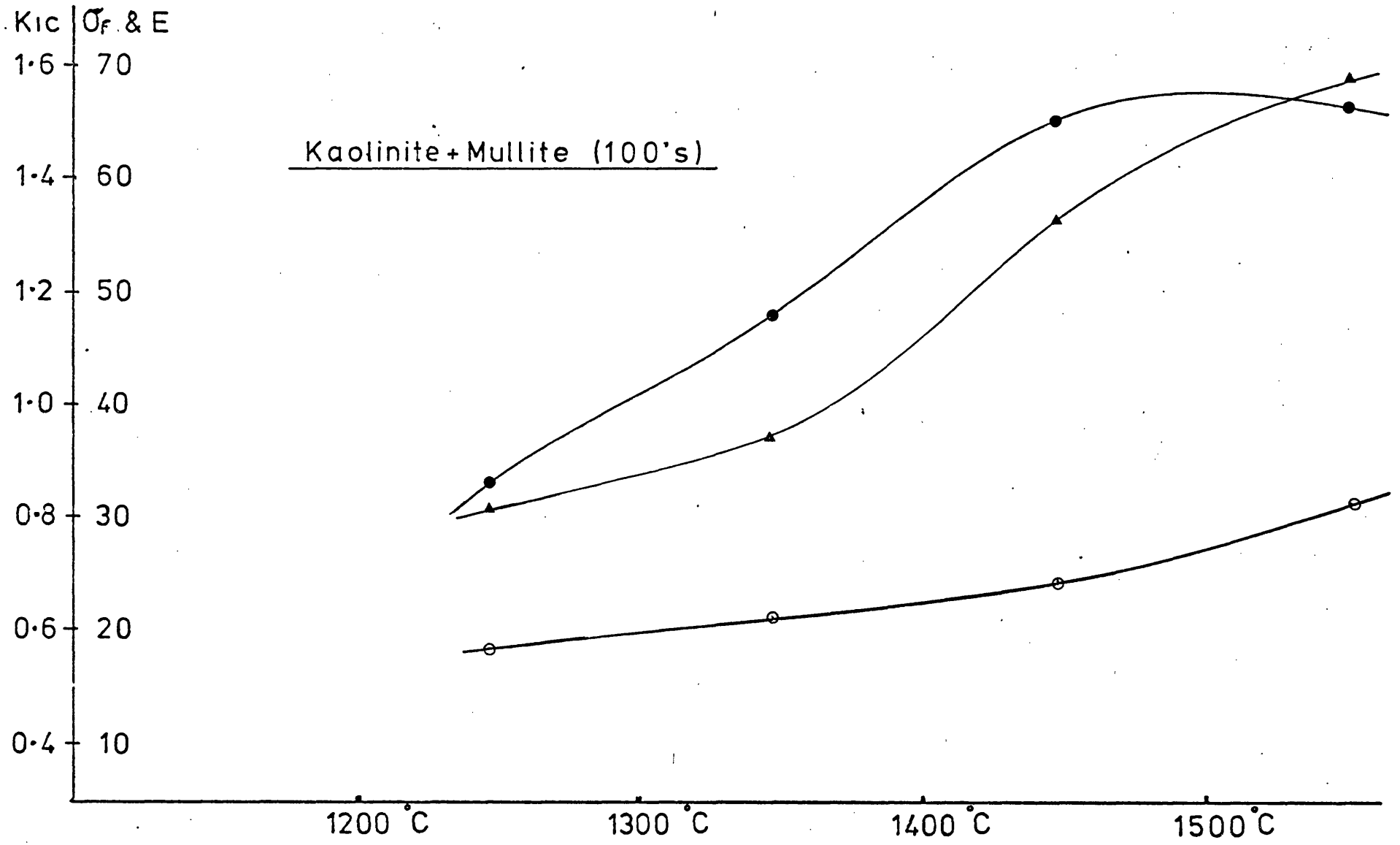
Kaolinite + Mullite (100's)
Kic
σ_f & E
1·6
1·4
1·2
1·0
0·8
0·6
0·4
70
60
50
40
30
20
10
1200 °C
1300 °C
1400 °C
1500 °C

Graph 12

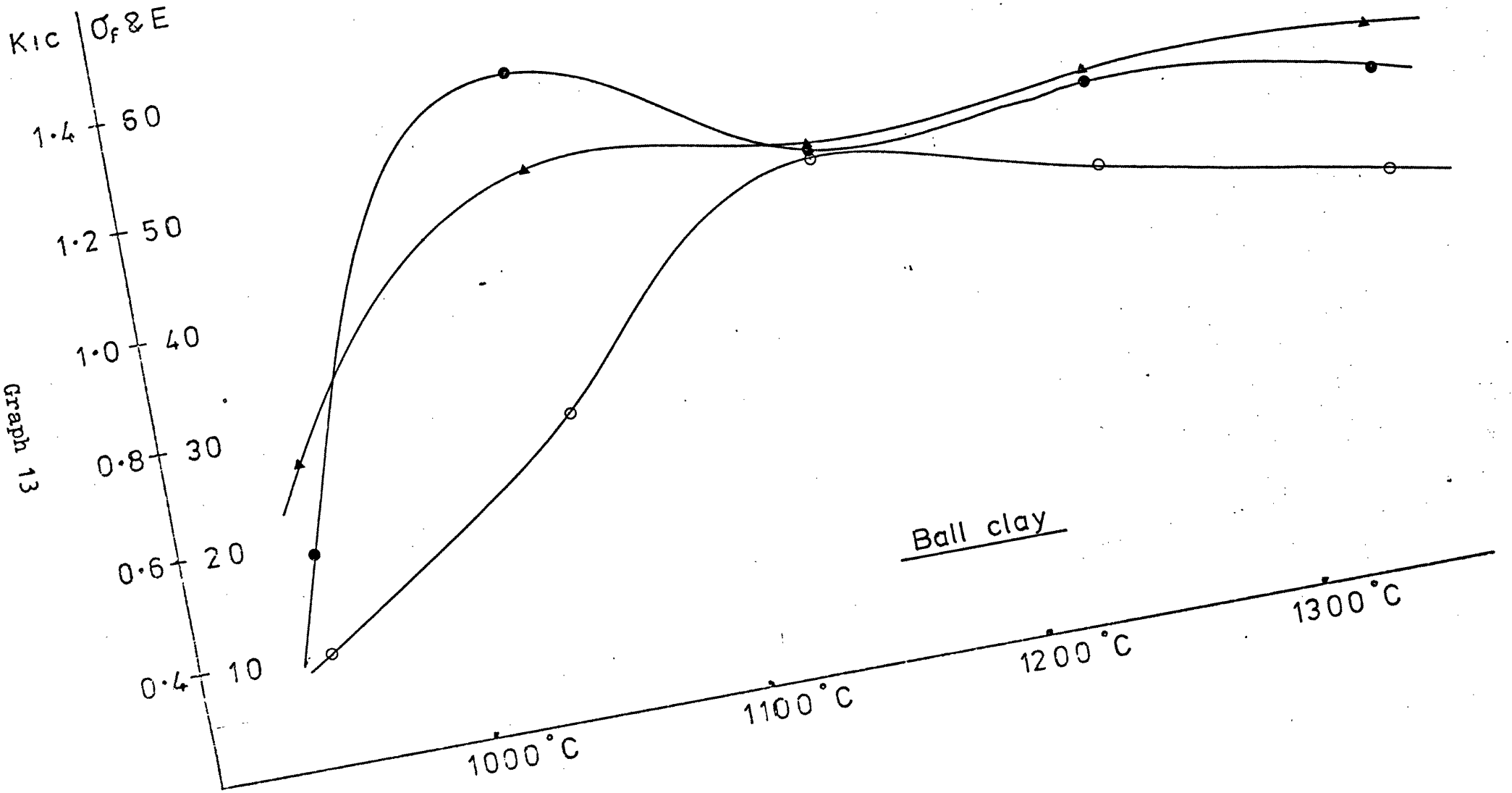
KIC
σ_f & E
1·4
1·2
1·0
0·8
0·6
0·4
60
50
40
30
20
10
1000 °C
1100 °C
1200 °C
1300 °C
Ball clay

Graph 13

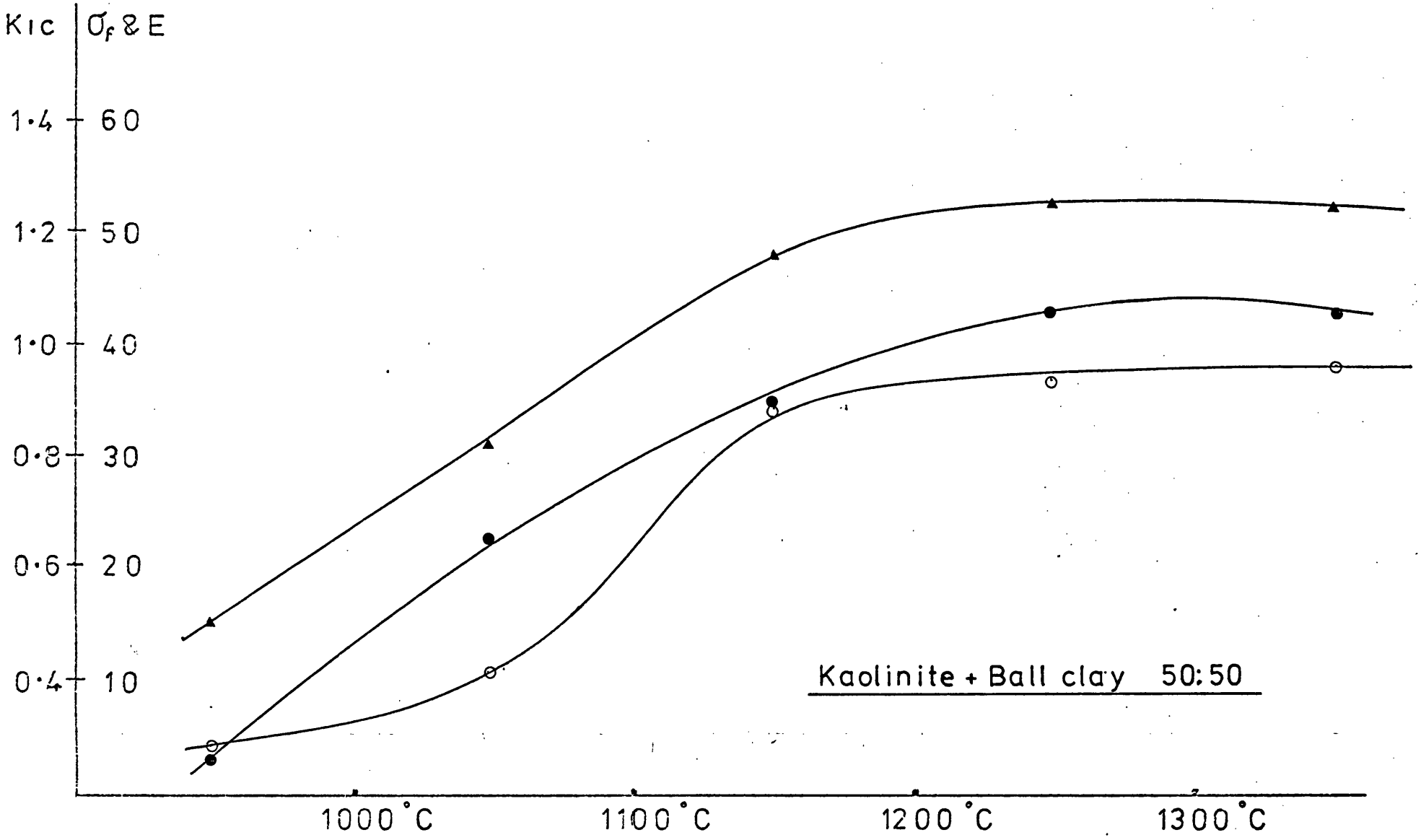
Kic
σ_f & E
1·4
1·2
1·0
0·8
0·6
0·4
60
50
40
30
20
10
1000 °C
1100 °C
1200 °C
1300 °C
Kaolinite + Ball clay 50:50

Graph 14

5. General Discussion

The previous chapter showed that the resistance of a polyphase clay bodied ceramic to fracture was related to the structure of the material. This was found to be the case whether the strength was measured in terms of the fracture stress σ_F or the critical stress intensity K_{ic}. It clearly throws some doubt on the customary view that K_{ic} measures the intrinsic strength of the material whilst σ_F is dependent on surface cracks or random flaws.

The present chapter aims to consider these points with particular reference to their implications for some of the equations previously defined and the findings of other workers.

5.1. Resumé of the Theoretical Approach.

The theoretical approaches to fracture mechanics discussed in chapter (2) either assumed matter to be a brittle elastic continuum with the equations of Inglis and Westergaard or as with Griffith treated the situation on energy grounds and assumed that at some distance ahead of the crack tip, continuum mechanics could be applied.

Individual examination of the equations shows that their extension to a real particular material will always impose limitations on one or more of the variables involved.

In the case of the Inglis equation

$$\sigma_t = 2\sigma\sqrt{a/\rho} \qquad \text{.....(18)}$$

ρ is the radius of the tip of an ellipse with a major axis of length 2a. When applied to a quasi brittle material, the plastic zone at the crack tip determines the minimum value of ρ. (A discussion of the term quasi brittle will be found in the following section 5.2.). Provided $a \gg \rho$ and, for example, the requirement for valid K_{Ic} determinations is that $a > 50\rho$, Brown and Srawley 1966; then equation (8) give a figure for σ_t which is acceptable both mathematically and also in terms of the material structure involved, Smith 1967.

When however equation (8) is applied to a fully brittle material, no clearly defined material feature provides a determining value of ρ. The minimum value will be set by inter-atomic spacing and possibly in an amorphous material such as glass this could have significance - Griffith 1921. In a polycrystalline or a polyphase material with which this thesis is concerned, grain boundaries will give rise to a larger but less determinate value of ρ - see for example plate (2) or (10) Additionally equation (8) was derived from laws governing linear elastic continuums and it is unlikely that they will hold for the separation of atoms or individual crystals.

Similarly, the Westergaard equation

$$\sigma_r = \sigma\sqrt{\frac{a}{2r}} \qquad \text{.....(5)}$$

gives the stress σ_r at a distance r just ahead of a sharp crack of length 'a'. As with the Inglis equation, in the case of quasi brittle materials, the plastic zone defines the minimum value of r. However given that r is

small compared with 'a' but large compared with atomic dimensions, the elastic solution for the stress in the neighbourhood of the crack is reasonably meaningful. Drucker 1968, Rice 1966.

In the case of fully brittle materials, the structure imposes limits on the minimum value of r and on the meaning of a 'sharp crack'. Whilst it may well be that the minimum value of r is less than that of the plastic zone in the quasi brittle material, it is the indeterminacy of r that causes difficulties and the point is discussed further in section 5.3. - page 133.

By considering the energy balance before and after crack propagation, Griffith was able to derive equat. (11)

$$\sigma_f = \sqrt{\frac{2E\gamma_e}{\pi a}}$$

without being forced to examine the stress position at the crack tip. Nevertheless there is still the assumption that linear elastic stress analysis will be valid from some point ahead of the crack tip. The Griffith equation states that an amount of energy γ_t is necessary for fracture. It does not state that γ_t, the thermodynamic surface energy is the only energy required for fracture. For most materials it is not. Nor does it give any information about the actual stress at the bottom of the crack which, depending on the sharpness of the crack, may or may not be sufficient to initiate fracture.

Griffith's own work was carried out on glass, probably the nearest approach to a continuum available in a real material. For this, he was able to show that his equation

held. His results were obtained by bursting pre-cracked spherical bulbs and circular tubes. In the nomenclature of this thesis, he compared

$$\sigma_f\sqrt{a} \quad \text{with} \quad \sqrt{\frac{2E\gamma_t}{\pi\nu}}$$

where ν is Poissons Ratio.

The average value obtained for $\sigma_F\sqrt{a}$ was 2391bs $in^{-3/2}$ with a maximum of 251. The calculated value for $\sqrt{\frac{2E\gamma_t}{\pi\nu}}$ was 266 lbs $in^{-3/2}$. It is important to note that Griffith was able to make direct independent assessments of E, ν and especially γ_t.

(note. γ_t which Griffith took as the surface tension of the glass, was obtained by measuring the surface tension at high temperatures when the glass was molten and extrapolating back to room temperature. This method cannot be applied to polycrystalline material. He obtained a figure of 0.5 Jm^{-2} which whilst fitting in well with his results is considerable less than γi determinations since - see table (5) page 127.)

Griffith's results show that for a brittle amorphous material such as glass, the thermodynamic surface energy accounts for the bulk of the energy released during fracture. Very little extra energy is required for non elastic events such as plastic flow or noise generation. Glass however, is a unique class of material in that it has no crystalline structure and fractures with a smooth surface, which allows a reasonable estimate to be made of the area of the new surface formed during fracture.

It is probable and perhaps unfortunate that because the Griffith equation worked well with glass, so much effort has since been spent trying to identify or relate the Griffith crack dimension 'a' with structural features in polycrystalline materials. - see section 2.8. page 26.

5.2. Quasi Brittle Fracture.

In section 2.7.1., brittle fracture was defined as occurring when the applied stress at fracture was less than the general yield stress. This implied the existence of cracks to act as stress raisers and did not rule out local yield as a form of crack extension prior to fracture. It is usual to refer to fracture where this occurs as quasi brittle.

Likewise a quasi brittle material is one in which a small zone of plastic flow is present at the crack tip. The zone is small compared with the length of the crack. It is also assumed, and essential to most discussions that the size of the plastic zone at fracture is constant and is independent of the crack length. e.g. in the calculation of the equivalent elastic crack.

Metals form the main bulk of the quasi brittle materials which accounts for the considerable emphasis and importance given to this type of fracture. It is well known that most metals are 'tough', which in the language of the Griffith equation is equivalent to saying that γ_t is only a small part of the energy needed for fracture- see table 5 over leaf.

Table of γ_i in Jm^{-2} from $\frac{K_{1c}^2}{2E}$.

Soda lime glass		0.5	Griffiths direct from surface tension
	(1)	4	
	(2)	8	
Alumina	(1)	3.5	Single crystal
	(2)	30	Polycrystalline
	(3)	15 - 40	"
Magnesia	(1)	1.5	Single crystal
	(2)	1.2	"
Sodium chloride	(2)	0.3	"
Magnesite refractories	(4)	5 - 15	
Kaolinite	(5)	20 - 25	
Kaolinite + Sand	(5)	20 - 35	
Kaolinite + Mullite 100's	(5)	20 - 40	
Kaolinite + Mullite 22's	(5)	40 - 65	
P.M.M.A. (Polymethylmethacrylate)	(1)	2×10^2	
	(2)	3.5×10^2	
Beryllium	(1)	0.5×10^3	
	(6)	1.5×10^3	
Aluminium alloy	(6)	85×10^3	
4340 steel	(6)	10×10^3	
Maraging steel	(6)	37×10^3	

1. Lawn and Wilshaw 2. Davidge
3. Meredith and Pratt 4. Uchno, Bradt and Hasselman
5. Present thesis 6. Averbach

Table 5

Orowan 1950 on experimental evidence suggested that the form of the Griffith equation still applied provided the thermodynamic energy γ_t was replaced by an energy term which included the virtual surface energy γ_p associated with plastic flow (plus noise and any other energy absorbing process).

In this context the term 'virtual' surface energy is used to distinguish it from real surface energy. That is, the additional energy γ_p does not subsequently appear on the surface but is dissipated. The same situation arises in the case of the work of fracture γ_F where the work, represented by the area under the stress strain curve, can contain a large component of virtual surface energy.

Thus $\gamma_i = 2\gamma_t + \gamma_p$. where γ_i is the energy required to initiate fracture and

$$\sigma_f = \sqrt{\frac{E(2\gamma_t+\gamma_p)}{\pi a}} = \sqrt{\frac{2E\gamma_i}{\pi a}} \quad \ldots\ldots\ldots(15)$$

Numerous workers (Knudsen 1959, Carniglia 1965, Lange 1973 and Rice 1972) have since confirmed the validity of this <u>form</u> of equation though disagreement has existed regarding the interpretation of 'a'.

Irwin 1958 in essentially the same modification as Orowan propsed the strain energy release rate, previously defined in terms of γ_t should include all other types of energy. Thus, by definition, at the critical value when fracture is just about to occur,

$$G_c = (2\gamma_t + \gamma_p) = 2\gamma_i$$

It will be recalled that a general relationship

$G = \frac{K_I^2}{E}$ was derived earlier in the thesis (equation 13 section 2.6.3.). Though this was obtained in terms of the thermodynamic energy γ_t, provided the plastic zone is small compared with the crack length, independent of the length and constant in size, the derivation would apply in relation to γ_i (i.e. γ_i defined originally in σ_F type measurements will, like γ_t, be constant)

Whence $$2\gamma_i = G_{Ic} = \frac{K_{Ic}^2}{E}$$

from which by substitution in $\sigma_F = \sqrt{\frac{2E\gamma_i}{\pi a}}$

gives $$\sigma_f = \sqrt{\frac{K_{Ic}^2}{\pi a}}$$

Use has frequently been made of this substitution both in the brittle and the quasi brittle field, Davidge and Tappin 1970, Averbach 1968, Chermont and Osterstock 1976. For the design engineer concerned with the fracture of metals (quasi brittle), it provides a basis for the specification of surface finish or for the calculation of the maximum safe crack. - Wessel, Clarke and Pryle 1969.

It is suggested here, that the plastic zone, present only in the quasi brittle case, is the chief reason why the 'fracture toughness' testing of metals has progressed to its present importance. Without such a zone to smear out both machining and material irregularities at the crack tip, comparative testing would be considerably more difficult.

The starting requirement in the application of the formula, is a valid determination of K_{Ic} . For this, the methods developed by Brown and Srawley 1966 under the

auspice of the A.S.T.M. are now generally accepted as satisfactory. The design of test pieces and the subsequent K calibrations have been extensively cross checked by experiment on a variety of different metals. The limitations on the test piece size are the points of interest in this thesis - see section 2.10.3.. Essentially they are concerned with ensuring that the starting crack is long compared with ρ, the radius of curvature of the crack tip, (additionally the crack should penetrate about half way through the sample which must also be sufficiently wide to ensure plane strain conditions at the crack tip).

Given that a valid K_{Ic} determination has been obtained; it is known that at fracture, the radius of curvature of the crack tip will always be the same value ρ since this is the radius of the plastic zone. Thus it can be expected that the stress field at the root of the crack of length 'a' in the formula $\sigma_f = \sqrt{\frac{K_{Ic}^2}{\pi a}}$ will be the same as that for the K_{Ic} test pieces.

(note, if the determination of K_{Ic} involves work hardening of the crack tip inorder to increase its sharpness by reducing the diameter of the plastic zone or if the fabrication of the product produces work hardened or embrittled portions (e.g. welding), then the argument does not hold.

i.e. With G_{Ic} defined equal to $2\gamma_i$, it is not permissible to write $G_{Ic} = K_{Ic}^2/E$ since one is considering a different set of conditions and γ_i is not necessarily the same.

Though work hardening of the test piece increases

the design safety factor, work hardening of the product reduces it. - see discussion on paper by Wessel, Clark and Pryle 1969)

5.3. Brittle Ceramic Materials.

Whilst it is accepted that metals develop a zone of plastic flow at the crack tip prior to fracture which contributes to subcritical crack growth - Johnson 1962, Kelly 1970, this is unlikely to be the case for ceramics, Evans and Toppin 1972, Lange 1973. The view of Carniglia 1965 that plastic flow at the crack tip was the mechanism of crack extension has been superceded by the view that flaw linking takes place in a series of discreet steps as the critical linking stress for that step is reached, Glucklich 1970. In the author's own work on clay ceramics, there has been no evidence of plastic flow. The brittle nature of the fracture can be seen, for example, on plates 3, 6, 10 and 11. Whilst these were taken a short distance from the start of the crack, examination of the starting area on the S.E.M. screen did not reveal any major differences.

The equations of Inglis and Westergaard indicate how dependent the stress field in the neighbourhood of the crack tip is on its sharpness. In the absence of a constant plastic zone at the crack tip to smear out any irregularities, it would be expected that completly random values of σ_f would be obtained. In practice, it is usually found that a Griffith type of equation can be

applied providing the surface energy term γ_t is increased to include other forms of energy dissipation. In this case, the additional energy requirement comes from the non-linear and non-elastic forces associated with the fracture of the crystal lattice and the separation of individual atoms. The type of energies involved are considerably smaller than for the quasi brittle material as table (5)* shows - ceramics are not tough.

It is obviously not possible to evaluate the particular atomic scale events leading to ultimate fracture. An examination of the S.E.M. plates shows it to be doubtful, in the case of a clay bodied material, whether it is possible even on the macro scale to identify the particular subcritical events leading to fracture. However, it is still possible to consider the situation at the crack tip and the following points can be made.

1) There is an intensification of the applied stress caused by the presence of a crack. At some distance ahead of the crack, linear elastic stress analysis may be expected to apply. A formula $G' = (K')^2/E$ can be derived in which G' and K' are some form of G and K. G' will contain, in addition to the thermodynamic surface energy, non-linear and non-elastic energy terms associated with the separation of the individual atoms. K' will be the usual form of K (i.e. $K = \sigma\sqrt{\pi a}$) at the point ahead of the crack where linear elastic stress analysis applies, but may be expected to differ from this form as non linear and non elastic conditions take over closer to the crack tip.

* p. 127

2) Energy will always be required to extend the crack and following the same argument as for quasi brittle materials gives

$$2\gamma_i' = G' = \frac{(K')^2}{E}$$

If by definition γ_i' is the critical value of surface energy required for the Griffith equation then $2\gamma_i' = G_c'$

In view of the uncertainty attached to K' close to the crack tip - (i.e. $K' \simeq \sigma\sqrt{\pi a}$), it is <u>not</u> possible to deduce directly from the mathematics that $G_c' = \frac{(K_{1c}')^2}{E}$

thus $$2\gamma_i' = G_c' \simeq \frac{(K_{1c}')^2}{E}$$

or $$\sigma_F = \sqrt{\frac{2E\gamma_i'}{\pi a}} \simeq \sqrt{\frac{(K_{1c}')^2}{\pi a}} \quad \ldots\ldots\ldots(26)$$

The same problem would have arisen in the quasi brittle material but in that case the plastic zone at the crack tip <u>ensured</u> at least similarity of the stress conditions for σ_F and K_{1c} measurements.

(note. If G had been defined as the crack extension force rather than the strain energy release rate,

then $$2\gamma_i' \simeq G_c' = \frac{(K_{1c}')^2}{E}$$

The difference would not affect the problem of the relationship between γ_i' and K_{1c}')

5.3.1 <u>Experimental Justifications of $\sigma_F = \sqrt{(K_{1c}')^2/\pi a}$</u>

Griffith was able to establish the validity of

$$\sigma_F = \sqrt{\frac{2E\gamma_i}{\pi a}}$$

for glass by the independent measurement of σ_F, E, γ_i and 'a'.

Subsequently he was able to make predictions about the value of 'a' in other configurations.

In the case of ceramic materials, where interest also lies in the value of 'a', it is not normally possible to obtain a direct measurement of γ_i and recourse is usually made to the expression $2E\gamma_i = K_{1c}^2$ -Davidge and Tappin 1970, Chermant and Osterstock 1975, and figures in table (5)* of this thesis. In terms of equation (26) this relies on establishing that $\sigma_F = \sqrt{\frac{(K_{1c})^2}{\pi a}}$ either by direct measurement or by reasonable inference.

The direct approach was undertaken by Meredith and Pratt 1974 on three grades of alumina. K_{1c} determinations were made using several standard shapes of test pieces (single edge notched bend, compact tension and double cantilever). Fractured σ_F specimens were then examined for flaws and possible flaw linking and from a knowledge of the flaw shapes, dispositions and K_{1c} for the material; a value of σ_F was calculated which agreed with the actual measured value.

The more usual approach is to examine the fracture origins of K_{1c} and σ_F test pieces and if no differences are apparent, to conclude the stress situations have been similar and the formula is valid, Davidge 1969. This is directly analagous to making assumptions about the plastic zone in the quasi brittle case. Davidge and Tappin 1968 point out that it has not been established that γ_i is a material property alone and that the values they quote are strictly relevant only to specimens prepared and tested in the same way.

* p. 127

The coarse non uniform structures of the polyphase clay bodied ceramic used in this thesis make it unlikely that much success in the justifying of writing $\sigma_F = \sqrt{\frac{(K_{1c}')^2}{\pi a}}$ could be achieved by the direct approach. Additionally, the variation in structure from one formulation to the next would necessitate a separate justification for every one. The alternative of examining the fracture origins of σ_F and K_{1c} test pieces was carried out in the S.E.M. and as far as could be seen there was no difference. This suggests that for a given formulation and firing, it is permissable to write $\sigma_F = \sqrt{\frac{(K_{1c}')^2}{\pi a}}$ and that some smearing out process, analagous, to but different in nature from, the plastic zone in the quasi brittle case is taking place.

Further confirmation of this is given by the ability to relate both σ_F and K_{1c} results to the structure of the material - (see section 4.2.7.)* and by the similar low variation in results in sets of σ_F and K_{1c} test pieces. If σ_F was controlled by random surface flaws whilst K_{1c}, with its reduced sensitivity to random flaws was controlled by the material structure it would be expected that sets of K_{1c} results would vary by considerably less than sets of σ_F results. This however is not so, the standard error of K_{1c} tests is about 4.0% and σ_F about 5.5%. It is suggested that both σ_F and K_{1c} fracture follows a period of random crack growth but because a large number of alternative growth paths are always available, the variations in the ultimate fracture stresses are small. The acoustic emission results

* p. 115

substantiate the view that a large number of subcritical crack events can occur prior to fracture - section 3.5.2.*

(note, in cases where the material features such as grain size and pore size are likely to be smaller than defects in the surface finish, it is not unreasonable to expect that random surface flaws, which may be few in number, will determine the value of σ_F and that material properties will determine the value of K_{Ic}. Irwin 1958)

5.3.2. Equivalent elastic crack. Given it is accepted that $\sigma_F = \sqrt{\frac{(K_{Ic}')^2}{\pi a}}$ or $(K_{Ic}')^2 = 2E\gamma_i$ then the determination of K_{Ic}', E and σ_F allows the calculation 'a', the Griffith flaw size and γ_i, the surface energy for the initiation of fracture. For completeness a table of γ_i is given overleaf but it is in the Griffith flaw size 'a' that the main interest lies.

It was shown in section (2.8) that numerous attempts had been made to link it to the grain size of the material and indeed for uniformly grained materials some success was achieved - Petch 1953, Knudsen 1959 and Carniglia 1965. In these cases the approach was to measure σ_F, a grain size parameter 'd' and to demonstrate that $\sigma_F = kd^{-\frac{1}{2}}$.

Latterly - see section 2.9., the emphasis has changed to relating the value of 'a' as calculated from σ_F and K_{Ic}, and referred to here as the equivalent elastic crack C_E, to observable features in test pieces. Kirchener, Gruver and Sotter 1976, working with hot pressed alumina and silicon nitride, found that with the presence of large

* p. 83

Table of γ_i in Jm^{-2}

Firing Temp °C	950	1050	1150	1250	1350	1450	1550
Kaolinite				25	22	24	20
Kaolinite + Felspar		11	12	15	15	21	
Kaolinite + Alumina 3				16	24	17	17
Kaolinite + Alumina 4				12	18	18	18
Kaolinite + Alumina 5				14	15	22	18
Kaolinite + Quartz				18	23	16	28
Kaolinite + Flint				21	25	17	21
Kaolinite + Sand				22	24	21	33
Kaolinite + Zircon Flour			15	20	24	33	24
Kaolinite + Zircon Sand			12	17	24	33	21
Kaolinite + Mullite (22's)				38	39	45	62
Kaolinite + Mullite(100's)				20	32	46	38
Ball Clay	18	39	14	17	17		
Kaolinite + Ball Clay	8	20	12	16	15		

Standard error of γ_i is about 9%

Table 6

crystals, there was reasonable agreement between the calculated value of C_E and the crystal size. With other types of flaw, less agreement was found.

In the case of the polyphase clay bodied structures examined in this thesis, it was also found that only in those cases where major flaws or large particles were visible on the S.E.M. was it possible to relate C_E directly to a material feature - section 4.2.1.* It should be noted that,for instance, in the case of a sand filled formulation, it was never possible to determine which particulargrain was responsible. The constancy and the repeatability of the results allowed the conclusion that sand grains were responsible for the increased value of C_E.

In all other cases, even Kaolinite + Ball Clay where $C_E \sim 100\mu$ - section 4.2.2.**, the value of C_E was larger than any observable feature and it had to be concluded that crack extension prior to fracture was taking place. A case is made in section 4.2.3.*** for the linking together of pores prior to the fracture of Kaolinite.

Thus the value of the equivalent elastic crack C_E, calculated from σ_F and K_{Ic}, will for a clay bodied ceramic be the shortest crack from which catastrophic fracture can occur. Unfortuntely from the aspect of the design or quality control engineer, the value of C_E is in the region of a few hundred microns and not readily detectable by inspection.

*p. 110
**p. 111
***p. 112

6. Conclusions.

Before commencing the experimental work on polyphase clay ceramics, it had been expected that K_{Ic} would be found to be a material parameter with the initiation of fracture dependent on the polyphase structure of the material, and σ_F would be found to be dependent on random or surface cracks. In the event both σ_F and K_{Ic} have been shown by the results to be material parameters normally following similar trends. Differences between them arose when gross flaws such as those caused by bloating or large particles such as sand were present. In these cases σ_F showed its greater sensitively to flaws but remained material dependent - the flaws were part of the structure of the material as opposed to damage due to preparation or handling.

The values determined for the equivalent elastic crack C_e, show that gross flaws are capable of initiating fracture with a minimum of crack extension. In their absence, acoustic emission evidence and the value of C_e being muchgreater than observable structural features, shows catastrophic fracture occurs only after a period of subcritical crack growth. It is considered this sub-critical crack growth which takes place in both σ_F and K_{Ic} determinations results in essentially identical stress conditions at the root of the crack immediately prior to fracture. Thus at the instant of fracture σ_F and K_{Ic} are governed by similar material features. The large values of C_e, relative to those found by workers on the polycrystalline single oxides, are believed to explain the

insensitivity of σ_F to random surface damage cracks.

The addition of particles to the kaolinite base has a different effect on fracture to particles grown in situ during the firing. S.E.M. photographs show crystals grown in situ do not divert the crack front and fracture values show they do not produce any reinforcing effect. Mullite or Zircon particles added directly to the formulation however give considerable reinforcement and S.E.M. photographs show a disturbed fracture path. It is suggested that at the firing temperatures used, fusion between kaolinite and the added particles never approaches that of particles grown in situ. Consequently the travelling crack front experiences some discontiuuity. Further work carried out with the addition of different proportions of added particles should help to clarify this point.

As with σ_F and K_{Ic}, the values of E could usually be related to visible features in the structure of the material. It was found to be affected by major cracks or flaws and in this it more closely paralleled σ_F than K_{Ic}.

The critical strain ϵ_c lay in the region of 1 or 2 millistrain, which is usual for brittle fracture. There was some evidence to suggest the results could be divided into two groups with values of ϵ_c of about 1.1 and 1.6. An unexplained feature which requires further investigation was that the variation of ϵ_c between firing temperatures of the same formulation as it changed from a point bonded structure to a glassy structure, was considerably less than the variation between different formulations. It would have been expected to find the variation less

between similar types of structure - see section 4.3.4.*

The effect of the plastic zone present in quasi brittle materials is discussed and shown to provide a smearing out of individual events at the crack tip. The result is to ensure that measurements of σ_F and K_{Ic} for quasi plastic materials are made under the same crack tip stress conditions, which thus provides a justification for relating in the case of quasi plastic materials, σ_F K_{Ic} and dependent variable such as C_E.

In the case of brittle fracture, the constancy and repeatability of the experimental results, and the ability to relate σ_F and K_{Ic} to the observable structure of the material, showed some form of smearing out existed. It is considered this arose by the subcritical crack growth causing (for a given formulation) the crack tip or crack front to develop in a similar manner from one test piece to the next. Thus at the instant of catastrophic fracture the crack tip was always seeing and was controlled by the structure of the material. Under these circumstances it was again justifiable to relate σ_F and K_{Ic} and to look for significance in the dependent variables.

The term crack tip has been used throughout the thesis and is consistent with the terminology of the literature. However, the crack develops along a line and the term 'crack front' more accurately describes the situation. For complex polyphase materials such as those discussed herin, the stress pattern will vary along the crack front but this will not prevent a similarity of conditions arising between test pieces prior to fracture.

*p. 119

Bibliography

Astbury, N.F. (1966). Proc. Br. Cer. Soc., 6. p103.

Averbach, B.L. (1968). Fracture. Vol 1. ed. Liebowitz, H., Pub. Academic Press. New York.

Bailey, J.E., Hill, N.A. (1970). Proc. Br. Cer. Soc., 15. p15.

Bishui, B.M., Nandi, A.K. (1972. Glass and Cer. Bull. 19. 4. p77.

Brindley, G.W., Nakahira, M. (1959). J. Am. Cer. Soc. 42. 7. p311.

Brown, W.F., Srawley, J.R. (1965). A.S.T.M. S.T.P. 381.

ibid, (1966). A.S.T.M. S.T.P. 410.

Carniglia, S.C. (1965). J. Am. Cer. Soc. 42. 8. p376.

ibid, (1966). Mat. Sci. Res. 3. p425.

Chermant, J.L., Osterstock, F. (1976). J. Mat. Sci. 11. p1939.

Chu, G.P.K. (1966). 3rd Int. Mat. Symp. Cer. Microstructures 38. p828.

Clark, F.J.P., Tattersall, H.G., Tappin, G. (1966). Proc. Br. Cer. Soc. 6. p168.

Comer, J.J. (1960). J. Am. Cer. Soc. 43. 7. p378.

ibid, (1961). J. Am. Cer. Soc. 44. 1. p561.

Coppola, J.A., Hasselman, D.P.H. (1973). Am. Cer. Soc. Bull. 52. 7. p578.

Cutler, I,B. (1957). J. Am. Cer. Soc. 40. 1. p20.

Davidge, R.W. (1969). Contemp. Physics 10. 2. p105.

Davidge, R.W., Evans A.G. (1970). Mat. Sci. Eng. 6 p281.

Davidge, R.W., Tappin, G. (1968). J. Mat. Sci. 3 p165.

ibid (1970). Proc. Br. Cer. Soc. 15 p47.

Dinsdale, A., Wilkinson, W.T. (1966). Proc. Br. Cer. Soc. 6. p119.

Drucker, D.C. (1968). Fracture. Vol 1. ed. Liebowitz, H. pub. Academic Press. New York.

Duckworth, W. (1953). J. Am. Cer. Soc. 36. 2. p65.

Evans, A.G. (1970). Proc. Br. Cer. Soc. 15. 10. p113.

Evans, A.G., Davidge, R.W. (1969). Phil. Mag. 20 p373.

Evans, A.G., Tappin, G. (1972). Proc. Br. Cer. Soc. 20. 4. p275.

Ghote, B.B., Hasselman, D.P.H., Spriggs, R.M. (1973). Am. Cer. Soc. Bull. 53 9 p670.

Glass, H.D. (1954). Am. Mineralogist. 39 p193.

Glucklich, J. (1970). Teck. Rep. 32 - 1438 N.A.S.A.

Griffith, A.A. (1921). Phil. Trans. Roy. Soc. London A Vol.221. p163.

ibid, (1924). Proc. 1st Int. Cong. App. Mech. p56.

Groves, G.W. (1970). Proc. Br. Cer. Soc. 15. 9. p103.

Hamano, K., Lee, E.S. (1972). Bull. Tokyo Inst. Tech. 108. p95.

Hariya, Y. Dollace, W.A., Kennedy, G.C. (1969). Amer. Mineralogist 54. p77.

Hartline, S.D., Bradt, R.C., Baumgarten, H.R., Rosebrooks, N.B. (1973). J. Am. Cer. Soc. 56 10 p550.

Inglis, C.E. (1913). Trans. Inst. Naval Arch. London55 p.219. quoted by Griffith (1921).

Irwin, G.R. (1948). Fracturing of Metals. 29th Congress 1947. pub. A.S. for Metals. Cleveland. 1948.

Irwin, G.R. (1958). Encyclopedia of Physics 6 p551 pub. Springer - Verlag, Berlin.

Irwin, G.R., Kies, J.A. (1954). Welding J. Res. Supp. p1953

Johnson, A.A. (1962). Phil. Mag. 7 p177.

Johnson R. (1975). Trans. and J. Br. Cer. Soc. 75 1 p1.

Kelly, A. (1970). Proc. Br. Cer. Soc. 15. p1.

Kingery, W.D. (1960). Introduction to Ceramics. p278 pub. John Wiley and Sons. New York.

Kirchener, H.P., Gru ver, R.M., Sotter, W.A. (1976). Mat. Sci. & Eng. 22 p147

Knott, J.F. (1973). Fundamental of Fracture Mechanics pub. Butterworths. London.

Knudsen, F.P. (1959). J. Am. Cer. Soc. 42. 8. p376.

Lach, V. (1974). Interceram. 1. p27.

Lange, F.F. (1973). Composite Materials 5. p1 -64. ed. Broutman, L.J., Krock, R.H.

Lundin, S.T. (1959). Studies on Triaxial Whiteware Bodies pub. Almquist and Wiksell. Stockholm.

Meredith, H., Pratt, P.L. (1974). Spec. Cer. 6. p107 pub. Br. Cer. Res. Ass. (1975).

Nakayama, J. (1965). J. Am. Cer. Soc. 4. p583.

Orowan, E. (1949). Prog. Phys. 12. p185.

ibid, (1950). M.I.T. Symp. p139. pub John Wiley and Sons. New York.

Passmore, E.M., Spriggs, R.M., Vasilos, T. (1965). J. Am. Cer. Soc. 48. 1. p1.

Penty, R.A., Hasselman, D.P.H., Spriggs, R.M. (1972) J. Am. Cer. Soc. 53. 3. p169.

Percival, H.J., Duncan, J.F. (1974). J. Am. Cer. Soc. 57. 2. p57.

Petch, N.J. (1953). J. Iron Steel Inst. (London) 174. 1. p25 -28.

Rice, J.R. (1966). A.S.T.M. S.T.P. 415.

Rice, R.W. (1972). Pro. Br. Cer. Soc. 20. p205.

ibid, (1973). Symp. on Frac. Mech. of Cer. Univ. of Pennsylvania.

ibid, (1975). J. Am. Cer. Soc. 58. 9 -10 p458.

Richardson, H.M., Wilde, F.G. (1952). Trans. Br. Cer. Soc. 51. p387.

Rossi, R.C. (1968). J. Am. Cer. Soc. 51. 8. p433.

Roy, R., Roy, D.M., Francis, E.E. (1955). J. Am. Cer. Soc. 38. 6. p198.

Rue, J.W., Ott, W.R. (1974). J. Thermal Anal. 6 p. 513 - 519.

Ryshkewitch, E. (1953). J. Am. Cer. Soc. 36. 2. p65 - 68.

Sambell, R.A.J., Bradley, R. (1964). Phil. Mag. 9 p161.

Sequit, E.K., Anderson, C.A. (1971). Am. Cer. Soc. Bull. 50. 5. p480.

Shand, E.B. (1961). J. Am. Cer. Soc. 44. 1. p21.

Simpson, L.A. (1974). J. Am, Cer. Soc. 57. 4. p151.

Smith, E. (1967). Proc. Roy. Soc. (London) 299 p455.

Soliman, M.R., Hamnad, E. (1970). Bull. Central Glass Cer. Res. Inst. Calcutta; 17. 1. p5.

Stokes, R.J. (1966). Pro. Br. Cer. Soc. 6. 17. p189.

Swanson, G.D. (1972). J. Am. Cer. Soc. 55. 1. p48.

Wessel, E.T., Clark, W.G., Pryle, W.H. (1969). Pro. 2nd Int. Conf. on Fracture. pub. Chapman and Hall.

Westergaard, H.M. (1939). J. App. Mech. 6. A. 49.

Acknowledgements

Thanks are due to the Science Research Council for the award of a Research Studentship; to Professors C.R.Tottle and B. Harris of the School of Materials Science for making available laboratory facilities; to Mr. H. Perrott for assistance with the scanning electron microscopy; and to Mr. B. Chapman of the School of Physics for the X-ray spectroscopy results. Particular thanks must go to Dr. R. G. Cooke for his supervision of this project; his sound suggestions and constructive cricism, both during the experimental work and the writing of this thesis, have been much appreciated.

Appendix 1.

Meledor China Clay

Suppliers:- English Clays. Lovering Pochin & Co. Ltd.

Chemical Analysis

SiO_2	46.58
Al_2O_3	38.08
Fe_2O_3	0.69
TiO_2	0.07
MgO	0.20
CaO	0.19
K_2O	1.47
Na_2O	0.08
Loss on Ignition	12.66

Rational Analysis

Clay	89.5
Felspathic Matter	9.4
Quartz	nil

Particle size distribution

% residue on 300 mesh B.S.S. sieve	0.03
% above 10 microns	26
% below 2 microns	37

Quartz, Flint and Sand

Suppliers:- Wengers Ltd.

Typical Analysis	Quartz 1136W	Flint 1122W
S_iO_2	96.20	98.30
Al_2O_3	1.41	0.82
K_2O	0.80	0.09
Fe_2O_3	0.15	0.05
CaO	0.05	0.05
M_gO	nil	0.06
Na_2O	0.09	0.03

Particle size - sieve analysis

Passes 38	8.9%	97.2%
63	82.8%	
150	7.6%	
150	0.7%	2.8%

Sand 1309W

Particle size - sieve analysis

Passes 63	1.3%
150	5.4%
300	77.3%
425	15.1%
425	0.9%

Potash Felspar - $K_2O.Al_2O_3.6Si_iO_2$

Suppliers:- Wengers Ltd.

Typical Analysis

Si_iO_2	66.11
A_2O_3	18.26
Fe_2O_3	0.1
CaO	0.76
M_gO	0.1
K_2O	10.38
Na_2O	3.75

Alumina (calcined)

Suppliers:- Wengers Ltd.

Ball Clay - High Mod KC.

Suppliers:- English Clays. Lovering Pochin & Co. Ltd.

Appendix 2

Clay Formulations

The figures give the parts by weight of the various components of the formulation. In some cases a possible mullite figure is given. This is the percentage by weight of mullite that would be produced by the complete reaction of all the alumina present in the mix based on chemical equation (4) - section 2.11 page 51.

Kaolinite + Quartz

Kaolinite 77

Quartz 23

Possible mullite 45%

Kaolinite + Flint

Kaolinite + Sand

} as Kaolinite + Quartz

Kaolinite

Kaolinite 100

Possible mullite 61%

Kaolinite + Alumina (3)

Kaolinite 73

Alumina 27

Possible mullite 84%

Kaolinite + Alumina (4)

Kaolinite 55

Alumina 45

Possible mullite 99%

Kaolinite + Alumina (5)

Kaolinite 48

Alumina 52

Excess Alumina 15%

Kaolinite + Felspar

Kaolinite 87

Felspar 13

Possible mullite 56%

Kaolinite + Zircon Flour and Kaolinite + Zircon Sand

Kaolinite 77

Zircon Flour or Sand 23

Possible mullite 24%

Kaolinite + Mullite (100's or 22's)

Kaolinite 77

Mullite 23

Possible mullite 70%

Kaolinite + Ball Clay

Kaolinite 50

Ball Clay 50